AD-A139 904 FOUR-DIMENSIONAL SATELLITE DATA ASSIMILATION(U) 1/2
COOPERATIVE INST FOR MESOSCALE METEOROLOGICAL STUDIES
NORMAN OK Y K SASAKI ET AL. JAN 84 N00014-79-C-0758
UNCLASSIFIED F/G 4/2 NL

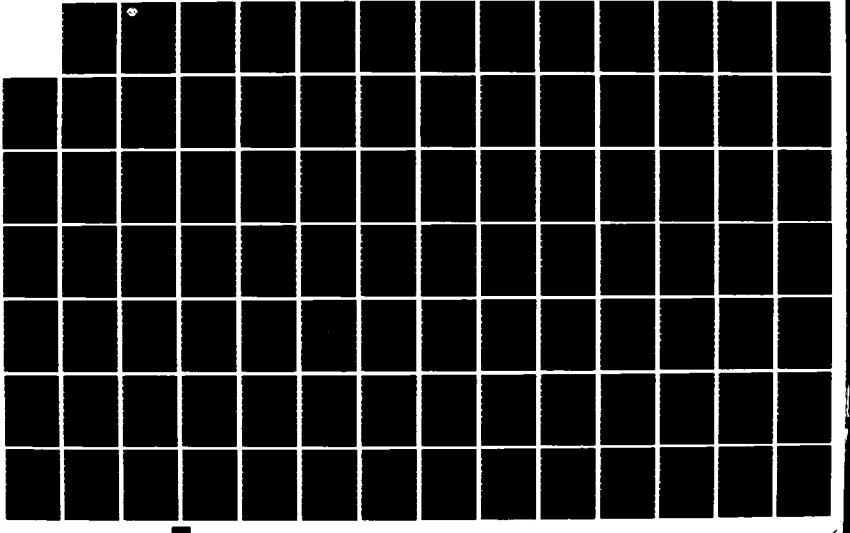

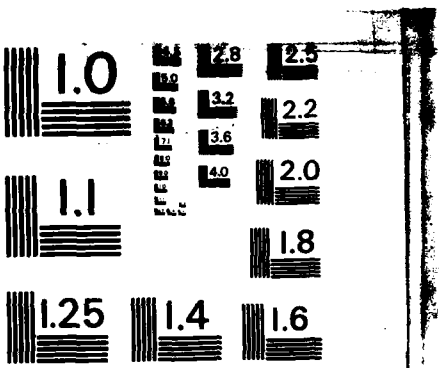

FINAL REPORT
FOR
DEPARTMENT OF THE NAVY
CONTRACT N00014-79-C-0758

FOUR-DIMENSIONAL SATELLITE DATA ASSIMILATION

SUBMITTED BY
YOSHI K. SASAKI, PRINCIPAL INVESTIGATOR
GEORGE LYNN CROSS RESEARCH PROFESSOR
SCHOOL OF METEOROLOGY, UNIVERSITY OF OKLAHOMA
AND
DIRECTOR, COOPERATIVE INSTITUTE FOR MESOSCALE METEOROLOGICAL STUDIES

AND

JAMES S. GOERSS, RESEARCH SCIENTIST
COOPERATIVE INSTITUTE FOR MESOSCALE METEOROLOGICAL STUDIES

NORMAN, OKLAHOMA

JANUARY, 1984

Final Report

for

Department of the Navy
Contract N00014-79-C-0758

Four-Dimensional Satellite Data Assimilation

Submitted by

Yoshi K. Sasaki, Principal Investigator
George Lynn Cross Research Professor
School of Meteorology, University of Oklahoma
and
Director, Cooperative Institute for Mesoscale Meteorological Studies

and

James S. Goerss, Research Scientist
Cooperative Institute for Mesoscale Meteorological Studies

Norman, Oklahoma

January, 1984

This work relates to Department of the Navy Contract N00014-79-C-0758 issued by the Office of Naval Research and funded by Naval Environmental Prediction Research Facility (NEPRF).

1. INTRODUCTION

Over the past several years our research efforts under this contract have been focused upon developing techniques to utilize satellite data assimilation in order to improve the forecasts made by global numerical weather prediction models. The accuracy of forecasts made by forecast models is dependent upon how realistically the model represents the actual processes of the atmosphere and by the ability to provide the model with initial conditions which reflect the true state of the atmosphere. Data assimilation research has concentrated on the second of these two problems. Before the development of satellite-borne measurement systems in the 1960's, the volume of asynoptic data available was limited and data assimilation schemes were designed primarily to handle the conventional surface and upper-air observations. Unlike the conventional data, the vast amount of satellite observations consists of measurements of meteorological variables (primarily temperature) which are widely distributed in both space and time. Beginning with a paper by Charney et al. (1969), a great deal of data assimilation research has been conducted to determine ways to use this new data source. In this report we will use the terminology conventions introduced in the review papers of McPherson (1975) and Bengtsson (1975).

Dynamic assimilation describes the use of a numerical prediction model as an integrator of observations distributed in space and time. We refer to the process of interpolating an observation to a number of surrounding model grid points using an objective analysis scheme as indirect insertion. Insertion of data into a numerical model which disagrees with the current model solution will result in the generation of gravity wave noise within the model. On the other hand insertion of data which is in perfect agreement with

the model solution adds no information. There are two ways to attack the data assimilation problem: use an insertion method which maximizes information and minimizes resulting model noise or control the model noise after insertion. Ghil et al. (1979) found in a global assimilation experiment using real data that forecast improvement was directly related to the sophistication of the continuous indirect insertion scheme used. On the other hand, in our research we have utilized techniques (Noise Freezing Methods I and II) to control the noise caused by the insertion. In the research described in Sasaki and Goerss (1982) we used a dry global primitive equations model with 3 vertical levels and 7.5^{o} resolution and a relatively simple indirect insertion scheme. Continuous assimilation of satellite temperatures was performed using Noise Freezing Methods I and II and the results were compared with a scheme designed to simulate most operational forecast centers. Significant forecast improvement was found when the noise control techniques were utilized.

In this report we describe the culmination of our global satellite data assimilation research efforts. A continuous temperature data assimilation scheme was designed to be implemented using the Navy Operational Global Atmospheric Prediction System (NOGAPS). In the next section the details of this scheme are described. Two experiments were run using the operational satellite temperature data available to Fleet Numerical Oceanographic Center (FNOC). Each experiment consisted of an assimilation and a control run. The results of these experiments are detailed in Section 3. We conclude our report by summarizing our research and discussing its future applications to the improvement of NOGAPS forecasts.

2. CONTINUOUS DATA ASSIMILATION TECHNIQUES

The key to successful data assimilation is to introduce information to the forecast model without "shocking" the model so much that the benefits of the added information are overcome by the noise induced by the insertion. As described by Miyakoda et al. (1978), when asynoptic data are inserted into an atmospheric model, they create discontinuity with the current model solution. The dynamical characteristics of the fluid enable it to remove this discontinuity in such a way as to maintain a state of approximate geostrophic balance. This geostrophic adjustment process results in the generation and dispersal of inertia gravity waves. Talagrand (1972) points out that the effectiveness of an assimilation scheme is dependent upon not only the amount of information introduced into the model but also upon how well the high frequency noise caused by this introduction can be damped.

The conclusion of two studies using simulated asynoptic data (Bengtsson and Gustavsson, 1971; Miyakoda and Talagrand, 1971) is that the spreading of information contained in an observation to several surrounding grid points using some sort of objective analysis scheme increases the effectiveness of assimilation. In an extensive experiment using real data and a number of indirect insertion schemes, Ghil et al. (1979) found that the success of assimilation (based on forecast improvement) was directly related to the level of sophistication of the insertion scheme used. The reason for this is that the asynoptic data is put into a form by the objective analysis scheme which makes it more "palatable" to the forecast model. The effectiveness of this transformation in terms of forecast improvement is dependent upon how much of the information contained in the asynoptic data is retained. In this study we have devised a two-step objective analysis

procedure to attack this problem. First, we utilize a variational adjustment scheme which we call vertical shape matching to modify each satellite-derived temperature sounding so that its information content is disturbed as little as possible but its form is changed so that it can be more readily accepted into the NOGAPS model. Then, the soundings are assimilated each time-step into the NOGAPS model using an objective analysis scheme patterned after that described by Barker (1982). The details of these procedures will be given later in this section.

Another aspect of data assimilation has been explored by Sasaki and Goerss (1982). In their study of Noise Freezing Methods they found that improved forecasts could be obtained utilizing continuous data assimilation and by modifying the numerical forecast model so that the noise induced by data insertion is controlled. Their work pointed out the need to examine closely the effects of the data insertion upon the model used in the assimilation process. In this section we will also discuss this aspect of the problem with respect to the NOGAPS model.

Vertical Shape Matching

The vertical resolution of satellite soundings is such that smoothing results for features such as frontal inversions and the tropopause which are better defined by forecast models. An example of this problem is illustrated in Fig. 1 where we have pictured a model sounding with two inversions and a satellite sounding in which these features are typically smoothed. Before the observed satellite-derived temperatures are inserted into the forecast model, a variational adjustment is made to each satellite sounding. This adjustment is accomplished by minimizing the functional:

$$J = \int [a(T - \hat{T})^2 + b(\frac{\partial T}{\partial \pi} - \frac{\partial \tilde{T}}{\partial \pi})^2 + c(\frac{\partial^2 T}{\partial \pi^2} - \frac{\partial^2 \tilde{T}}{\partial \pi^2})^2] \, d\pi,$$

where the vertical coordinate is $\pi = \ln (1000/p)$. The mean layer temperatures implied by the satellite sounding are given by $\hat{T}$ while the model-derived temperatures at the location of the satellite sounding are given by $\tilde{T}$. The resulting adjusted satellite sounding, given by T, is such that the vertical structure of the model is preserved along with the mean layer temperatures implied by the satellite sounding. The results of applying this technique are illustrated in Fig. 1. Thus, by applying this scheme we produce satellite soundings which have been modified in a way so that the information content that we can expect from such a sounding is preserved and yet at the same time the sounding has been made more consistent with the model into which it will be inserted.

Indirect Insertion Scheme

The indirect insertion scheme used in this study is an objective analysis procedure patterned after that described by Barker (1982). For a particular time-step the model temperature fields are modified by performing a two-pass Barnes analysis using all satellite soundings to be applied at that time. Let K represent the number of asynoptic observations taken during a block of time within radius R of a model grid point. For this study R was chosen to be 800 km. For each assimilation time-step, a two-pass Barnes analysis is performed. On the first pass the forecast temperature T_f, at each grid point, is replaced by

$$T = T_f + [\sum_{i=1}^{K} W_i(T_i - T_{fi})/(W_o + \sum_{i=1}^{K} W_i)],$$

where T_i is the observed temperature at the pressure level of the grid point and T_{fi} is the model forecast temperature interpolated to the location and pressure level of the observation. The weight associated with the observation is

$$W_i = \exp\ [-D_i^2/(\gamma\beta^2)],$$

where D_i is the distance from the grid point to the location of the ith observation and β is chosen to be 450 km. The value W_0 is a "background" weight which results in the value of the forecast field being given weight as if it were an observation 450 km from the grid point. This prevents a "noisy" analysis at grid points on the fringes of areas where satellite observations are taken. The process is repeated on the second pass with the value of γ reduced from 1.0 to 0.3 and with the forecast values being replaced by the results of the first pass.

Continuous Data Assimilation into NOGAPS

The main forecast tool of Fleet Numerical Oceanographic Center is the Navy Operational Global Atmospheric Prediction System (NOGAPS). NOGAPS consists of objective analysis, initialization, and forecast model. The NOGAPS model is with minor modifications a version of the UCLA general circulation model described by Arakawa and Lamb (1977). Specific details about the NOGAPS model are given by Rosmond (1981). Details on the objective analysis method and initialization procedure are given by Barker (1981).

In this study we utilized a version of the NOGAPS model for which the time-step was 240 seconds and one "cycle" of integration consisted of a Matsuno time-step and four leap-frog time-steps. The last of the leap-frog

time-steps included most of the physical parameterizations of diabatic processes. The Matsuno time-step has a damping effect upon the "noise" induced within the forecast model by the full physics computations performed every five time-steps. In Fig. 2 we see the sawtooth pattern this cycle produces in the global root mean square pressure tendency for a six-hour forecast beginning at 06Z, 27 March 1983. Over the six-hour period the level of this quantity is virtually constant at roughly 0.0006 mb/sec.

The satellite data used in this study were those routinely available on an operational basis at FNOC. The data we used consisted of observations of geopotential height at the ten standard pressure levels between 1000 mb and 100 mb, inclusive. Using the hypsometric equation these observations were converted to a mean layer temperature which was then assumed to represent the atmospheric temperature at the pressure level at the middle of the layer. Thus, for each satellite sounding we obtained nine temperatures at pressure levels ranging from 922 mb to 122 mb, inclusive. We then blocked the satellite data into one-hour blocks centered upon the hour of observation. Typically each block consisted of around 100 observations and global coverage was effected by about twelve hours worth of data. The vertical shape matching discussed previously in this section was performed for each block of satellite data immediately before that block was introduced into the model. Thus, for a block of satellite data centered on 09Z the model fields valid at 0830Z were used along with the satellite observations themselves in order to modify the soundings which would be inserted into the model between 0830Z and 0930Z. The data insertion was performed during each of the three interior leap-frog time-steps of each NOGAPS cycle.

As mentioned previously Sasaki and Goerss (1982) found that forecast

improvement from data assimilation was dependent upon how well the numerical forecast model controlled the noise induced by data insertion. For the forecast model they used in that study, they found that data assimilation without use of one of the Noise Freezing Methods resulted in a gradual increase in the global root mean square pressure tendency over the forecast period. The use of Noise Freezing Method I, in which a constant was subtracted from all values of surface pressure carried within the model, resulted in the same gradual increase in this quantity but at a substantially reduced level. The results of applying Noise Freezing Method II, in which periodically during the assimilation process the mass divergence fields were smoothed and the model winds adjusted to agree with the smoothed mass divergence, showed a sawtooth pattern in which the level of the global rms pressure tendency is constant but higher than the level of that quantity for a non-assimilation forecast. In Fig. 2, we can see that the results obtained for a six-hour assimilation forecast beginning at 06Z, 27 March 1983 are similar to those obtained by Sasaki and Goerss (1982) using Noise Freezing Method II. The Matsuno time-step every cycle provides the noise control necessary for the data assimilation forecast.

One final aspect of data assimilation will now be discussed. There are two extremes which can be considered when performing data assimilation. If the information to be added is directly inserted into the forecast model with no modification whatsoever, the resulting noise induced within the model will be maximal. On the other hand, if the information is modified so much that it agrees perfectly with the model solution at time of insertion, then no noise will be induced but no information will be added to the model. Recall that our assimilation procedure calls for the satellite data to be broken up into one-hour blocks centered on the hour of observation. During

each of these blocks, the data is inserted into the model on each of the three interior leap-frog time-steps of each model cycle. In Fig. 2 the astericks represent the beginning of a new block of satellite information. At the top of the figure is plotted the root mean square of the temperature differences between the model solution for that time-step at the location of the observation and the value of the observation itself. This is for the satellite observations for temperature at about 592 mb and these results are typical of those found at all levels except for the uppermost level (about 122 mb) where the rms was typically three to four times greater. The important things to note from this plot are that the satellite information is different from the model solution (as indicated by the high rms values for the first two time-steps) and that the information is being successfully introduced into the model (as indicated by the low rms values for the succeeding time-steps). Thus, we conclude that our data assimilation procedures are sound and proceed with the experiment itself.

3. EXPERIMENTAL RESULTS

Two continuous data assimilation experiments were conducted, the first between May 12-18, 1983 and the second between August 22-27, 1983. Each experiment consisted of an assimilation run and a control run using NOGAPS and the satellite data operationally available to FNOC. A six-hour update cycle was utilized in these experiments. Each experiment consisted of a start-up period climaxed by 72-hour forecasts made from the global fields produced by the assimilation and control runs. In this section we will describe the differences between an assimilation and a control run, outline how each experiment was conducted, and evaluate the results of the forecasts made at the end of each experiment.

Both assimilation and control runs used NOGAPS as described by Rosmond (1981) and Barker (1981). The version of the forecast model used here possessed six vertical layers, 2.4^{0} x 3.0^{0} horizontal resolution, and a 4 minute time step. At six-hour intervals objective analysis and initialization were performed using all data operationally available at that time <u>including satellite observations</u>. The only difference between the assimilation run and the control run was the first-guess fields used by the objective analysis procedure each six hours. For the control run these fields were simply the six-hour model forecast valid at that time. For the assimilation run these fields were the result of <u>re-running</u> that six-hour model forecast while the satellite observations collected over that time period were continuously assimilated into the model. Thus, the additional expense of utilizing a continuous data assimilation scheme in an operational setting would be that of an extra six-hour forecast each update cycle.

Next we will describe how each experiment was conducted. Beginning with the same set of initial fields from 18Z, 12 May 1983 both assimilation and

conventional forecasts were made producing fields valid at 00Z, 13 May 1983. The satellite observations taken between 18Z and 00Z were continuously assimilated into the forecast model producing the assimilation forecast. Using the 00Z data and the respective first-guess fields, objective analysis and initialization were performed for both the assimilation and control runs. This process was repeated each six hours until objectively analyzed and initialized fields were produced for 00Z, 15 May 1983. Over the course of this two-day period the fields (especially temperature) for the assimilation run evolved quite differently than those for the control run. Finally, 72-hour forecasts were made using the conventional forecast model using the 00Z, 15 May 1983 fields from the assimilation and control runs. The second experiment was conducted in an identical fashion beginning with the same set of initial fields from 18Z, 21 August 1983 and ending with 72-hour forecasts made using the 00Z, 24 August 1983 fields from the assimilation and control runs.

One of the most striking results of these experiments was the marked changes effected in the temperatures in the upper levels of the NOGAPS forecast model by continuous temperature data assimilation. During the course of the two-day start-up period in each experiment the global mean temperatures for the four lowest model layers were virtually unaffected by data assimilation while those for the top two layers were significantly altered. This is illustrated in Table 1 where the results from the second experiment are tabulated. Similar results were found from the first experiment.

TABLE 1. Global Mean Temperatures for NOGAPS Model Layers

Time	Run	Model Layer 1	2	3	4	5	6
83082200	A	-50.3	-65.0	-39.9	-14.0	0.6	12.0
	C	-49.5	-65.1	-40.0	-14.1	0.5	11.9
83082212	A	-53.9	-64.0	-40.1	-14.0	0.7	12.3
	C	-49.4	-64.8	-39.9	-14.1	0.4	11.9
83082300	A	-56.3	-63.4	-40.4	-14.0	0.7	12.3
	C	-49.6	-64.9	-39.9	-14.1	0.3	11.8
83082312	A	-59.0	-62.7	-40.5	-13.9	0.8	12.6
	C	-49.5	-64.8	-39.8	-14.1	0.3	11.9
83082400	A	-60.5	-62.3	-40.6	-13.9	0.8	12.4
	C	-49.5	-64.8	-39.9	-14.2	0.2	11.8

As can be seen in the table the mean temperatures for the top two layers stay relatively constant throughout the period for the control run while the top layer ($\sim$75 mb) cools over 10^{o}C and the second layer ($\sim$150 mb) warms almost 3^{o}C for the assimilation run. More modest temperature changes are recorded for the lower four layers. The result is a more realistic representation of the atmospheric temperature profile in the upper layers of the model.

In order to evaluate the impact of data assimilation upon the NOGAPS forecasts, root mean square errors were computed for the differences between actual observations and the value of the initial or forecast field interpolated to the location of the observation. Tables 2 and 3 illustrate the results of these computations for the first experiment. The initial height fields at various levels at 00Z, 15 May 1983 for the control and assimilation runs, respectively, are featured in these tables. Globally, we can see that the fields from the assimilation run display rms improvement which increases with

Table 2. Root mean square error (m) for initial height fields at 00Z, 15 May 1983 for the control run.

	Global		NH		SH	
Level (mb)	Obs.	RMSE	Obs.	RMSE	Obs.	RMSE
850	645	13.8	572	13.6	73	15.3
500	1247	23.6	859	22.3	388	26.1
300	1227	36.5	840	34.0	387	41.5
100	1152	58.6	770	53.8	382	67.3

Table 3. Root mean square error (m) for initial height fields at 00Z, 15 May 1983 for the assimilation run.

	Global		NH		SH	
Level (mb)	Obs.	RMSE	Obs.	RMSE	Obs.	RMSE
850	645	14.5	572	14.2	73	16.6
500	1247	21.8	859	20.8	388	23.9
300	1227	33.2	840	32.0	387	35.8
100	1154	48.8	771	47.0	383	52.3

Table 4. Root mean square error (^{o}C) for initial temperature fields at 00Z, 15 May 1983 for the control run.

	Global		NH		SH	
Level (mb)	Obs.	RMSE	Obs.	RMSE	Obs.	RMSE
850	628	3.14	555	3.20	73	2.63
500	1246	2.32	859	2.21	387	2.53
300	1228	2.06	840	2.20	388	1.72
100	976	5.30	664	5.15	312	5.61

Table 5. Root mean square error (^{o}C) for initial temperature fields at 00Z, 15 May 1983 for the assimilation run.

	Global		NH		SH	
Level (mb)	Obs.	RMSE	Obs.	RMSE	Obs.	RMSE
850	628	3.05	556	3.09	72	2.75
500	1246	1.74	859	1.83	387	1.52
300	1227	2.14	839	2.23	388	1.92
100	1120	3.87	744	4.02	376	3.57

height and is most pronounced at 100 mb. This pattern holds true in both hemispheres as well with the most marked improvement displayed at 100 mb for the Southern Hemisphere (over 20% reduction in the rmse). At 850 mb the assimilation fields globally and in each hemisphere show a slight rms degradation. The improvements are also greater in the Southern Hemisphere than they are in the Northern Hemisphere for the levels above 850.

The results of rmse computations for initial temperature fields are shown in Tables 4 and 5. At both 500 mb and 100 mb the assimilation fields show large rms reduction globally and in each hemisphere. The slight global improvement shown at 850 mb is entirely due to the improvement in the Northern Hemisphere. Slight degradation is seen uniformly at 300 mb. A large part of the reduction at 100 mb is due to the reduction in bias effected by satellite data assimilation. Recall how the NOGAPS model tends to be too warm at its upper level without data assimilation. It should also be pointed out at this time that a gross error check is performed before the rms calculations are made. At all levels but 100 mb the number of rejected observations is negligible. We can seen in Tables 4 and 5 that nearly 150 100 mb observations were rejected for the control run fields. Thus, the actual rms improvement at 100 mb is even greater than that shown in these tables. These results are consistently observed throughout both experiments.

Next we will examine the results for the 24-hour forecasts valid at 00Z, 16 May 1983 displayed in Tables 6-9. With the exception of the 100 mb level, slight degradation is shown at each level for assimilation height forecasts, globally and in each hemisphere. At 100 mb significant improvement is still seen (almost 20% in the Southern Hemisphere). On the other hand the assimilation temperature forecasts (with the exception of 850 mb

Table 6. Root mean square error (m) for 24-hour forecast height fields valid at 00Z, 16 May 1983 for the control run.

	Global		NH		SH	
Level (mb)	Obs.	RMSE	Obs.	RMSE	Obs.	RMSE
850	653	23.7	577	22.0	76	34.2
500	994	32.3	739	29.1	255	40.2
300	965	48.0	713	43.3	252	59.2
100	890	69.9	642	66.6	248	77.7

Table 7. Root mean square error (m) for 24-hour forecast height fields valid at 00Z, 16 May 1983 for the assimilation run.

	Global		NH		SH	
Level (mb)	Obs.	RMSE	Obs.	RMSE	Obs.	RMSE
850	653	25.4	577	23.7	76	35.7
500	993	33.8	738	30.4	255	42.0
300	966	48.7	713	44.2	253	59.6
100	886	62.4	640	61.3	246	65.3

Table 8. Root mean square error (^{o}C) for 24-hour forecast temperature fields valid at 00Z, 16 May 1983 for the control run.

	Global		NH		SH	
Level (mb)	Obs.	RMSE	Obs.	RMSE	Obs.	RMSE
850	630	3.87	555	3.95	75	3.25
500	993	2.43	739	2.36	254	2.63
300	970	2.43	715	2.44	255	2.39
100	747	5.26	558	5.00	189	5.97

Table 9. Root mean square error (^{o}C) for 24-hour forecast temperature fields valid at 00Z, 16 May 1983 for the assimilation run.

	Global		NH		SH	
Level (mb)	Obs.	RMSE	Obs.	RMSE	Obs.	RMSE
850	627	3.58	553	3.58	74	3.60
500	993	2.10	739	2.07	254	2.16
300	970	2.42	715	2.36	255	2.58
100	860	3.99	621	4.01	239	3.94

and 300 mb in the Southern Hemisphere) all show improvement with the most marked improvement at 100 mb.

The results for the 48-hour forecasts valid at 00Z, 17 May 1983 are shown in Tables 10-13. As for the 24-hour forecasts, only at 100 mb is significant improvement seen in assimilation height forecasts (roughly 10% in each hemisphere). Only slight improvements or degradations are observed at other levels. For the temperature forecasts, except at 300 mb where slight degradations are seen, improvements are observed at every level. Again the greatest improvement results at 100 mb where it is approximately 30% globally and even larger in the Southern Hemisphere.

Finally, the 72-hour forecast results are tabulated in Tables 14-17. For the height fields, only slight improvements or degradation are seen for the lower three levels while significant forecast improvement is realized for the assimilation run at 100 mb (about 10% in the Southern Hemisphere). A similar pattern holds true for temperature also. Large forecast improvement is observed at 100 mb for the assimilation run while at the lower levels no significant improvement or degradation is noted.

In summary, for the first forecast experiment we have seen that, in terms of root mean square error, the most marked improvements in forecasts due to continuous temperature data assimilation are seen at 100 mb for both the height and temperature fields. Although the initial height fields at the lower levels for the assimilation run showed smaller rmse's than those for the control run, no significant forecast improvement was seen at those levels. On the other hand, the forecast temperature fields at 500 mb consistently showed improvement due to assimilation while those at 850 mb did so less consistently. Little improvement or degradation was observed for temperature

Table 10. Root mean square error (m) for 48-hour forecast height fields valid at 00Z, 17 May 1983 for the control run.

	Global		NH		SH	
Level (mb)	Obs.	RMSE	Obs.	RMSE	Obs.	RMSE
850	677	31.7	600	30.1	77	42.0
500	1418	47.9	939	43.9	479	54.9
300	1365	64.1	900	60.6	465	70.3
100	1279	84.6	820	84.5	459	84.7

Table 11. Root mean square error (m) for 48-hour forecast height fields valid at 00Z, 17 May 1983 for the assimilation run.

	Global		NH		SH	
Level (mb)	Obs.	RMSE	Obs.	RMSE	Obs.	RMSE
850	677	33.7	600	32.7	77	40.3
500	1423	50.2	941	45.6	482	58.3
300	1365	64.0	900	59.9	465	71.1
100	1286	76.5	828	76.6	458	76.1

Table 12. Root mean square error (^{o}C) for 48-hour forecast temperature fields valid at 00Z, 17 May 1983 for the control run.

	Global		NH		SH	
Level (mb)	Obs.	RMSE	Obs.	RMSE	Obs.	RMSE
850	637	4.23	562	4.29	75	3.77
500	1426	2.73	940	2.56	486	3.04
300	1385	2.51	903	2.50	482	2.53
100	1077	5.15	729	5.02	348	5.43

Table 13. Root mean square error (^{o}C) for 48-hour forecast temperature fields valid at 00Z, 17 May 1983 for the assimilation run.

	Global		NH		SH	
Level (mb)	Obs.	RMSE	Obs.	RMSE	Obs.	RMSE
850	634	4.03	558	4.05	76	3.83
500	1425	2.50	939	2.36	486	2.76
300	1383	2.60	901	2.56	482	2.67
100	1294	3.62	824	3.64	470	3.60

Table 14. Root mean square error (m) for 72-hour forecast height fields valid at 00Z, 18 May 1983 for the control run.

	Global		NH		SH	
Level (mb)	Obs.	RMSE	Obs.	RMSE	Obs.	RMSE
850	609	39.0	540	39.0	69	39.6
500	906	52.2	669	48.8	237	60.8
300	868	74.1	639	70.5	229	83.6
100	810	93.1	580	94.8	230	88.6

Table 15. Root mean square error (m) for 72-hour forecast height fields valid at 00Z, 18 May 1983 for the assimilation run.

	Global		NH		SH	
Level (mb)	Obs.	RMSE	Obs.	RMSE	Obs.	RMSE
850	609	41.5	540	42.3	69	35.2
500	906	53.3	670	51.1	236	59.3
300	864	74.0	637	71.1	227	81.6
100	827	86.5	599	88.9	228	79.9

Table 16. Root mean square error (^{o}C) for 72-hour forecast temperature fields valid at 00Z, 18 May 1983 for the control run.

	Global		NH		SH	
Level (mb)	Obs.	RMSE	Obs.	RMSE	Obs.	RMSE
850	568	4.40	500	4.41	68	4.37
500	907	2.90	668	2.80	239	3.18
300	877	2.87	636	2.91	241	2.76
100	714	5.00	528	4.69	186	5.81

Table 17. Root mean square error (^{o}C) for 72-hour forecast temperature fields valid at 00Z, 18 May 1983 for the assimilation run.

	Global		NH		SH	
Level (mb)	Obs.	RMSE	Obs.	RMSE	Obs.	RMSE
850	572	4.44	505	4.47	67	4.17
500	908	2.84	669	2.77	239	3.02
300	883	2.96	641	3.04	242	2.74
100	825	3.97	595	3.92	230	4.11

forecasts at 300 mb.

Next we'll examine the results for the second experiment. The rmse's for the initial height and temperature fields valid at 00Z, 24 August 1983 are shown in Tables 18-21. The rms improvement for the heights due to assimilation is most pronounced at 500 mb and 100 mb with more modest improvements at 850 mb and 300 mb. This pattern also holds true for the temperature fields with the largest improvements noted at 100 mb. Again, we'll point out that the improvements shown in these tables at 100 mb are understated due to the number of rejected observations for the control runs.

In Tables 22-25 are displayed the results for the 24-hour forecasts valid at 00Z, 25 August 1983. Small forecast improvements and degradations are observed for the height fields below 100 mb. At 100 mb the assimilation forecast heights show improvement over those for the control run but not to the degree that was seen in the first experiment. Also, the improvement seen in the Northern Hemisphere is larger than that in the Southern Hemisphere. The assimilation temperature forecasts show consistent improvement with the most marked improvement at 100 mb for the Northern Hemisphere (over 40%).

The results for the 48-hour forecasts valid at 00Z, 26 August 1983 are shown in Tables 26-29. For the most part the assimilation height fields show slight improvement over those from the control run but none of the fields shows significant improvement. More consistent improvement is displayed for the assimilation forecast temperature fields. Again the most notable improvement is seen at 100 mb for the Northern Hemisphere (over 40%).

Finally, the rmse computations for the 72-hour forecasts valid at 00Z, 27 August 1983 are shown in Tables 30-33. Modest improvement for the height

Table 18. Root mean square error (m) for the initial height fields at 00Z, 24 August 1983 for the control run.

	Global		NH		SH	
Level (mb)	Obs.	RMSE	Obs.	RMSE	Obs.	RMSE
850	662	14.4	584	13.8	78	18.4
500	1358	28.3	1012	23.5	346	39.2
300	1323	37.6	979	33.6	344	47.2
100	1244	57.8	909	58.2	335	56.6

Table 19. Root mean square error (m) for the initial height fields at 00Z, 24 August 1983 for the assimilation run.

	Global		NH		SH	
Level (mb)	Obs.	RMSE	Obs.	RMSE	Obs.	RMSE
850	662	14.3	584	13.9	78	17.3
500	1358	24.9	1012	21.8	346	32.4
300	1323	35.3	979	32.1	344	43.0
100	1247	51.2	912	51.8	335	49.8

Table 20. Root mean square error (^{o}C) for the intial temperature fields at 00Z, 24 August 1983 for the control run.

	Global		NH		SH	
Level (mb)	Obs.	RMSE	Obs.	RMSE	Obs.	RMSE
850	652	3.05	574	3.07	78	2.97
500	1354	2.36	1009	2.39	345	2.27
300	1324	2.04	979	1.97	345	2.22
100	1084	5.87	768	6.28	316	4.73

Table 21. Root mean square error (^{o}C) for the initial temperature fields at 00Z, 24 August 1983 for the assimilation run.

	Global		NH		SH	
Level (mb)	Obs.	RMSE	Obs.	RMSE	Obs.	RMSE
850	657	2.77	579	2.77	78	2.74
500	1354	1.80	1009	1.80	345	1.81
300	1324	1.97	979	1.85	345	2.29
100	1208	3.94	874	3.98	334	3.83

Table 22. Root mean square error (m) for 24-hour forecast height fields valid at 00Z, 25 August 1983 for the control run.

	Global		NH		SH	
Level (mb)	Obs.	RMSE	Obs.	RMSE	Obs.	RMSE
850	663	21.9	583	21.5	80	24.1
500	1377	37.5	994	28.3	383	54.6
300	1332	47.8	954	40.1	378	63.2
100	1269	70.8	896	65.3	373	82.5

Table 23. Root mean square error (m) for 24-hour forecast height fields valid at 00Z, 25 August 1983 for the assimilation run.

	Global		NH		SH	
Level (mb)	Obs.	RMSE	Obs.	RMSE	Obs.	RMSE
850	662	23.9	582	23.4	80	26.9
500	1377	36.5	994	28.4	383	51.9
300	1332	48.7	954	42.8	378	61.0
100	1277	66.7	903	60.9	374	79.1

Table 24. Root mean square error (^{o}C) for 24-hour forecast temperature fields valid at 00Z, 25 August 1983 for the control run.

	Global		NH		SH	
Level (mb)	Obs.	RMSE	Obs.	RMSE	Obs.	RMSE
850	655	3.39	575	3.32	80	3.89
500	1376	2.37	990	2.29	386	2.56
300	1340	2.28	956	2.14	384	2.59
100	1102	5.75	760	6.06	342	4.99

Table 25. Root mean square error (^{o}C) for 24-hour forecast temperature fields valid at 00Z, 25 August 1983 for the assimilation run.

	Global		NH		SH	
Level (mb)	Obs.	RMSE	Obs.	RMSE	Obs.	RMSE
850	657	2.96	577	2.84	80	3.74
500	1377	2.13	991	2.04	386	2.34
300	1341	2.24	956	2.04	385	2.68
100	1252	3.67	880	3.40	372	4.24

Table 26. Root mean square error (m) for 48-hour forecast height fields valid at 00Z, 26 August 1983 for the control run.

	Global		NH		SH	
Level (mb)	Obs.	RMSE	Obs.	RMSE	Obs.	RMSE
850	665	31.1	588	30.3	77	37.1
500	1412	41.6	1008	34.8	404	55.1
300	1389	55.9	988	49.5	401	69.3
100	1306	75.5	931	70.5	375	86.6

Table 27. Root mean square error (m) for 48-hour forecast height fields valid at 00Z, 26 August 1983 for the assimilation run.

	Global		NH		SH	
Level (mb)	Obs.	RMSE	Obs.	RMSE	Obs.	RMSE
850	664	29.6	588	28.6	76	36.7
500	1414	41.5	1008	33.8	406	56.3
300	1388	56.2	988	49.8	400	69.5
100	1300	73.1	930	67.4	370	85.6

Table 28. Root mean square error (^{o}C) for 48-hour forecast temperature fields valid at 00Z, 26 August 1983 for the control run.

	Global		NH		SH	
Level (mb)	Obs.	RMSE	Obs.	RMSE	Obs.	RMSE
850	658	3.82	581	3.81	77	3.89
500	1416	2.39	1006	2.26	410	2.69
300	1400	2.49	990	2.41	410	2.68
100	1149	5.36	795	5.45	354	5.15

Table 29. Root mean square error (^{o}C) for 48-hour forecast temperature fields valid at 00Z, 26 August 1983 for the assimilation run.

	Global		NH		SH	
Level (mb)	Obs.	RMSE	Obs.	RMSE	Obs.	RMSE
850	660	3.37	583	3.30	77	3.88
500	1415	2.32	1006	2.14	409	2.70
300	1401	2.50	991	2.31	410	2.90
100	1318	3.51	926	3.25	392	4.06

Table 30. Root mean square error (m) for 72-hour forecast height fields valid at 00Z, 27 August 1983 for the control run.

	Global		NH		SH	
Level (mb)	Obs.	RMSE	Obs.	RMSE	Obs.	RMSE
850	657	34.8	579	34.2	78	39.2
500	1250	51.8	890	45.6	360	64.5
300	1206	69.6	858	64.2	348	81.5
100	1115	82.8	788	78.4	327	92.4

Table 31. Root mean square error (m) for 72-hour forecast height fields valid at 00Z, 27 August 1983 for the assimilation run.

	Global		NH		SH	
Level (mb)	Obs.	RMSE	Obs.	RMSE	Obs.	RMSE
850	657	34.4	579	31.7	78	50.3
500	1249	51.2	890	42.1	359	68.6
300	1203	69.8	863	63.7	340	83.2
100	1105	79.3	785	75.4	320	88.3

Table 32. Root mean square error (^{o}C) for 72-hour forecast temperature fields valid at 00Z, 27 August 1983 for the control run.

	Global		NH		SH	
Level (mb)	Obs.	RMSE	Obs.	RMSE	Obs.	RMSE
850	645	4.18	568	4.16	77	4.30
500	1249	2.93	887	2.78	362	3.27
300	1231	2.87	866	2.93	365	2.71
100	984	5.56	679	5.33	305	6.04

Table 33. Root mean square error (^{o}C) for 72-hour forecast temperature fields valid at 00Z, 27 August 1983 for the assimilation run.

	Global		NH		SH	
Level (mb)	Obs.	RMSE	Obs.	RMSE	Obs.	RMSE
850	646	3.76	573	3.72	73	4.05
500	1249	2.84	887	2.67	362	3.22
300	1223	2.70	859	2.61	364	2.90
100	1121	3.86	790	3.60	331	4.41

forecasts due to assimilation is seen at all levels in the Northern Hemisphere but only at 100 mb in the Southern Hemisphere. Again, the temperature forecasts reflect more consistent improvement with the largest seen at 100 mb in the Northern Hemisphere.

In summary, the results from the second experiment were a little different than those from the first. The improvements in 100 mb height forecasts were not nearly as pronounced for the second experiment although the temperature forecast improvements were. Again, consistent improvement was noted in the temperature forecasts although the 300 mb level again showed little improvement or degradation. For the second experiment more improvement was evidenced in the Northern Hemisphere while in the first experiment the largest improvements were seen in the Southern Hemisphere. We can only speculate about the possible causes for these differences. One reason might be the difference in seasons as the first experiment was run in mid-May while the second was run in late August. The rmse calculations were made using all available observations (conventional and satellite) but that still does not provide truly global coverage. There very well could be fluctuations in these rmse calculations due to the extent of the observational coverage. In any case, however, it is encouraging to note that in both experiments the initial fields from the assimilation runs showed rms improvement over those from the control runs and that temperature forecasts also showed consistent and often marked improvement. The fact that the height fields did not always display the same improvement that the temperature fields did indicates that some attention needs to be paid to the pressure forecasts made during the assimilation runs.

The forecast fields for 24, 48, and 72 hours from 00Z, 24 August 1983 are displayed in Figs. 3-62 for both the control run and assimilation run. Comparing Figs. 3 and 13, 23 and 33, and 43 and 53 we see that only subtle

differences between the two runs are apparent for forecasts of sea-level pressure in the Northern Hemisphere. In Figs. 4 and 14 we see that after 24 hours the assimilation forecast for sea-level pressure depicts lows at about 60S, 90E and at about 50S, 90W to be deeper than the control forecast. Also the high latitude low at around 150W is portrayed quite differently. After 48 hours we see in Figs. 24 and 34 that the low at 60S, 90E is only slightly deeper now but that the low off the tip of South America is deeper and defined differently. Again the high latitude low near 150W is much different and a high has developed in the control forecast at about 40S, 110W. Finally, an inverted trough at about 30S, 180W is more pronounced for the assimilation run. In Fig. 44 and 54 we see that the lows at 60S, 90E are defined quite differently as is the high latitude low near 150W amd the low off the tip of South America. The high near 40S, 105W is much stronger for the control run while the assimilation run has developed a deeper low near 30S, 170W. Thus, we have seen in these figures that especially in the Southern Hemisphere significant qualitative differences in the depiction of meteorological features have developed between the control and assimilation forecasts for sea-level pressure. In this study we do not have the information necessary to assess the quality of these forecasts but it is important to note the differences that occur. Only by daily operational testing could one expect to determine which run (control or assimilation) actually produces better forecasts of these meteorological features.

Looking at the forecast of 850 mb heights in the Northern Hemisphere, we see in Figs. 5 and 15 that after 24 hours the assimilation run portrays the structure of the low near Kamchatka differently along with that of the trough off the west coast of the U.S. A low in the area of the Alps is also deeper

for the assimilation run. After 48 hours we can still see differences in Figs. 25 and 35 between these features for the two runs although they appear to be more subtle. In Figs. 45 and 55 we see that after 72 hours the low off Kamchatka is depicted by the assimilation run to be deeper with a distinct trough approaching the dateline, a low center has developed in the Alaskan Panhandle area, and only minor differences are evident in the handling of the Alpine low. In the Southern Hemisphere Figs. 6 and 16 show that after 24 hours differences in structure are seen between the two runs in the handling of the low at about 60S, 90E, the high southwest of New Zealand, the troughing around 150W, and the low off the western tip of South America. After 48 hours we see in Figs. 26 and 36 that the most notable differences are in the forecasts for the trough around 150W and the low off the tip of South America. For the 72-hour forecasts we see in Figs. 46 and 56 that the assimilation run develops a relatively deep low center at about 30S, 170W while the control run displays only weak troughing. The trough at about 140W and the low off the tip of South America are also portrayed quite differently.

As we look higher in the atmosphere the differences between the assimilation and control forecast fields become more and more subtle. In Figs. 7 and 17 the only really noticeable difference between the 24-hour Northern Hemisphere 500 mb forecasts is in the depiction of the trough off the west coast of the U.S. and the low near Kamchatka. We can make the same observations for the 48- and 72-hour forecasts displayed in Figs. 27 and 37 and Figs. 47 and 57, respectively. The same can be said for the Southern Hemisphere where we see in Figs. 8, 18, 28, 38, 48, and 58 that the only noticeable differences are in the treatment of the trough east of New Zealand, the

trough around 150W and the trough off the tip of South America. In the remaining figures we see that for the forecasts at 300 mb and 100 mb only subtle differences are apparent with a few exceptions. Comparing Figs. 10 and 20 we see that the trough off the South American tip at 300 mb is much sharper for the 24-hour assimilation forecast and the low at about 60S, 90E is closed off. In Figs. 30 and 40 the trough off the tip of South America is still sharper for the 48-hour assimilation forecast and the same holds true after 72-hours as evidenced by Figs. 50 and 60.

4. CONCLUSIONS AND RECOMMENDATIONS

In the previous section we described the results of two continuous data assimilation experiments conducted using NOGAPS and the satellite data operationally available to FNOC. The techniques used in these experiments, described in Section 2, were tailored for application with NOGAPS. In this section we shall summarize our findings and make recommendations for the future application of our research.

The first important result we obtained is that the NOGAPS model is ideal for continuous data assimilation. Over the course of our data assimilation research we have found that one way to obtain forecast improvement is to control the model noise induced by data insertion. The Noise Freezing Methods described in Sasaki and Goerss (1982) were developed to accomplish this. We saw in Section 2 that the Matsuno time-step which initiates each integration cycle of the NOGAPS model has a damping effect upon this noise. Thus, we found that we were able to continuously assimilate temperature data into the model without having to make any changes to the model itself.

The variational adjustment scheme we call vertical shape matching was designed to preserve the information content of each satellite sounding and yet modify it to make it easier for the forecast model to digest. Its success was demonstrated in Section 2 where we saw that the damping properties of the NOGAPS model kept the noise under control while the temperature data was assimilated into the model without any indications of rejection.

We described in Section 3 one of the most striking results of continuous assimilation. The global mean temperatures for the upper two layers of the NOGAPS model showed marked changes due to assimilation during the start-up period for each experiment. After the two-day start-up period, the upper

level field for the assimilation run was about 10^{o}C colder than that for the control run. Recall that the satellite data was also used in the control run but only in the objective analysis scheme applied each update cycle (every six hours). At the next lower level the mean temperature for the assimilation run was about 3^{o}C warmer than that for the control run. This modification to the mean NOGAPS model sounding caused by continuous data assimilation resulted in a more accurate depiction of the conditions in the actual atmosphere.

Next, forecasts made from the assimilation and control runs for each experiment were quantitatively evaluated by computing root mean square errors for the differences between actual observations of geopotential height and temperature and the values of forecast fields interpolated to the location of the observations. In general, improvement was noted due to assimilation. The most significant improvements were seen at 100 mb for both geopotential height and temperature. The improvements for temperature were much more widespread and marked than those for height. Differences were noted for the results between the two experiments which could have been seasonal or due to the observational coverage. In summary, however, the results of the rmse computations implied that continuous data assimilation had a positive impact overall on the NOGAPS forecasts.

Finally, a qualitative assessment of the forecasts was made for the second experiment. Conclusive statements could only be made about these results if the assimilation and control runs were compared on a daily basis in an operational evaluation over a significant period of time. However, in this study we found that noticeable differences were seen in the handling of meteorological features by the two runs, especially in the Southern Hemisphere.

From our research we conclude that the forecasts produced by NOGAPS can be improved by the use of continuous data assimilation. The operational expense of this technique would be that required to run an additional six-hour assimilation forecast each update cycle. It was very encouraging to discover that the NOGAPS model lends itself so well to continuous assimilation without modification. There are very few parameters that need to be considered in order to fine tune the continuous data assimilation techniques described in Section 2 for application in a truly operational setting. Minor adjustments to the weighting parameters in the indirect insertion scheme (which was patterned after that described by Barker (1982) and is similar to the objective analysis scheme used in NOGAPS) could be made and forecasts evaluated. Special attention needs to be paid to the effects of assimilation upon the forecasts of surface pressure during this "tuning" process. Although the impact of continuous satellite data assimilation upon the NOGAPS forecasts can only be determined after extensive operational testing, the results of our research reported here indicate that significantly positive impact can be expected.

REFERENCES

Arakawa, A. and V.R. Lamb, 1977: Computational design of the basic dynamical processes of the UCLA general circulation model. In Methods in Computational Physics, Vol. 17, Academic Press, Inc., New York.

Barker, E.H., 1981: Analysis and initialization procedure for the Navy Operational Global Atmospheric Prediction System. NEPRF Report.

_____, 1982: A comparison of two initialization methods in data assimilation. Ph.D. Dissertation, Naval Postgraduate School, Monterey, California, 160 pp.

Bengtsson, L., 1975: 4-dimensional assimilation of meteorological observations. GARP Publ. Ser., No. 15, 76 pp.

_____ and N. Gustavsson, 1971: An experiment in dynamic analysis. Tellus, 23, 328-336.

Charney, J., M. Halem and R. Jastrow, 1969: Use of incomplete historical data to infer the present state of the atmosphere. J. Atmos. Sci., 26, 1160-1163.

Ghil, M., M. Halem and R. Atlas, 1979: Time-continuous assimilation of remote-sounding data and its effect on weather forecasting. Mon. Wea. Rev., 107. 140-171.

McPherson, R., 1975: Progress, problems, and prospects in meteorological data assimilation. Bull. Amer. Meteor. Soc., 56, 1154-1166.

Miyakoda, K. and O. Talagrand, 1971: The assimilation of past data in dynamical analysis: I. Tellus, 23, 310-317.

_____, R. Strickler and J. Chludzinski, 1978: Initialization with the data assimilation method. Tellus, 30, 32-54.

Rosmond, T.E., 1981: NOGAPS: Navy Operational Global Atmospheric Prediction System. Preprints, Fifth Conference on Numerical Weather Prediction, Monterey, California, 74-79.

Sasaki, Y. and J.S. Goerss, 1982: Satellite data assimilation using NASA Data Systems Test 6 observations. Mon. Wea. Rev., 110, 1635-1644.

Talagrand, O., 1972: On the damping of high-frequency motions in four-dimensional assimilation of meteorological data. J. Atmos. Sci., 29, 1571-1574.

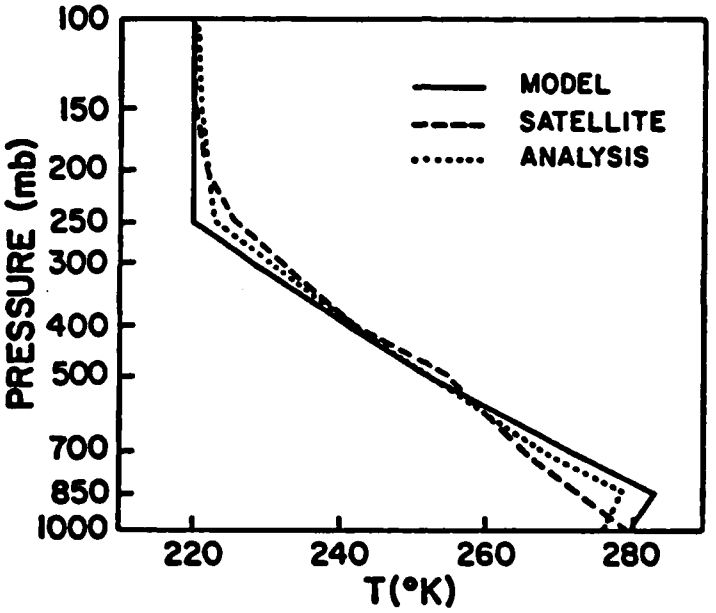

Fig. 1. Variational adjustment of a satellite temperature sounding.

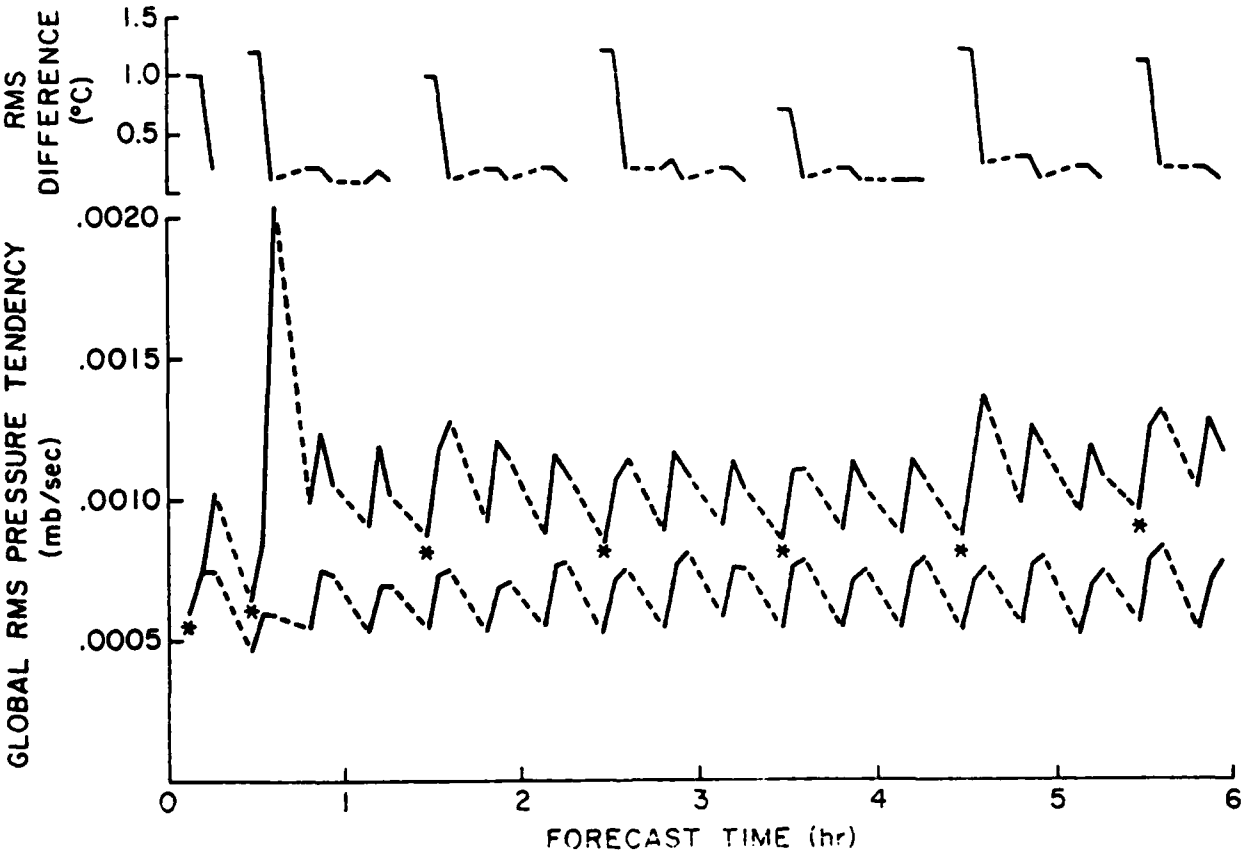

Fig. 2. (Top) Root mean square difference (^{o}C) between satellite temperature observations at 592 mb and NOGAPS model temperatures.
(Bottom) Global root mean square pressure tendencies (mb/sec) for assimilation (top) and non-assimilation NOGAPS forecasts.

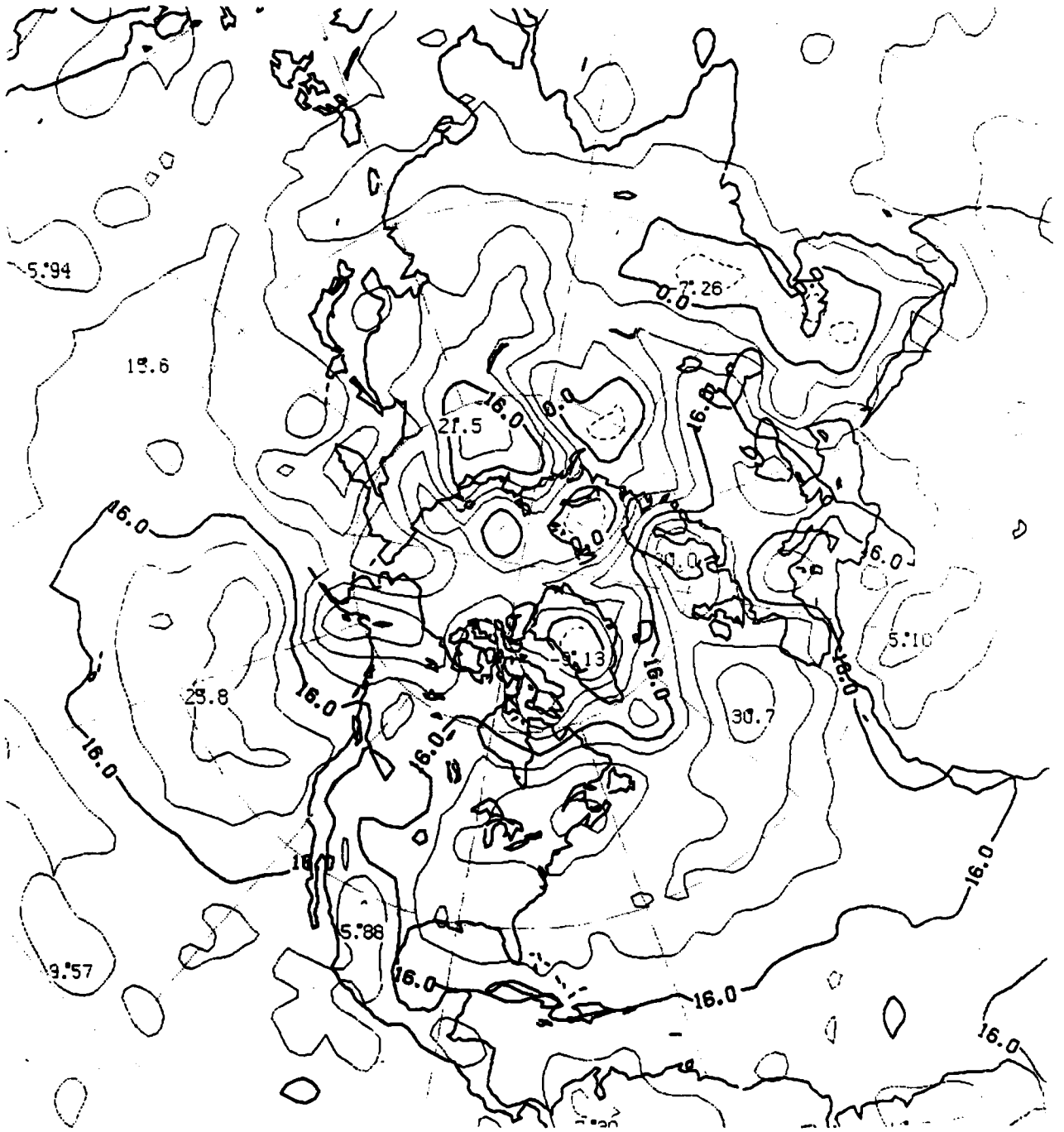

Fig. 3. 24-hour Northern Hemisphere assimilation run forecast for sea-level pressure (mb) valid at 00Z, 25 August 1983.

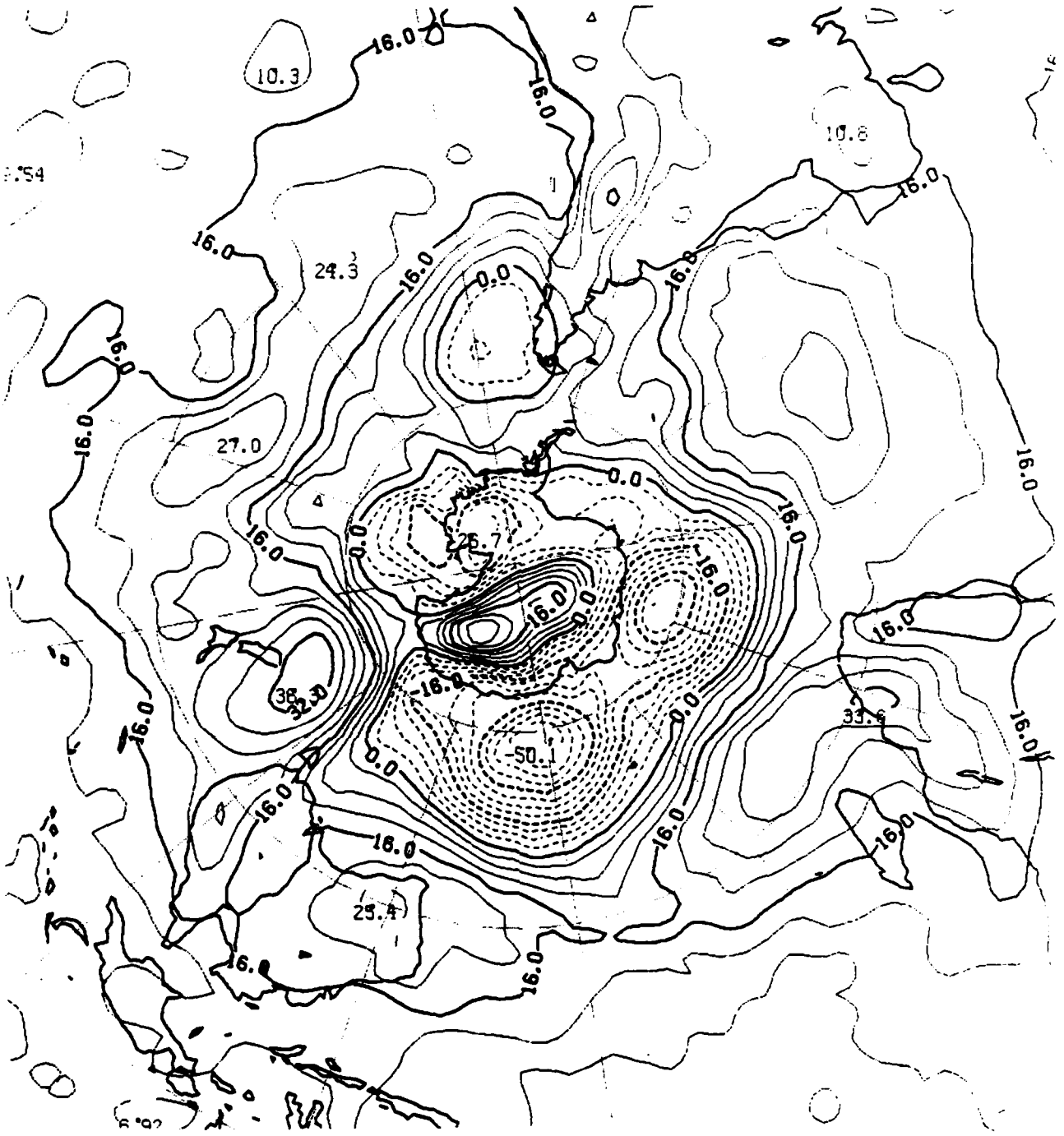

Fig. 4. 24-hour Southern Hemisphere assimilation run forecast for sea-level pressure (mb) valid at 00Z, 25 August 1983.

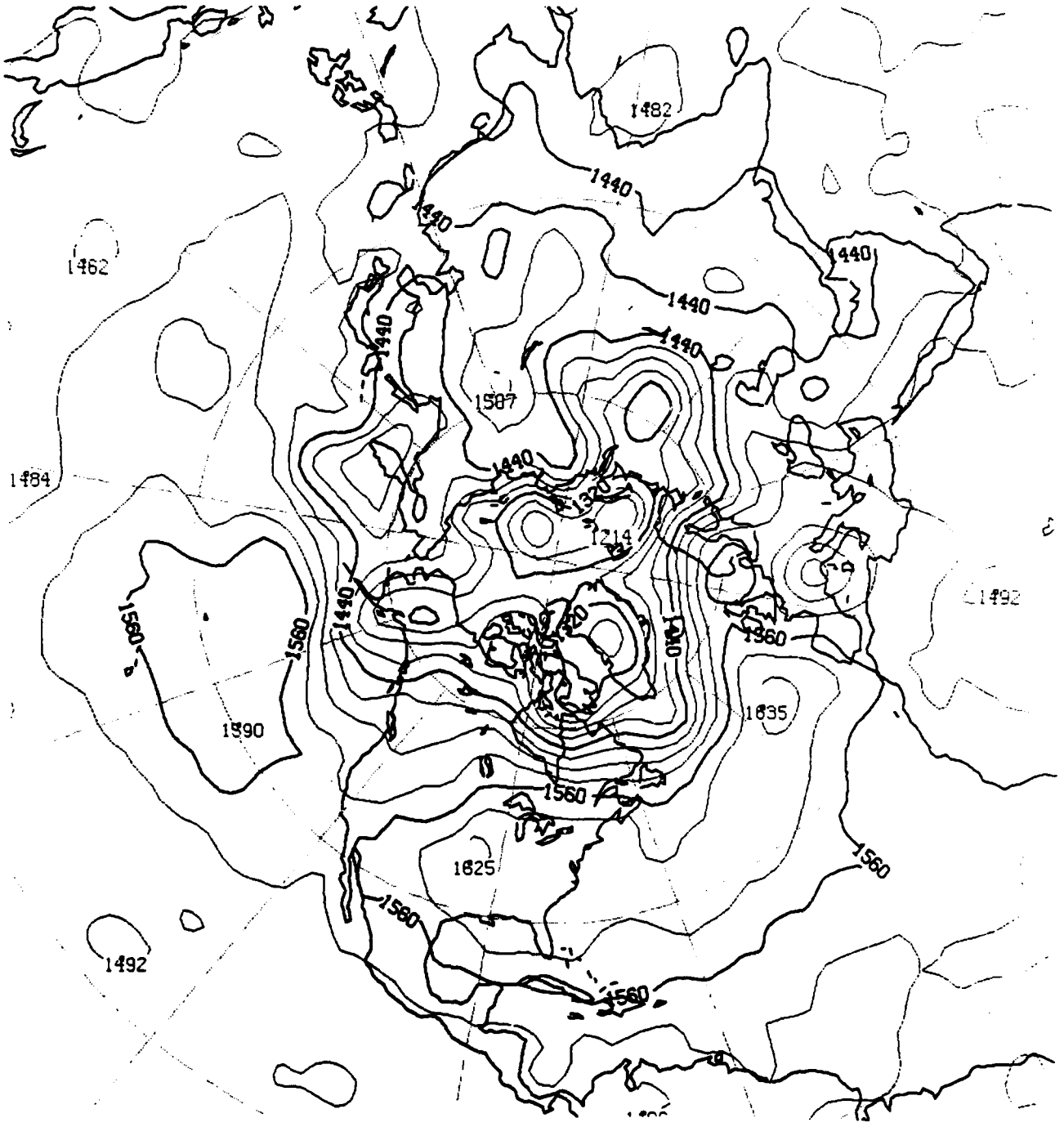

Fig. 5. 24-hour Northern Hemisphere assimilation run forecast for 850 mb heights (m) valid at 00Z, 25 August 1983.

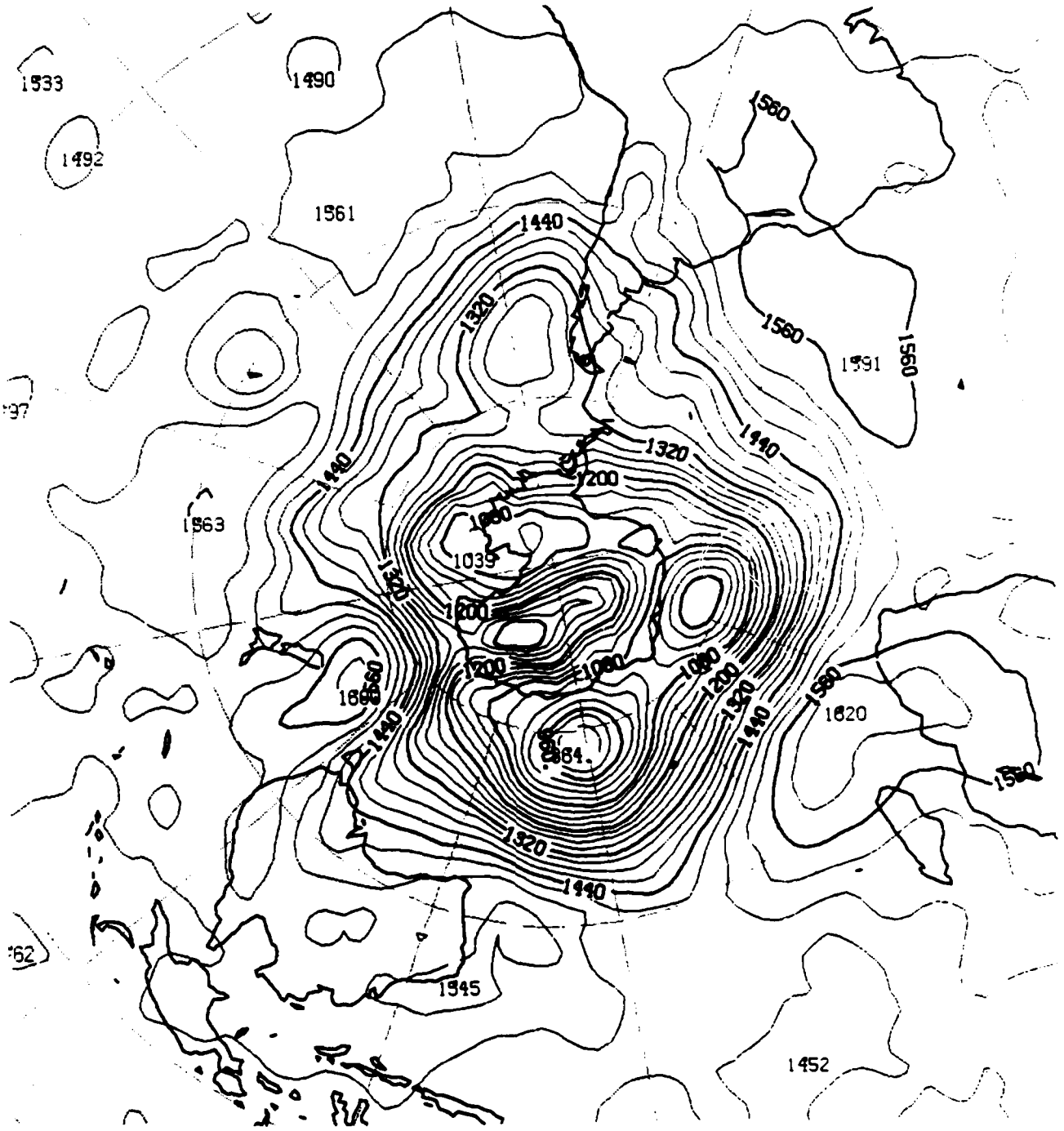

Fig. 6. 24-hour Southern Hemisphere assimilation run forecast for 850 mb heights (m) valid at 00Z, 25 August 1983.

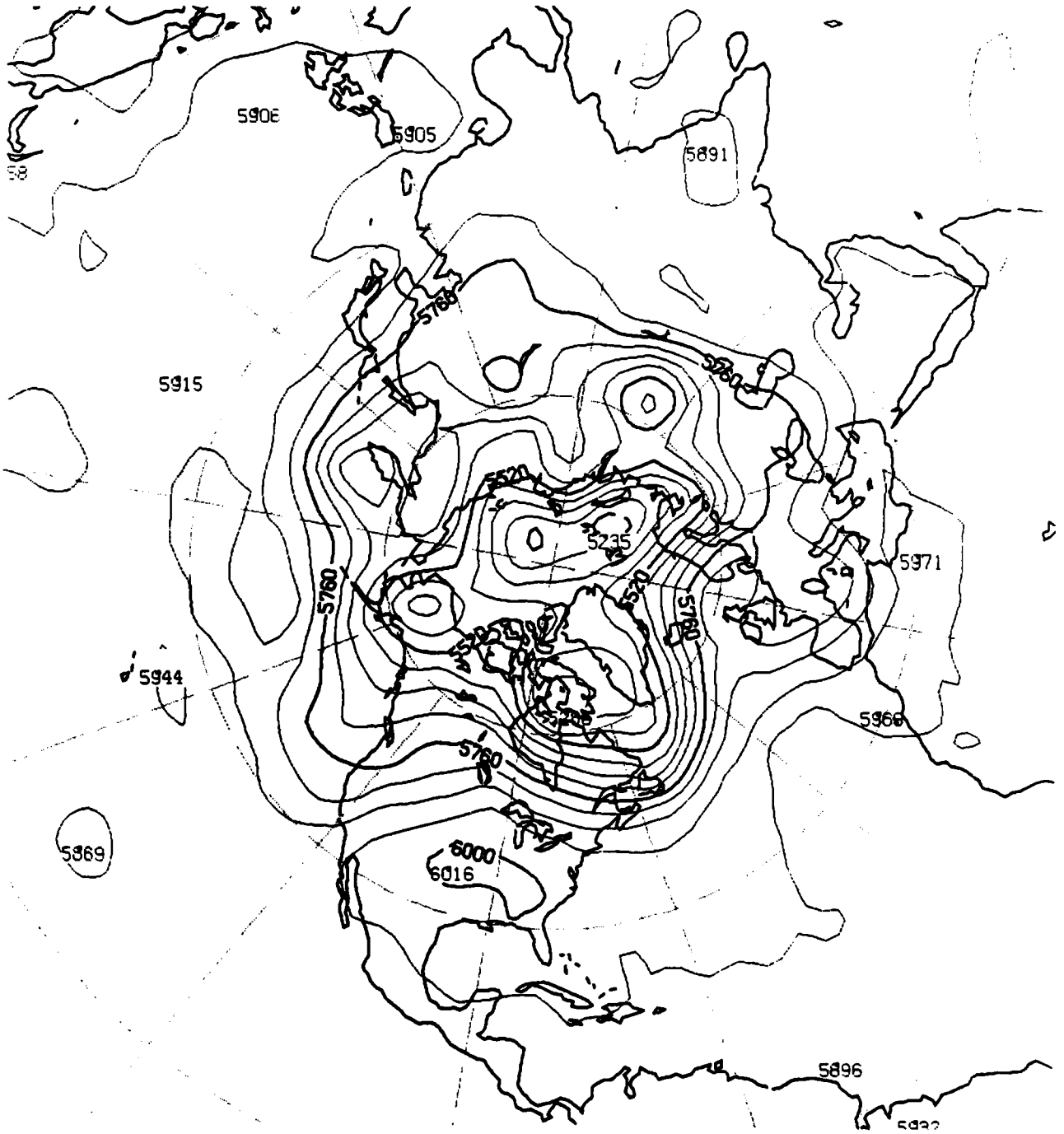

Fig. 7. 24-hour Northern Hemisphere assimilation run forecast for 500 mb heights (m) valid at 00Z, 25 August 1983.

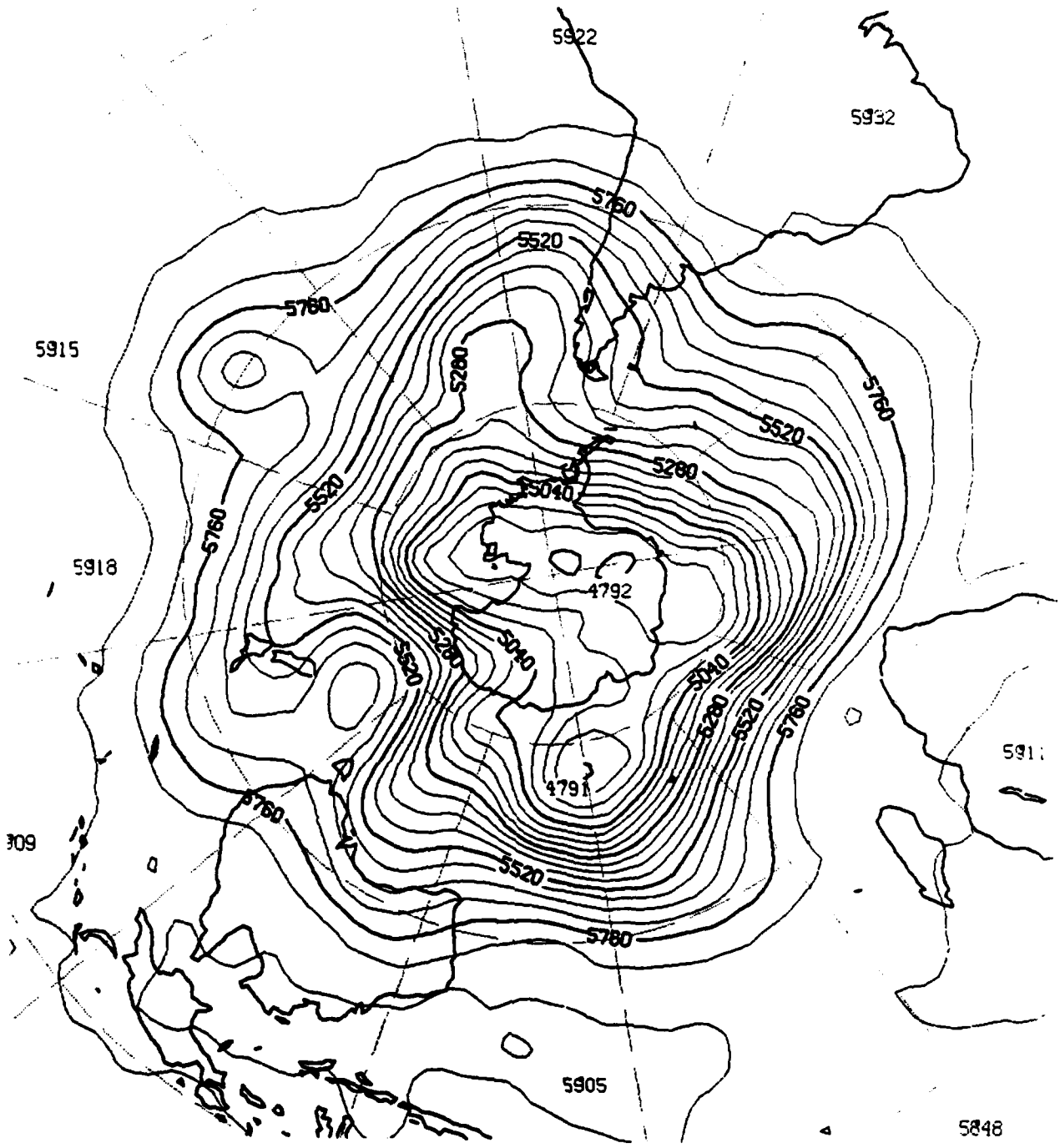

Fig. 8. 24-hour Southern Hemisphere assimilation run forecast for 500 mb heights (m) valid at 00Z, 25 August 1983.

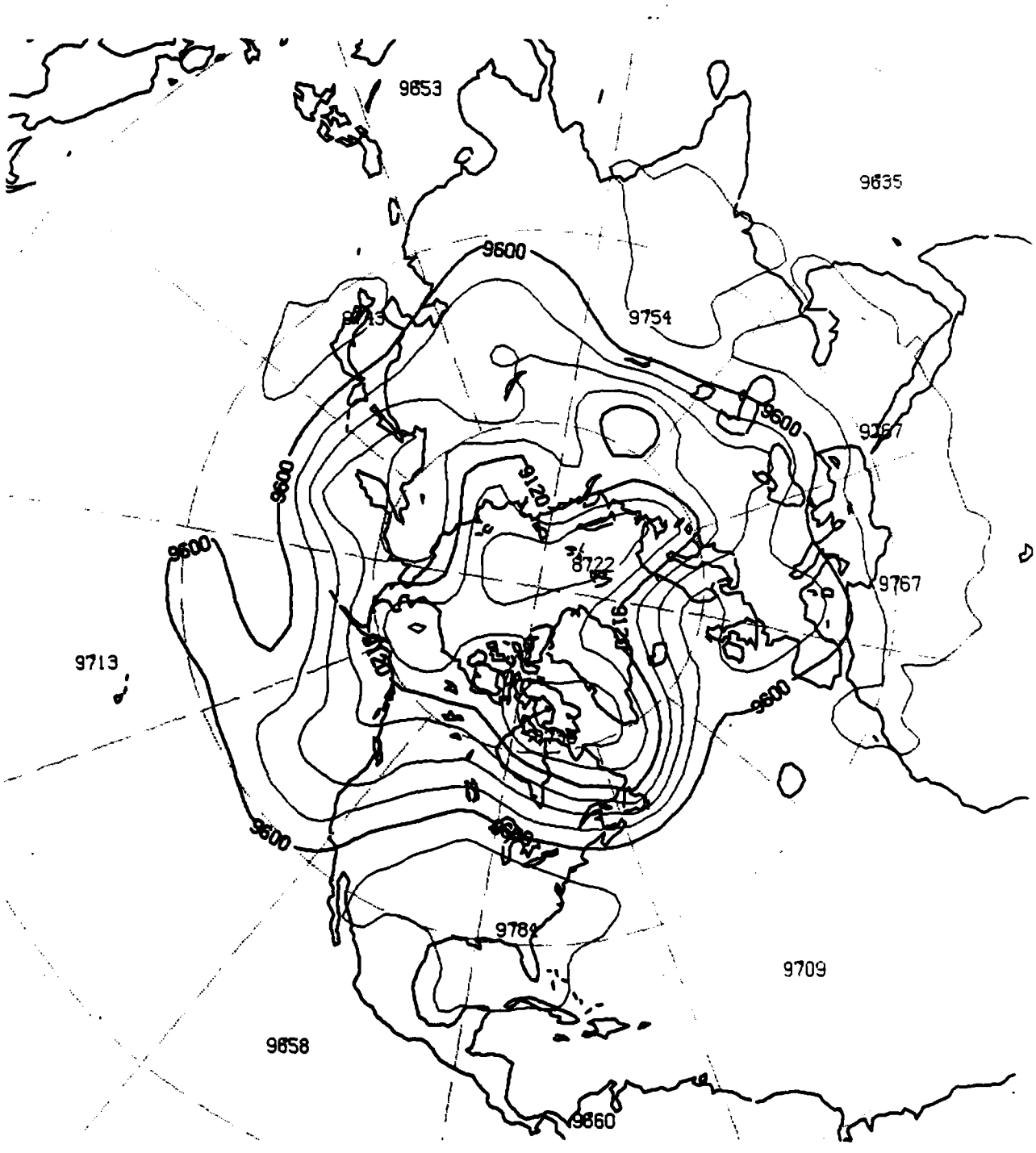

Fig. 9. 24-hour Northern Hemisphere assimilation run forecast for 300 mb heights (m) valid at 00Z, 25 August 1983.

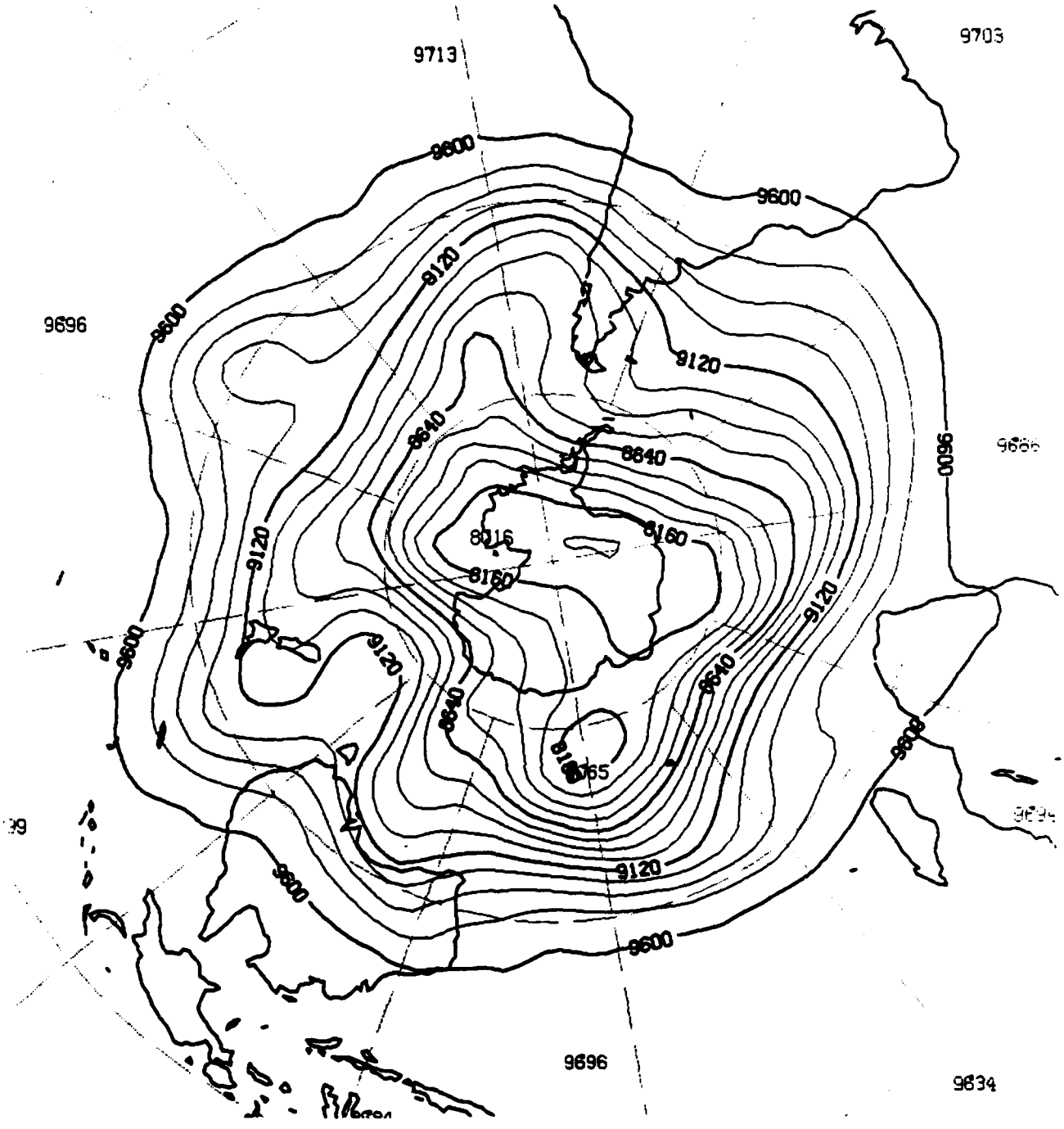

Fig. 10. 24-hour Southern Hemisphere assimilation run forecast for 300 mb heights (m) valid at 00Z, 25 August 1983.

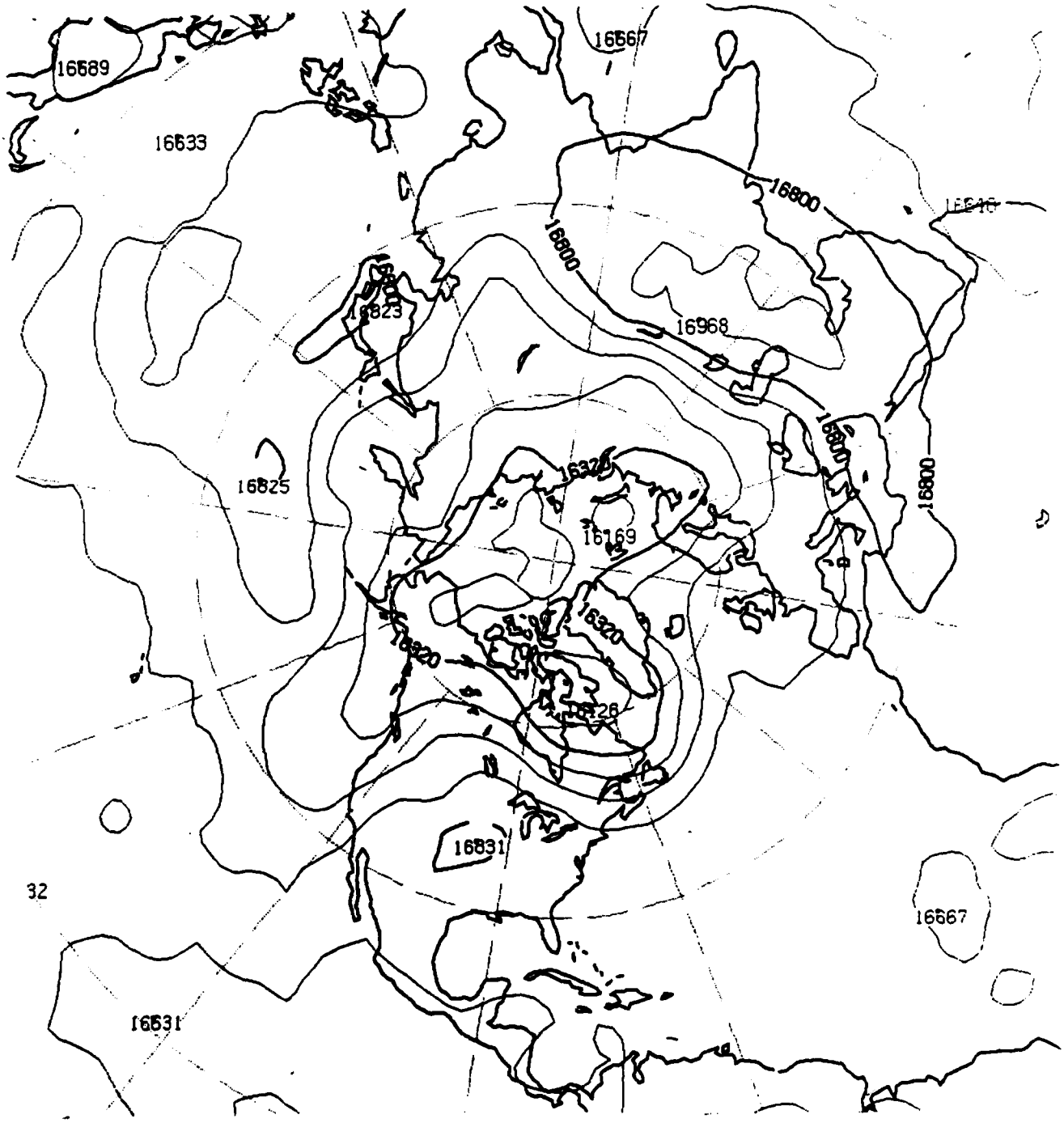

Fig. 11. 24-hour Northern Hemisphere assimilation run forecast for 100 mb heights (m) valid at 00Z, 25 August 1983.

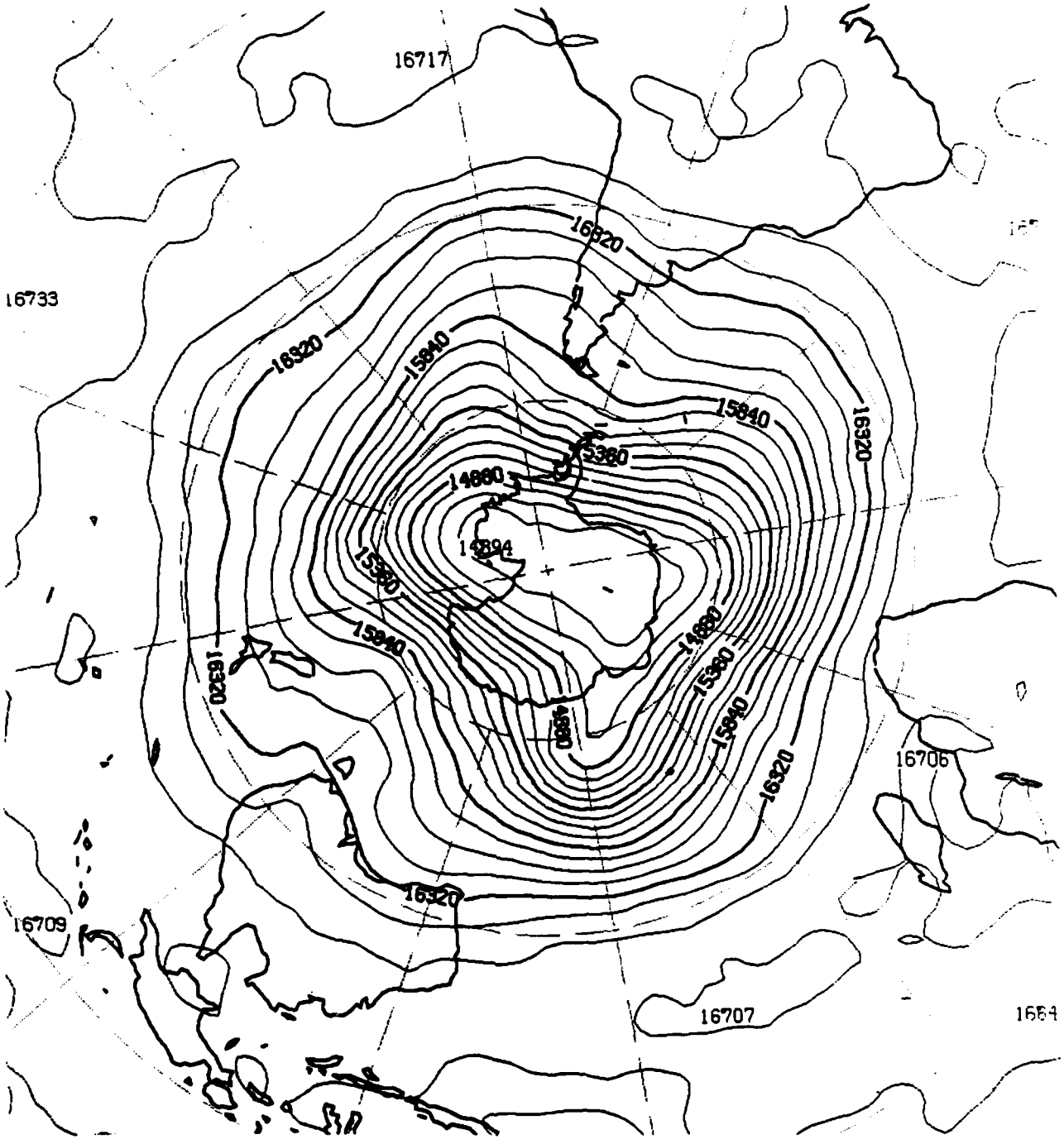

Fig. 12. 24-hour Southern Hemisphere assimilation run forecast for 100 mb heights (m) valid at 00Z, 25 August 1983.

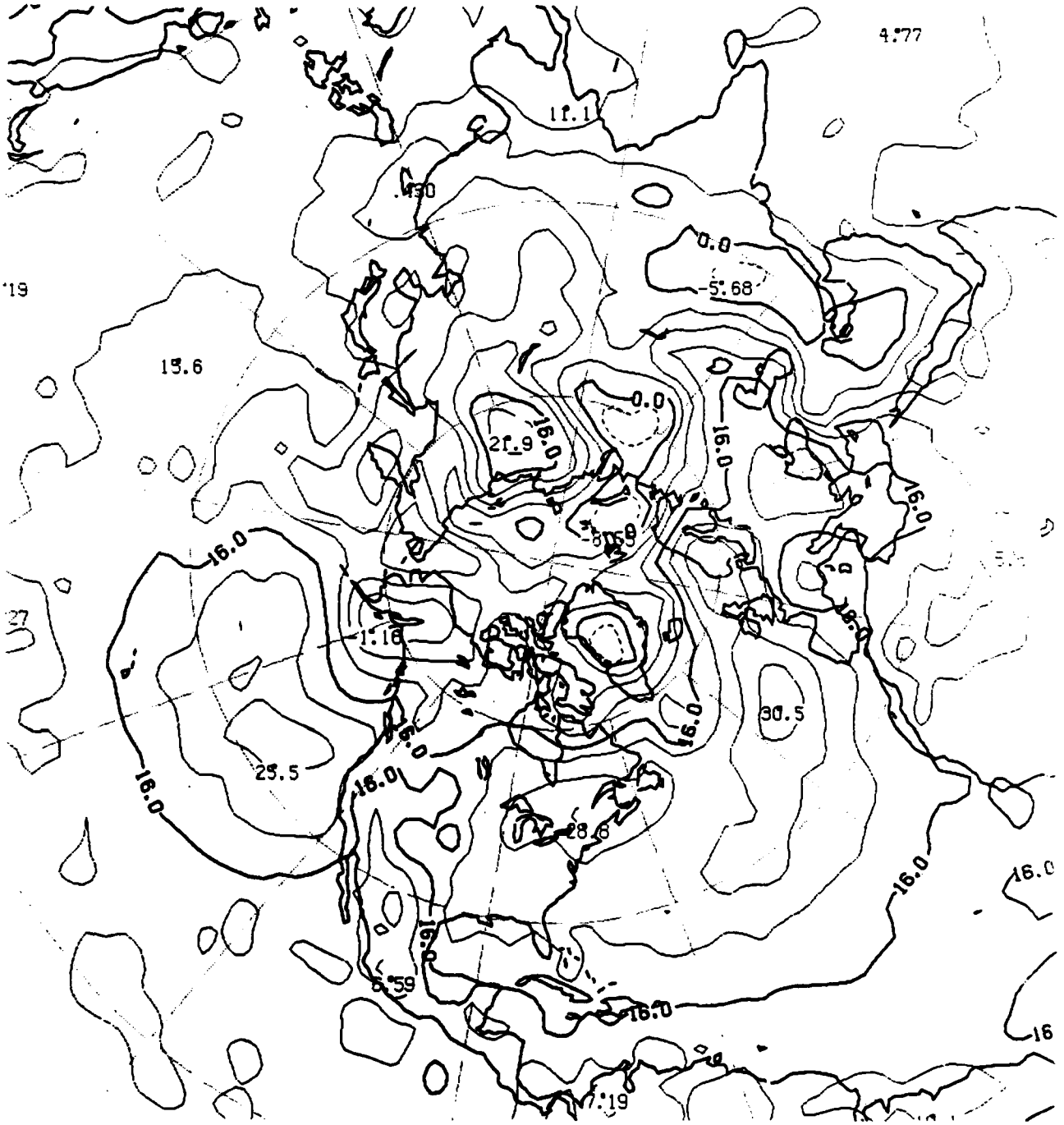

Fig. 13. 24-hour Northern Hemisphere control run forecast for sea-level pressure (mb) valid at 00Z, 25 August 1983.

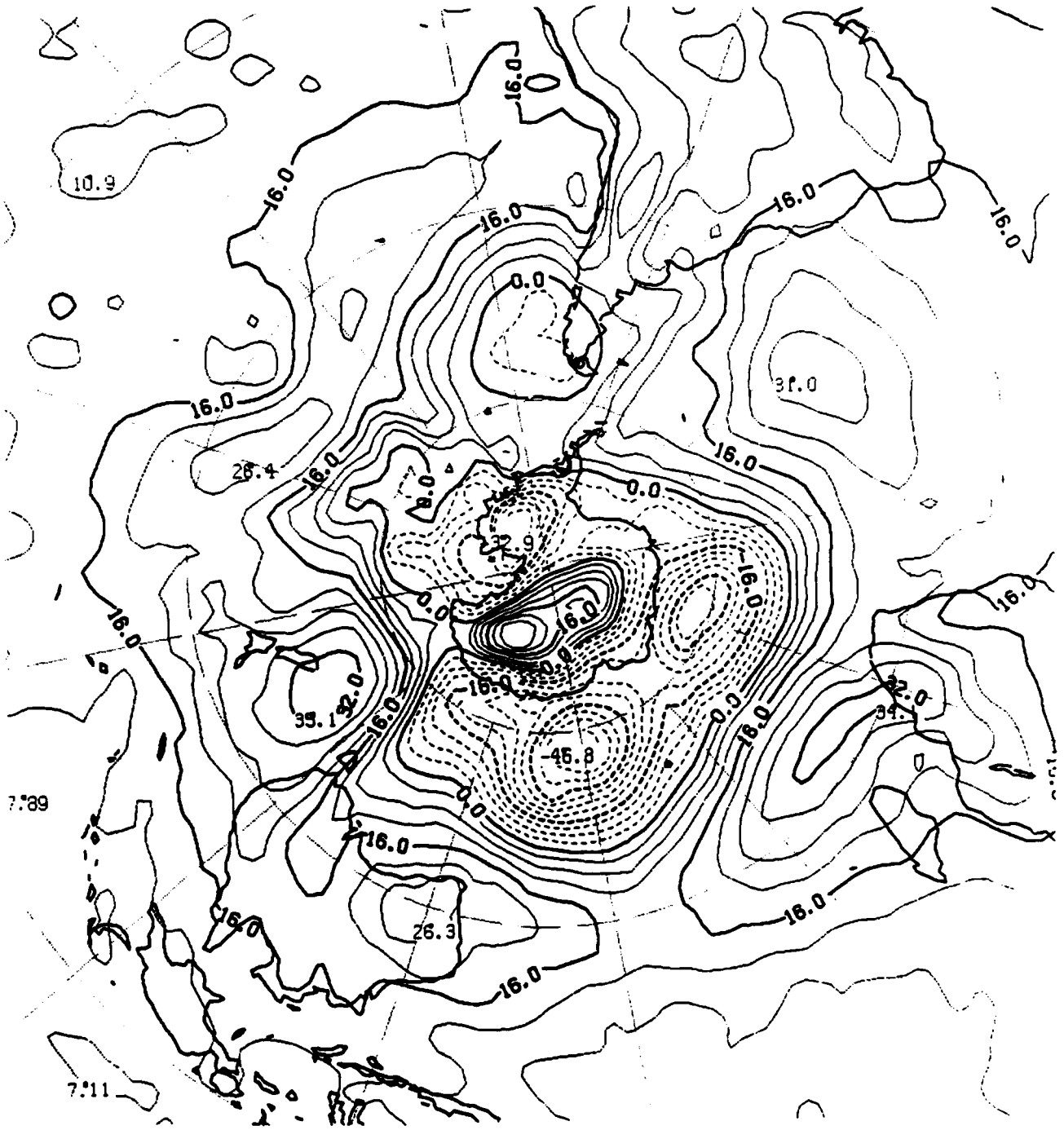

Fig. 14. 24-hour Southern Hemisphere control run forecast for sea-level pressure (mb) valid at 00Z, 25 August 1983.

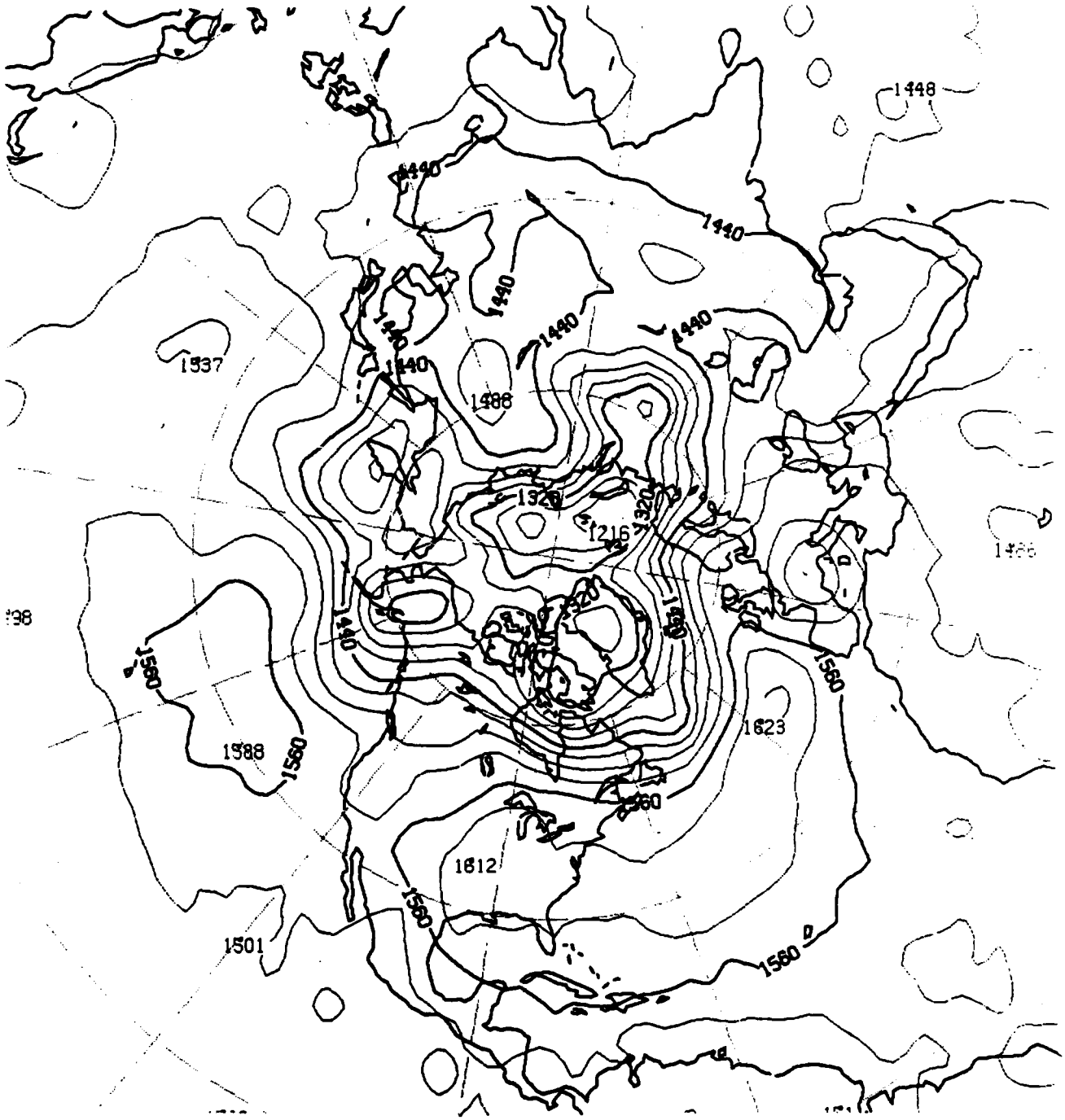

Fig. 15. 24-hour Northern Hemisphere control run forecast for 850 mb heights (m) valid at 00Z, 25 August 1983.

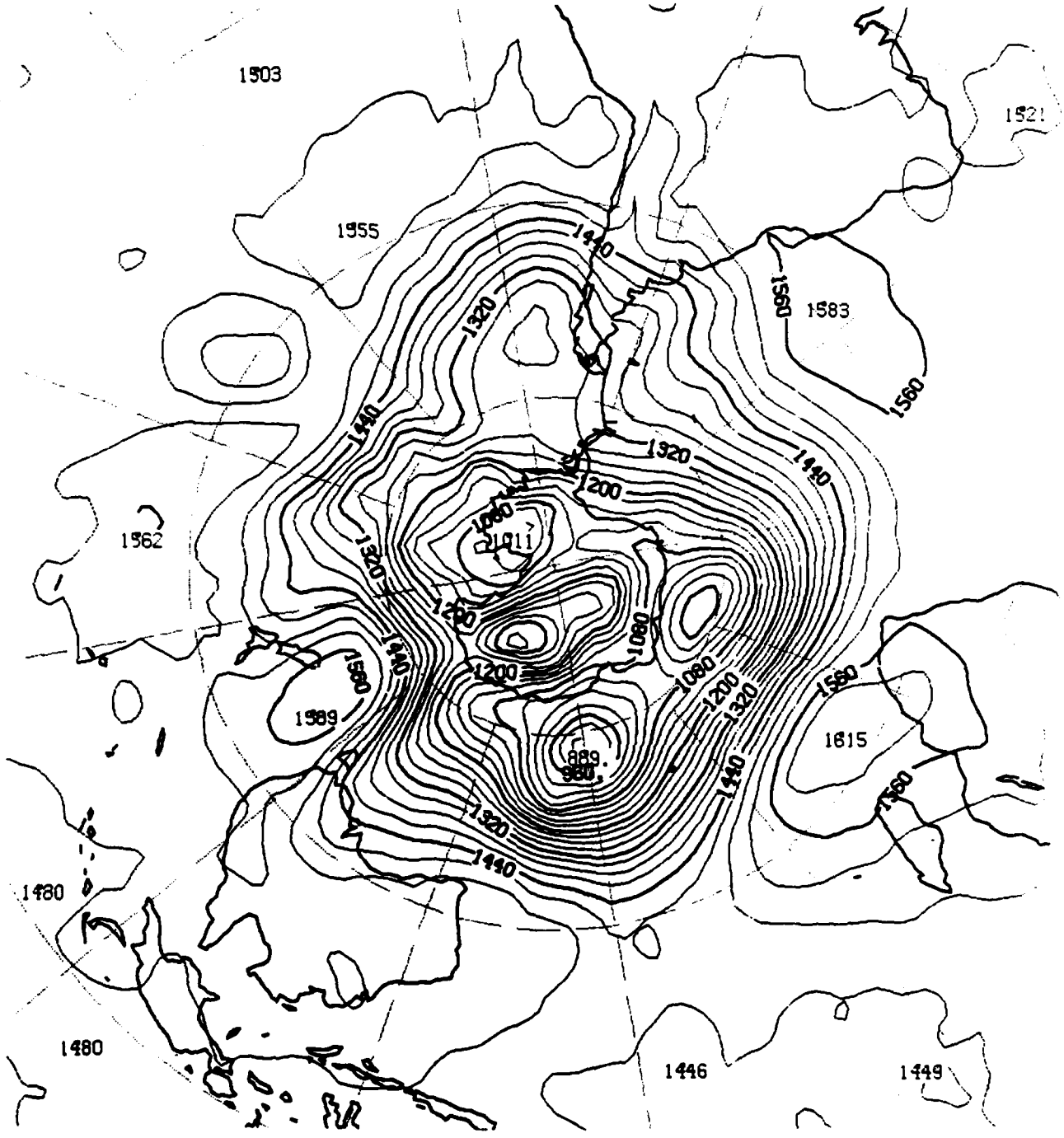

Fig. 16. 24-hour Southern Hemisphere control run forecast for 850 mb heights (m) valid at 00Z, 25 August 1983.

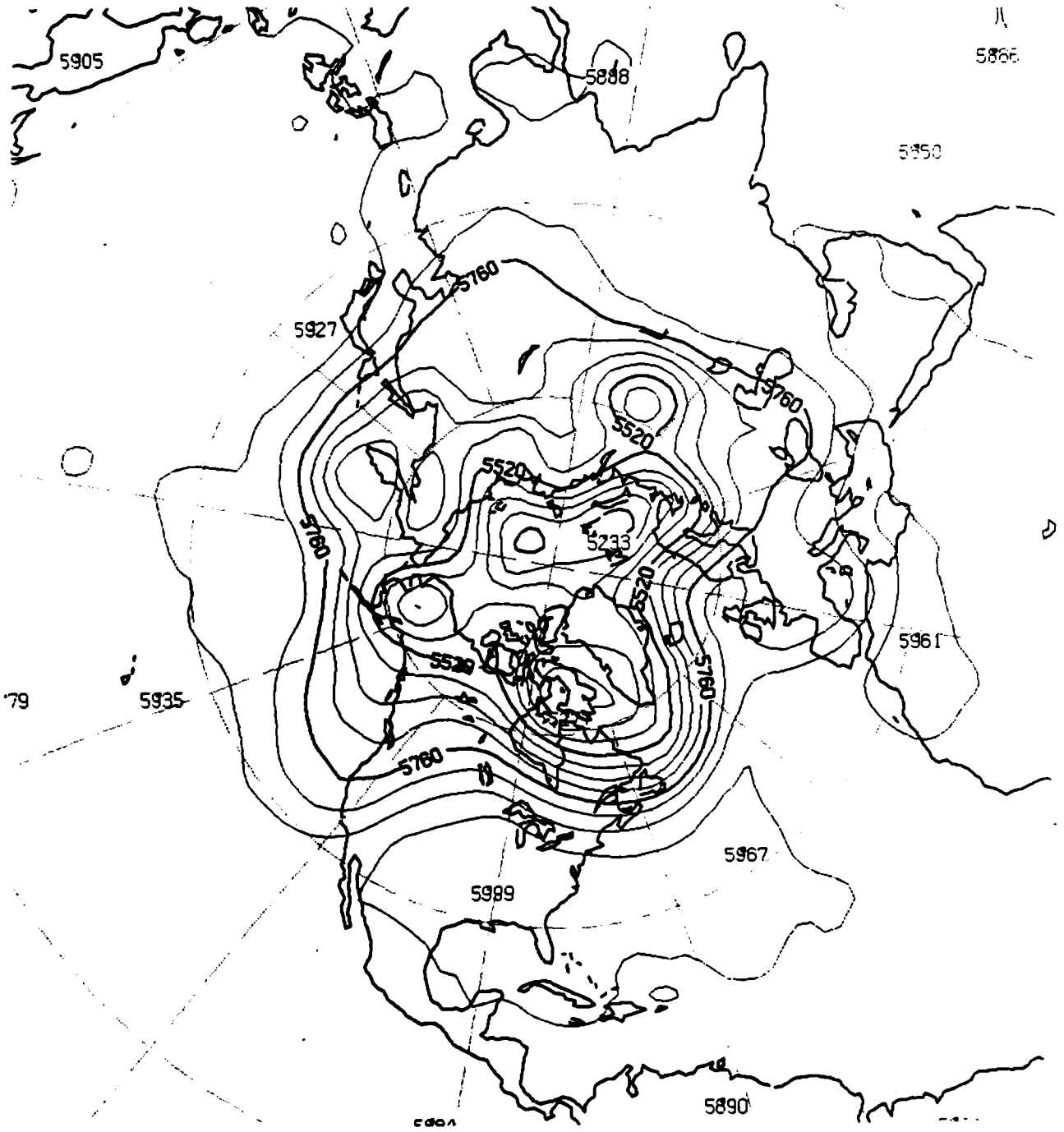

Fig. 17. 24-hour Northern Hemisphere control run forecast for 500 mb heights (m) valid at 00Z, 25 August 1983.

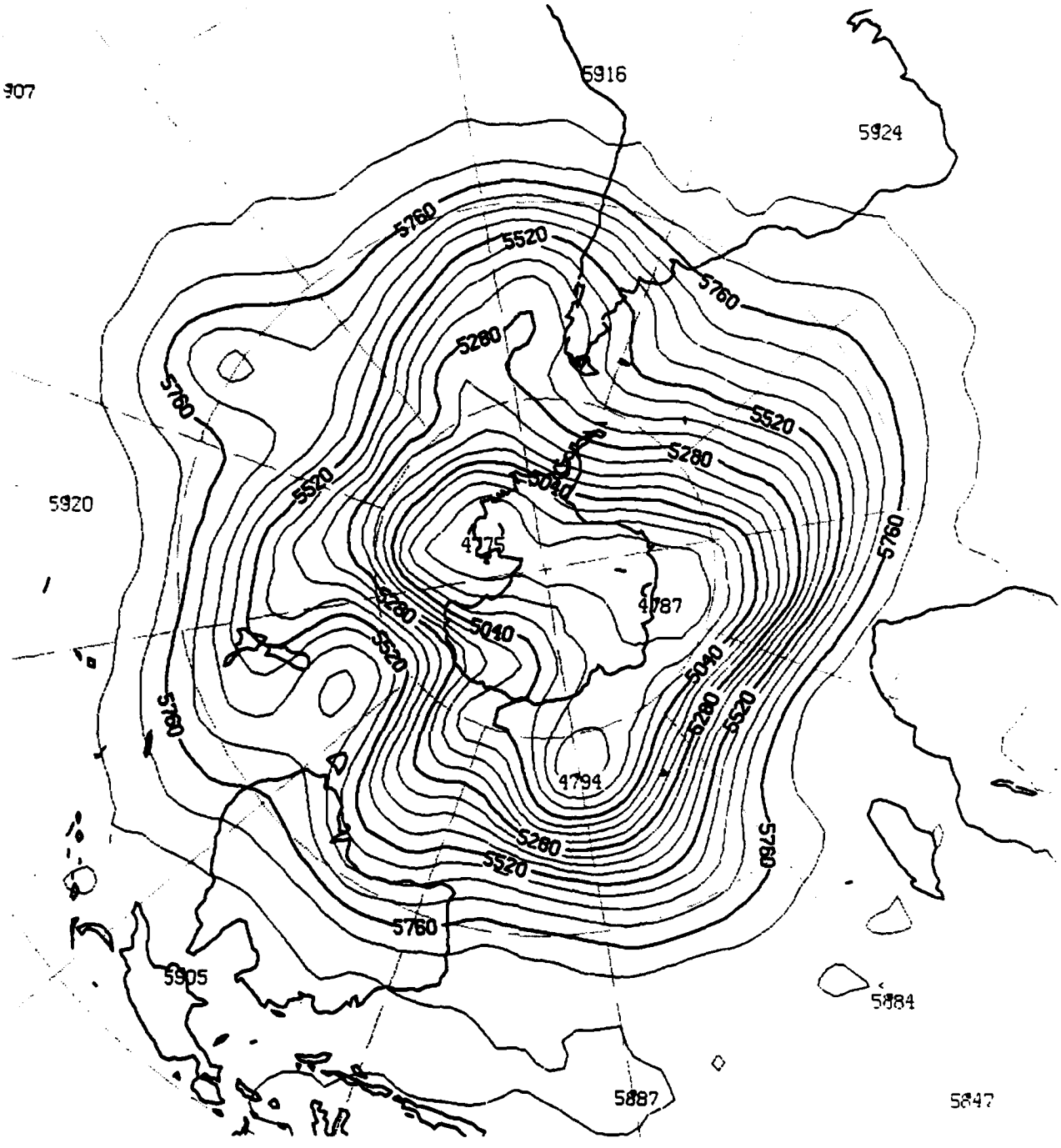

Fig. 18. 24-hour Southern Hemisphere control run forecast for 500 mb heights (m) valid at 00Z, 25 August 1983.

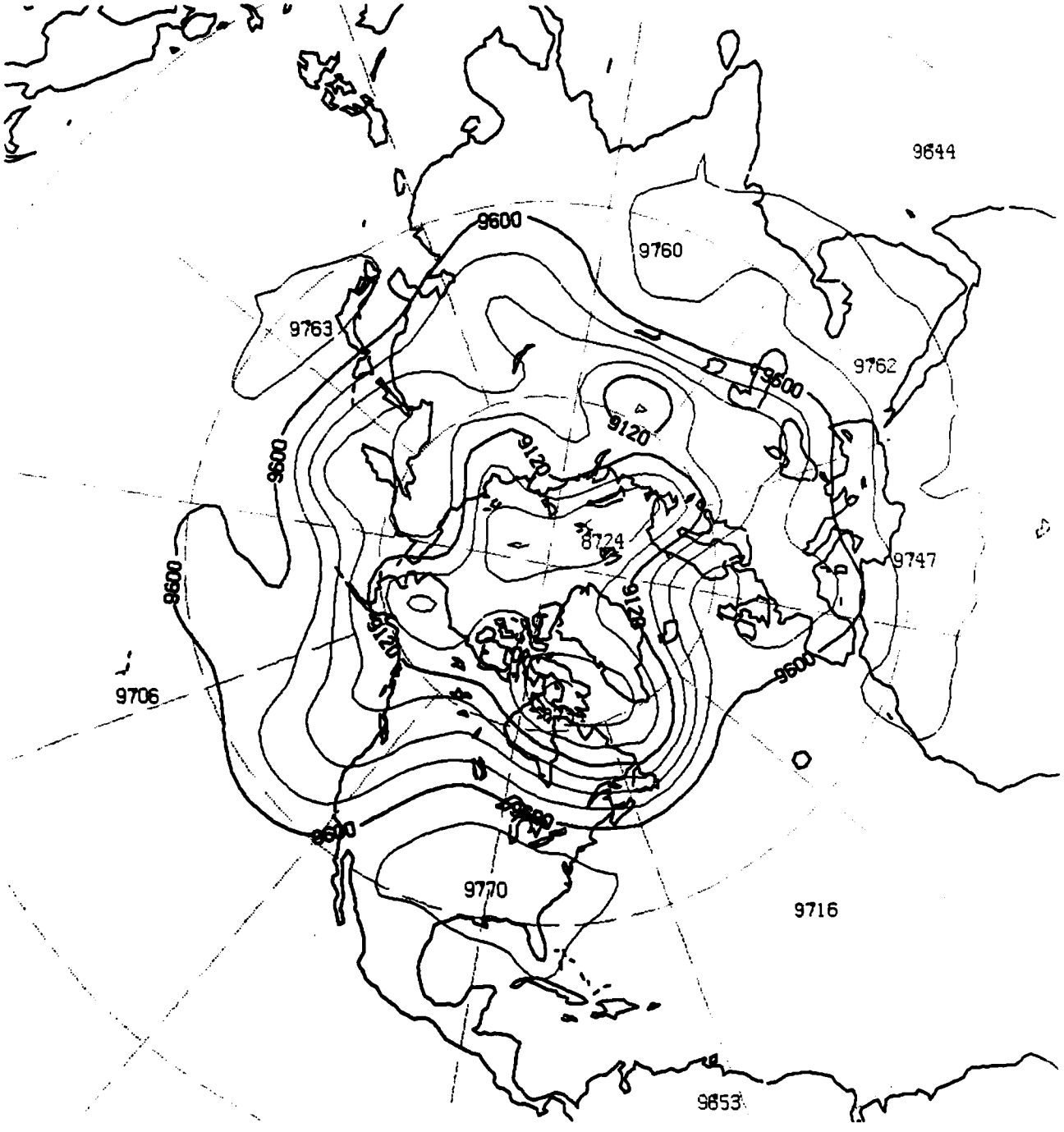

Fig. 19. 24-hour Northern Hemisphere control run forecast for 300 mb heights (m) valid at 00Z, 25 August 1983.

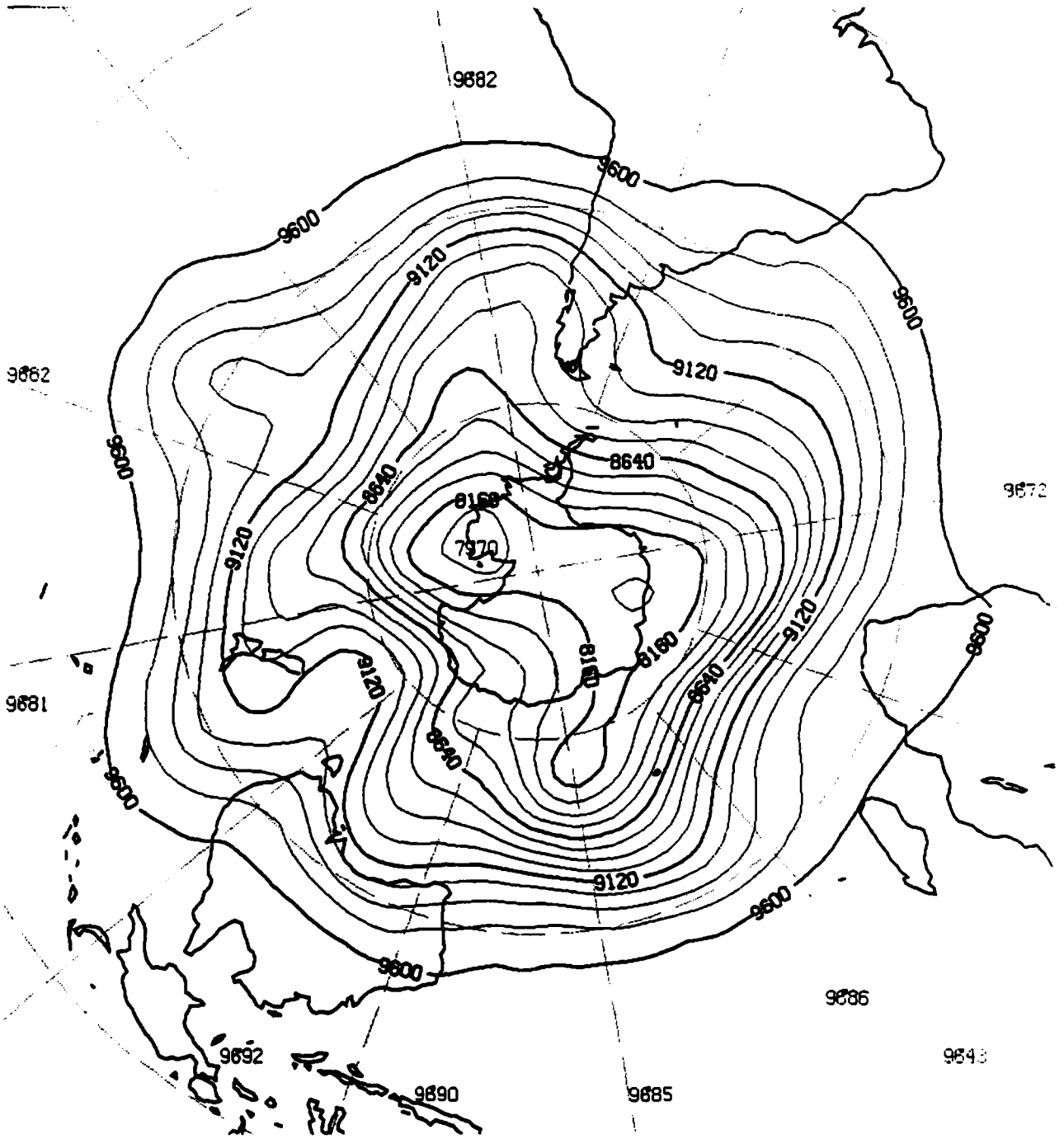

Fig. 20. 24-hour Southern Hemisphere control run forecast for 300 mb heights (m) valid at 00Z, 25 August 1983.

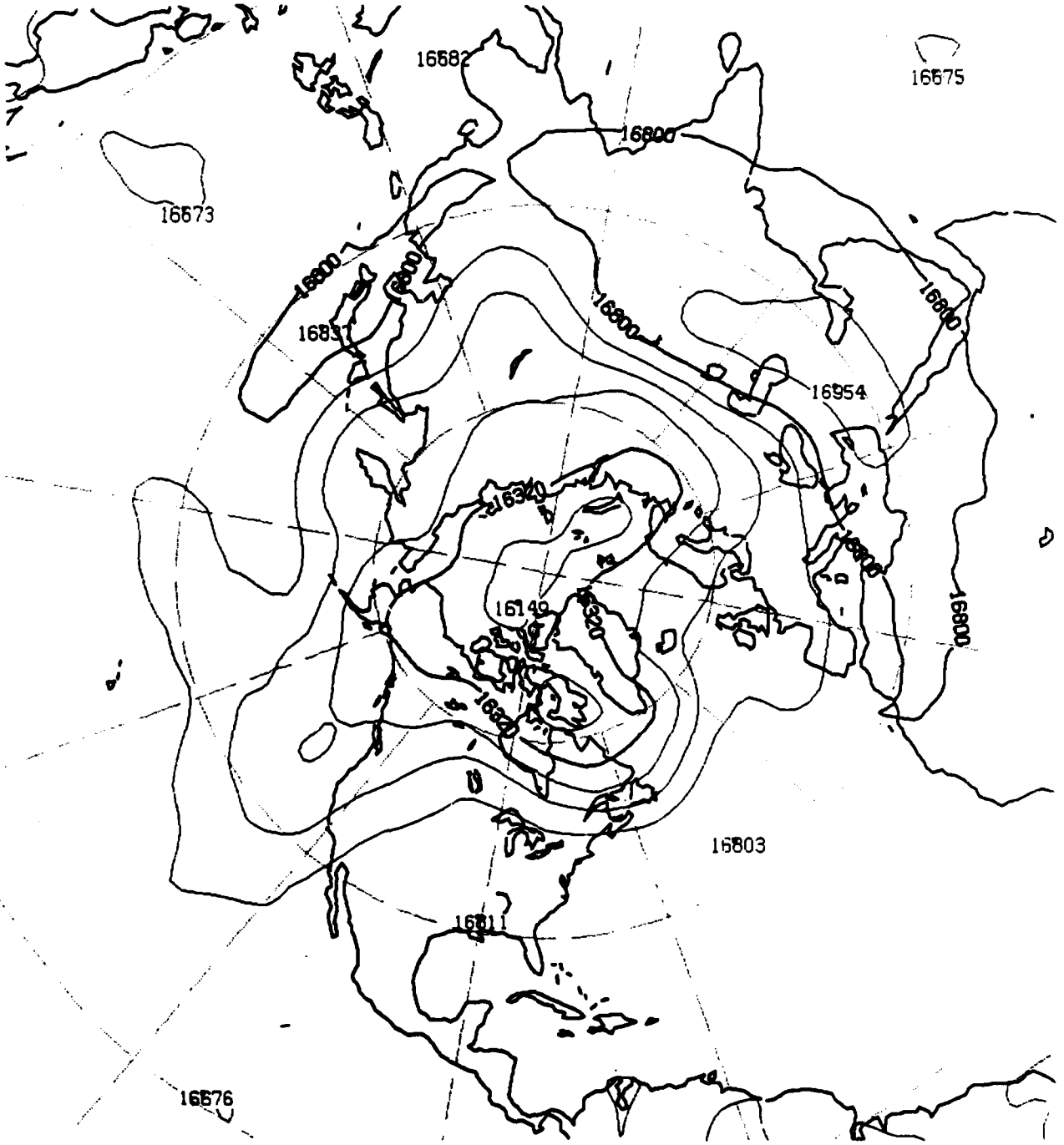

Fig. 21. 24-hour Northern Hemisphere control run forecast for 100 mb heights (m) valid at 00Z, 25 August 1983.

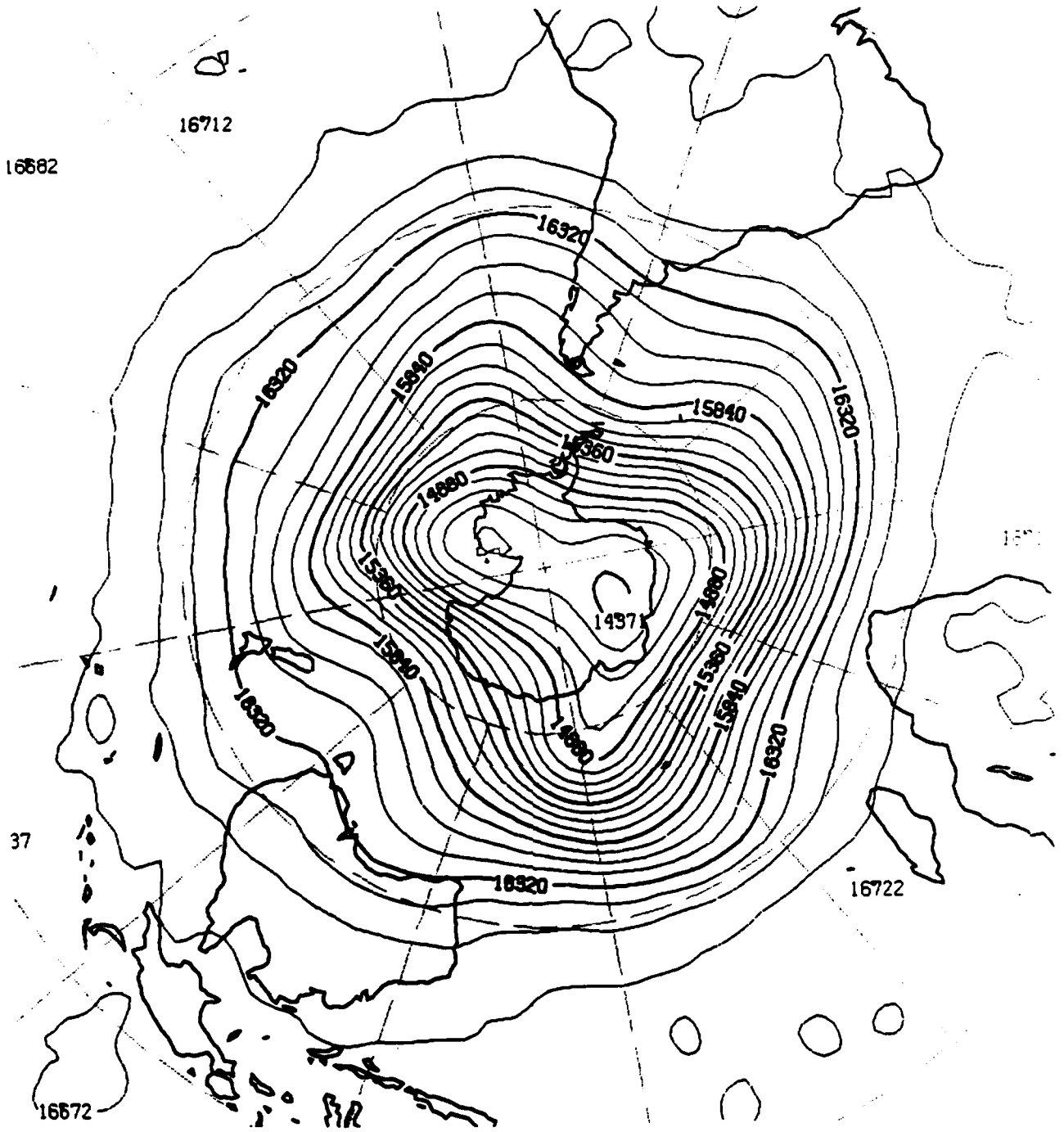

Fig. 22: 24-hour Southern Hemisphere control run forecast for 100 mb heights (m) valid at 00Z, 25 August 1983.

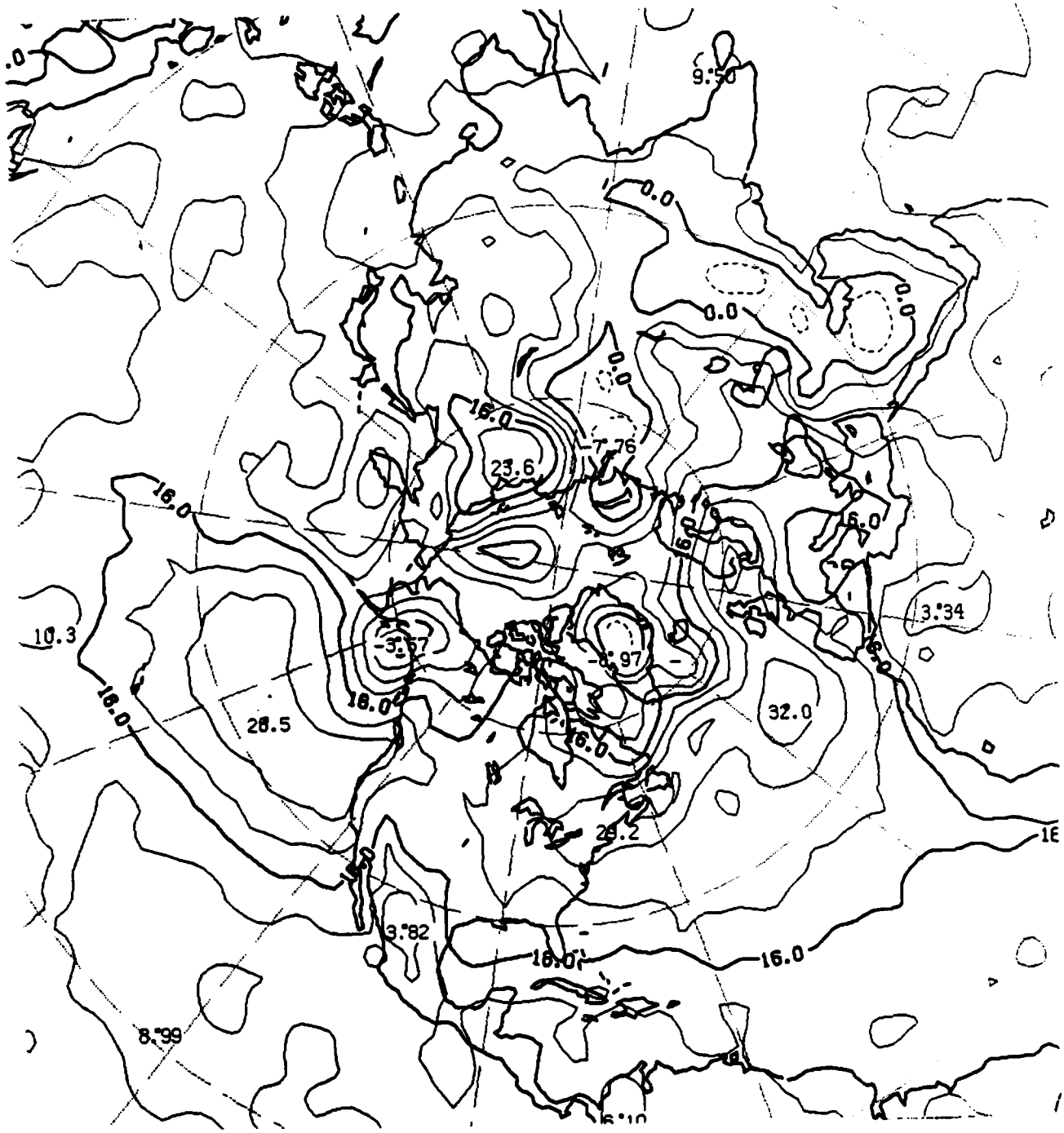

Fig. 23. 48-hour Northern Hemisphere assimilation run forecast for sea-level pressure (mb) valid at 00Z, 26 August 1983.

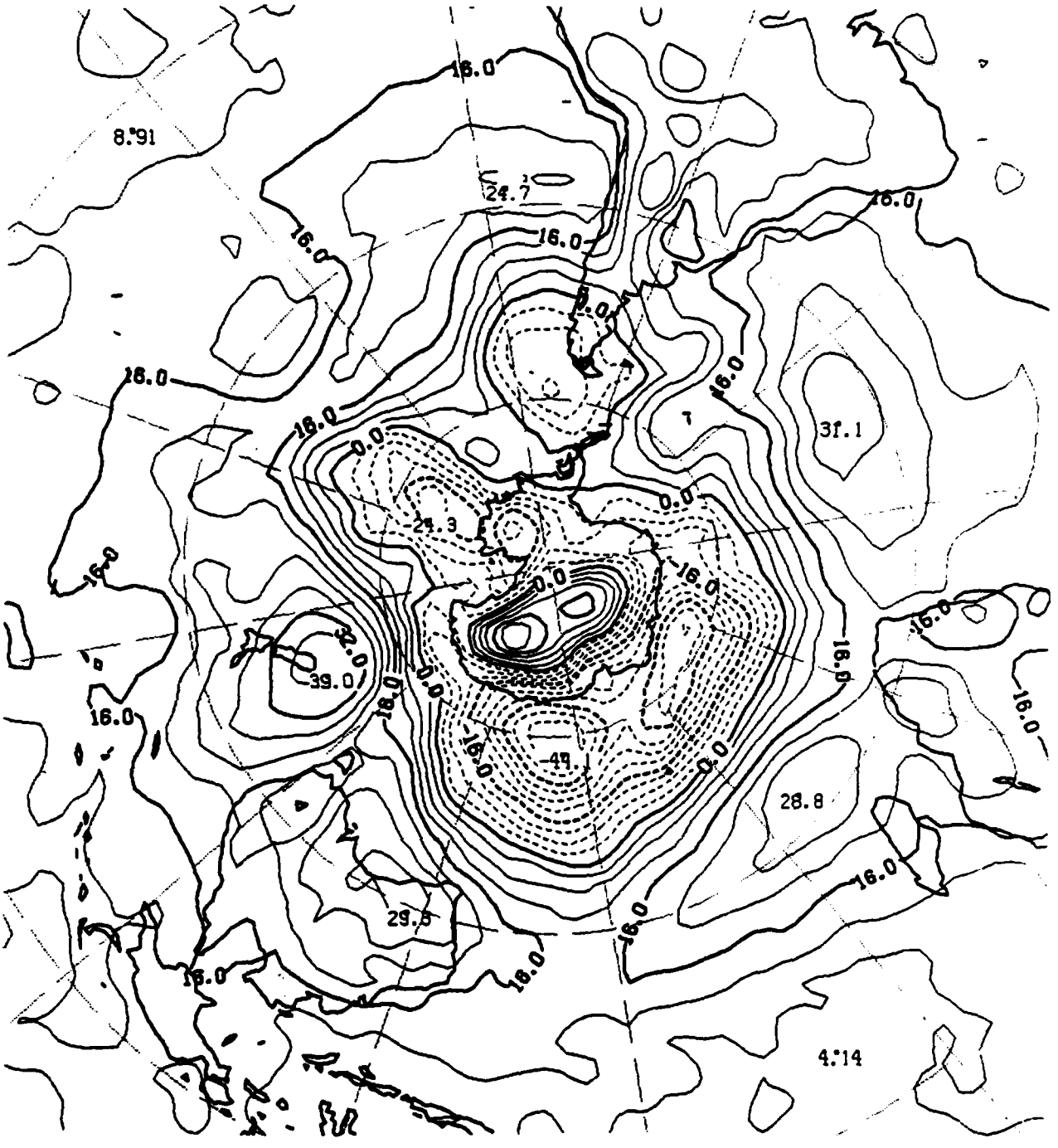

Fig. 24. 48-hour Southern Hemisphere assimilation run forecast for sea-level pressure (mb) valid at 00Z, 26 August 1983.

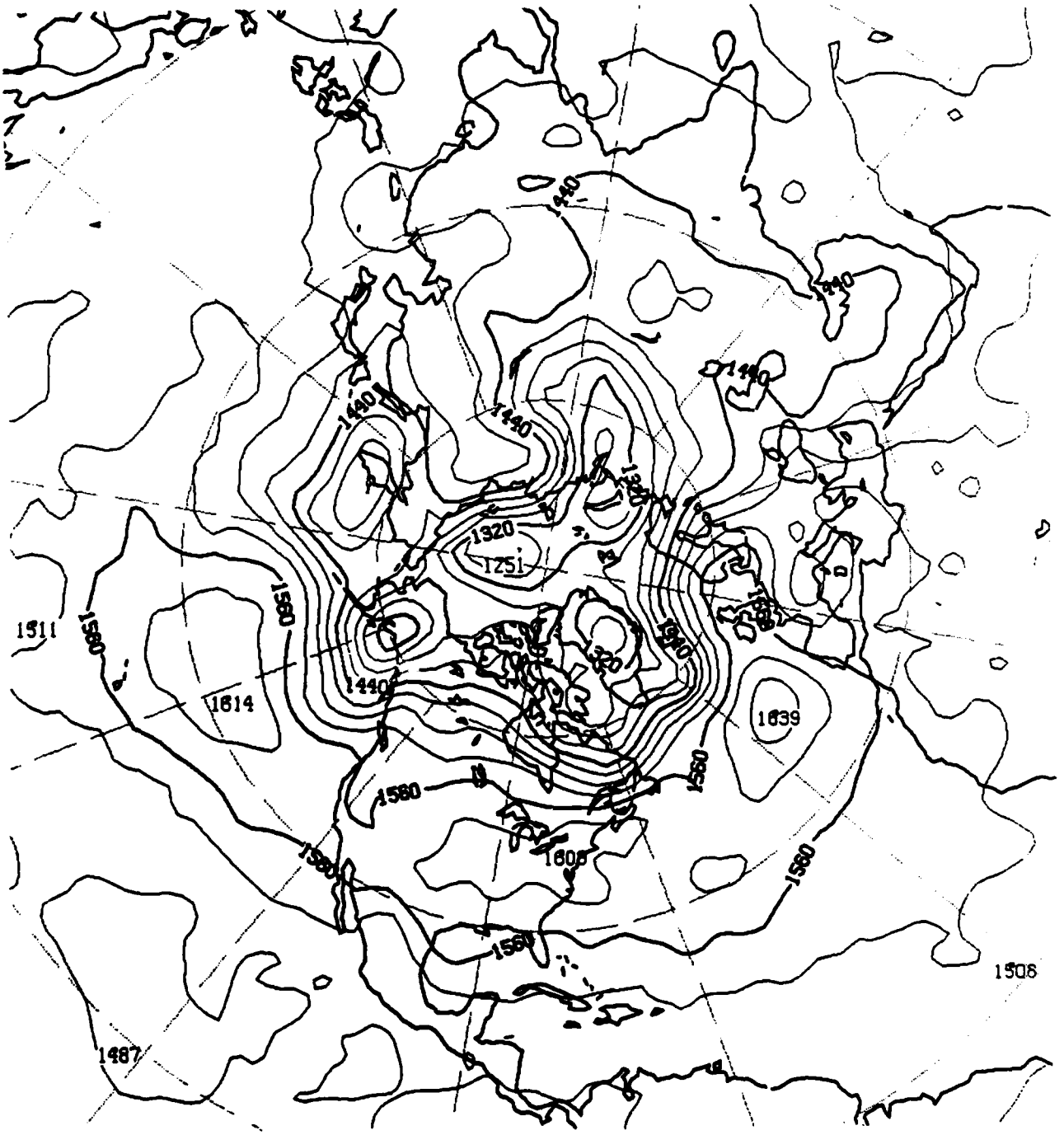

Fig. 25. 48-hour Northern Hemisphere assimilation run forecast for 850 mb heights (m) valid at 00Z, 26 August 1983.

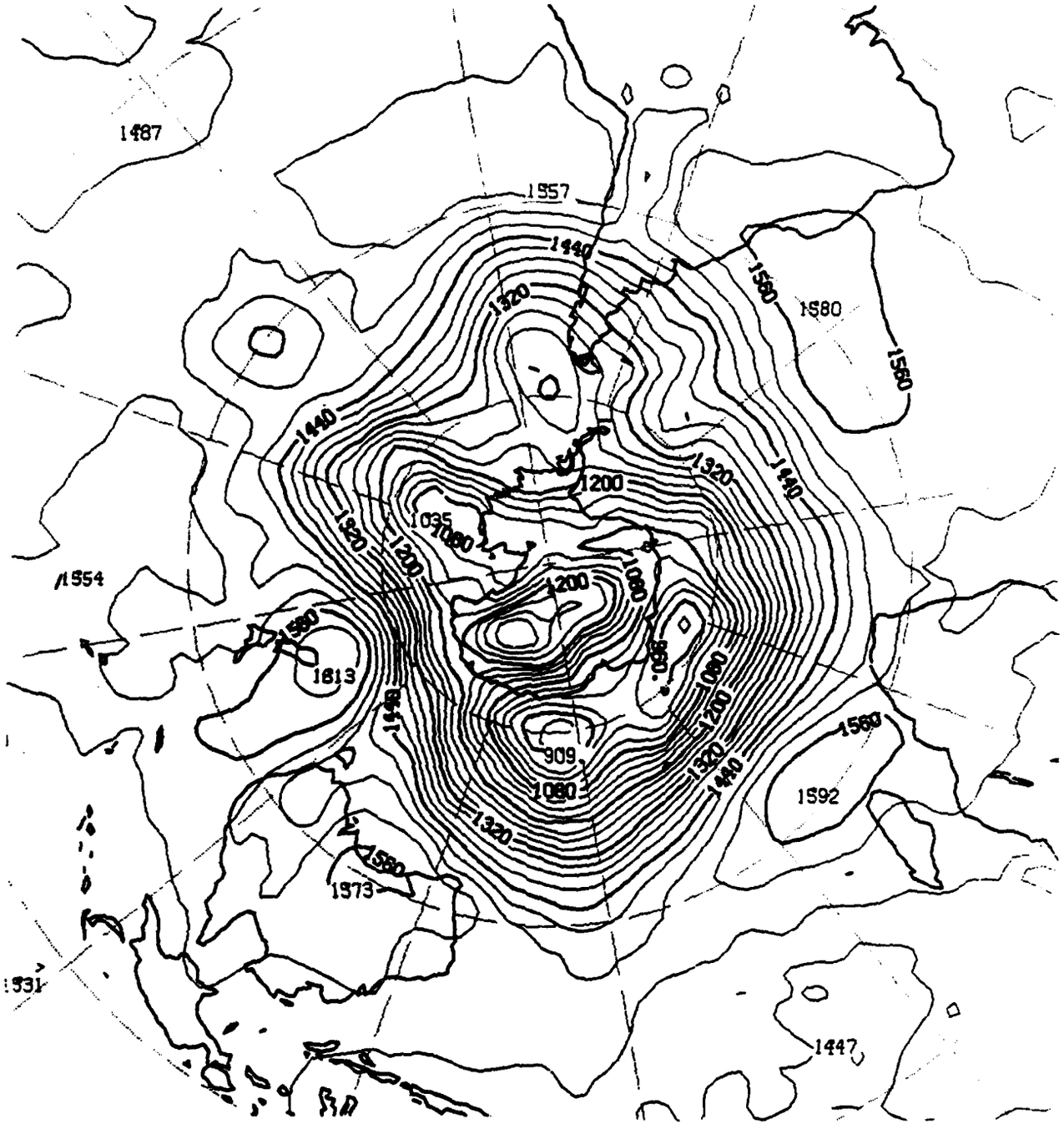

Fig. 26. 48-hour Southern Hemisphere assimilation run forecast for 850 mb heights (m) valid at 00Z, 26 August 1983.

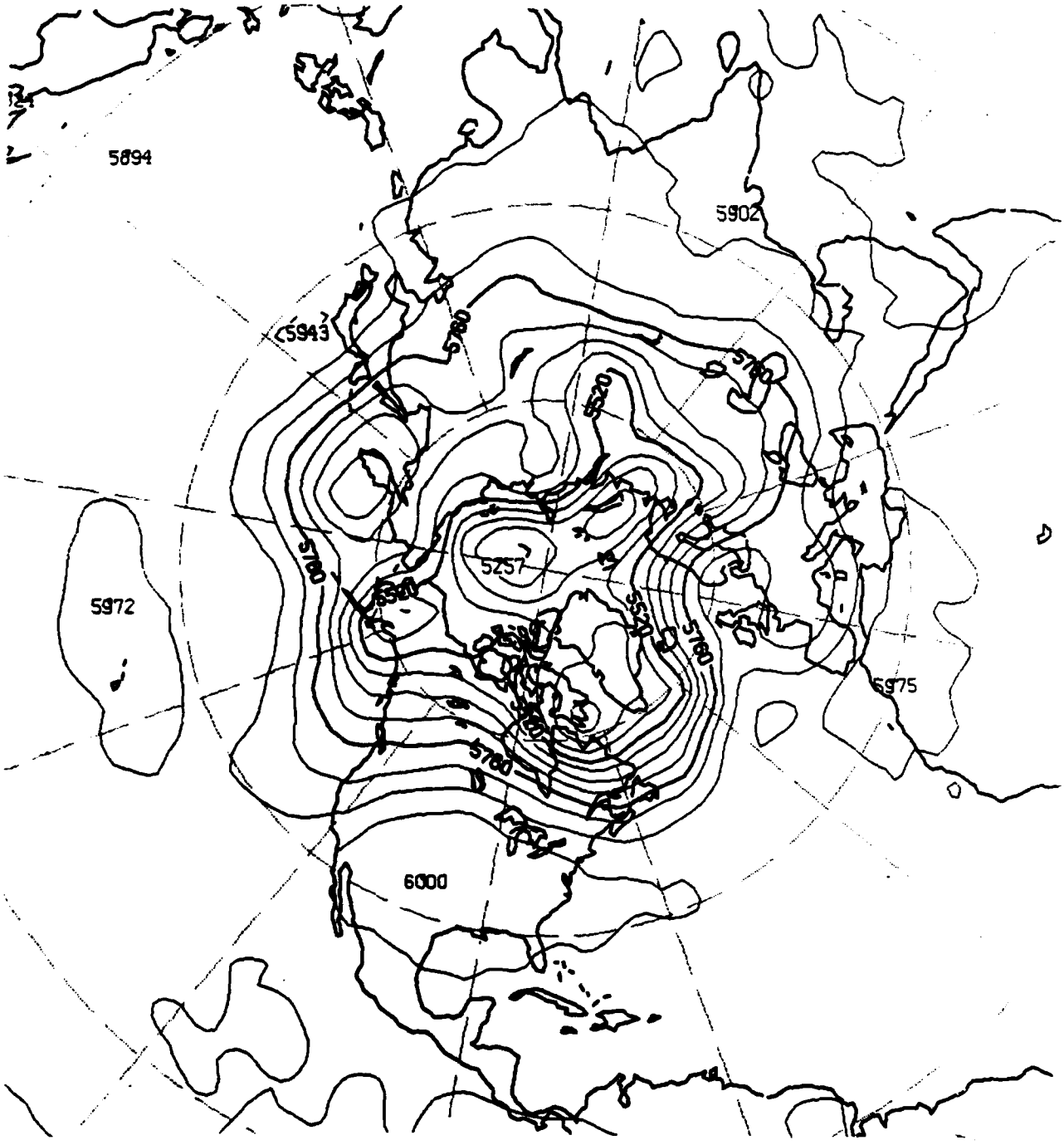

Fig. 27. 48-hour Northern Hemisphere assimilation run forecast for 500 mb heights (m) valid at 00Z, 26 August 1983.

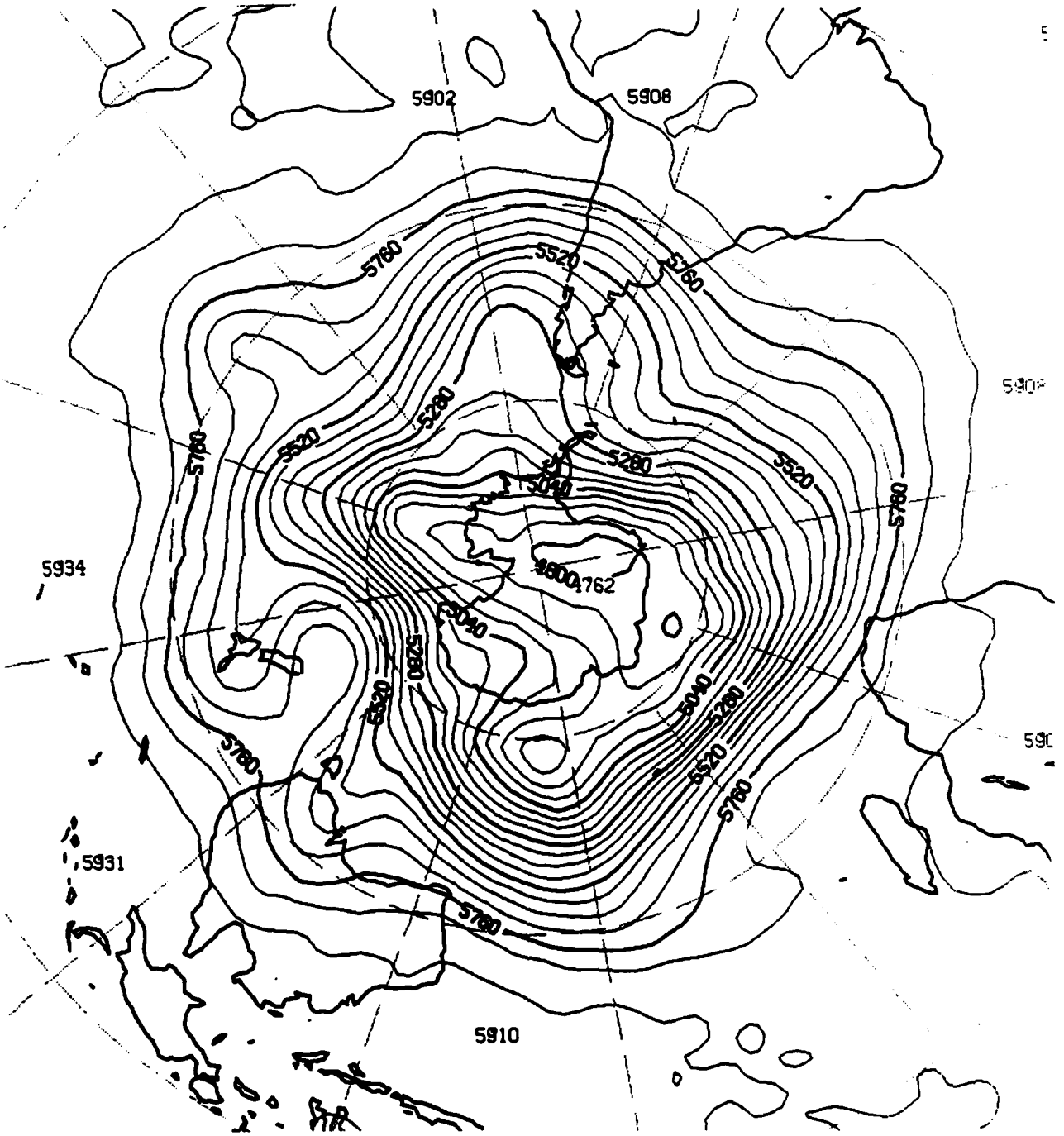

Fig. 28. 48-hour Southern Hemisphere assimilation run forecast for 500 mb heights (m) valid at 00Z, 26 August 1983.

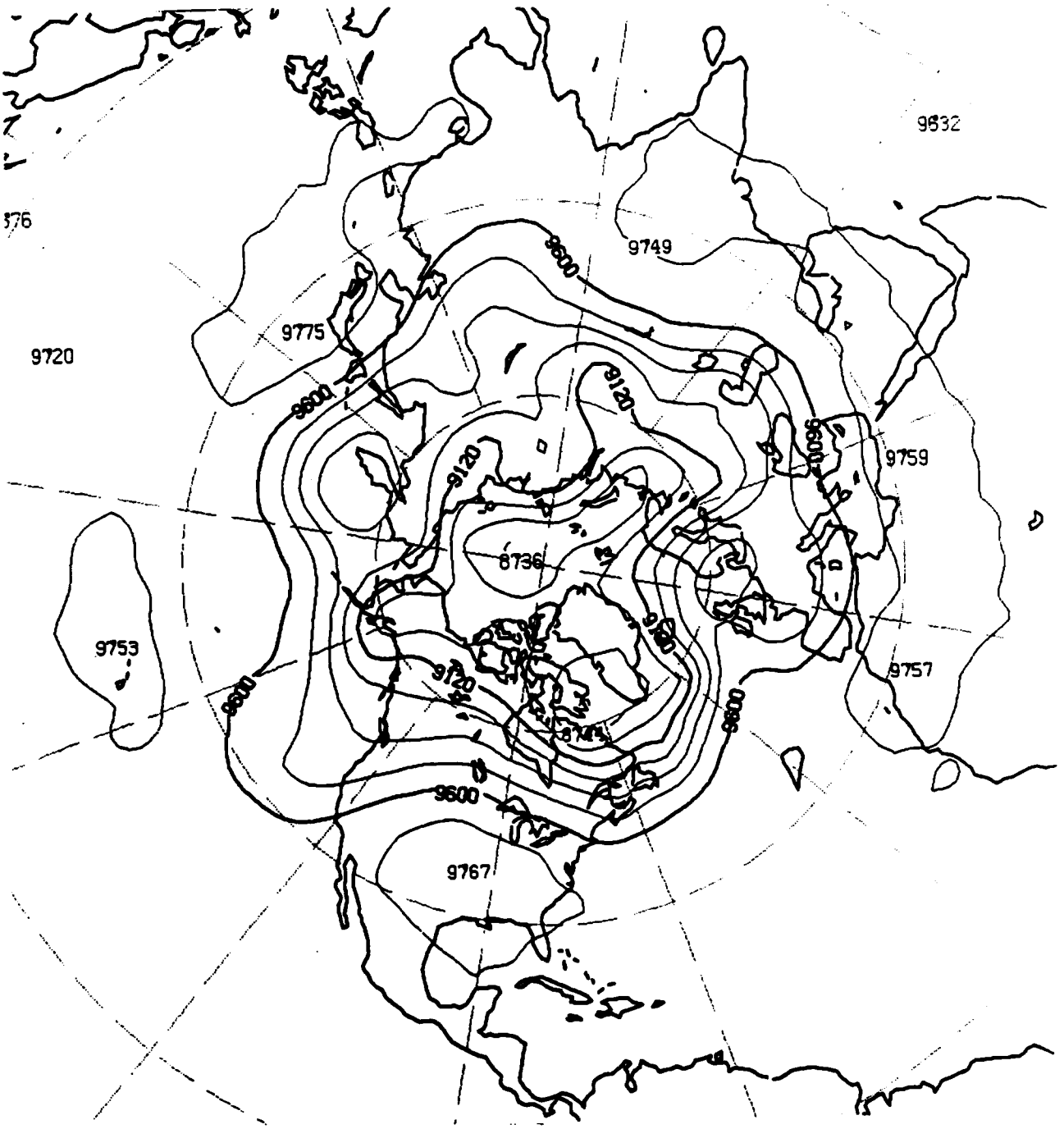

Fig. 29. 48-hour Northern Hemisphere assimilation run forecast for 300 mb heights (m) valid at 00Z, 26 August 1983.

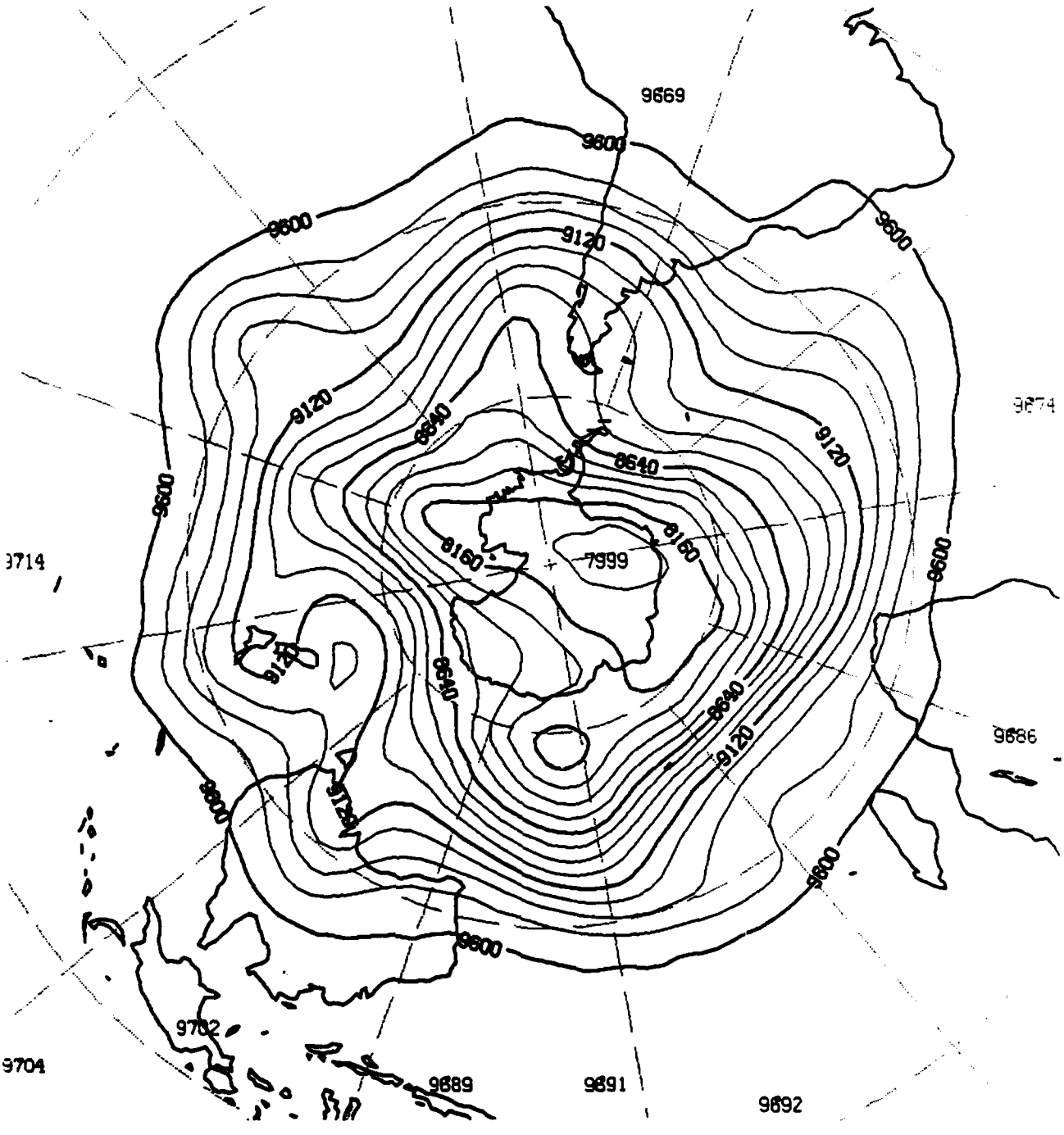

Fig. 30. 48-hour Southern Hemisphere assimilation run forecast for 300 mb heights (m) valid at 00Z, 26 August 1983.

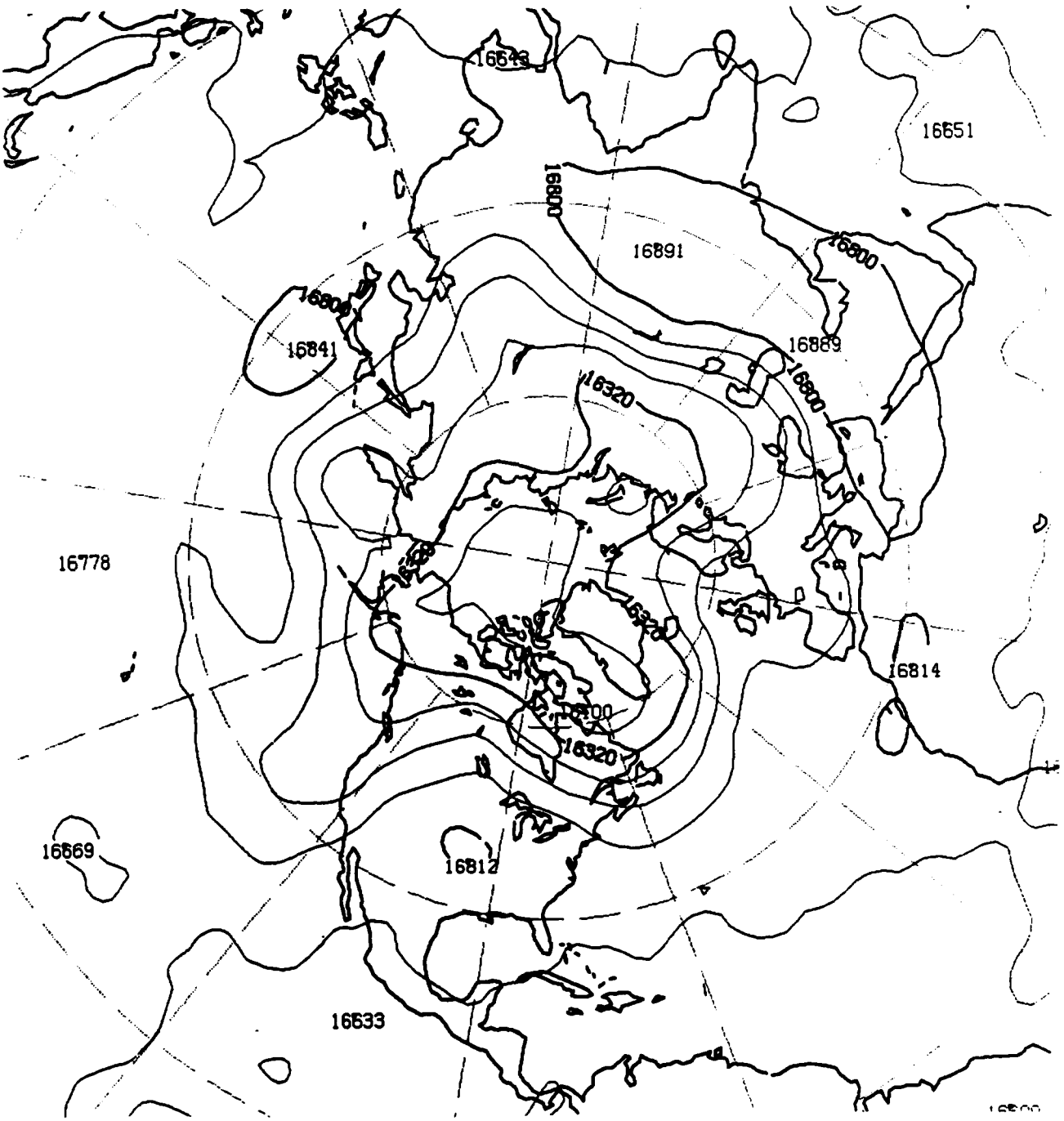

Fig. 31. 48-hour Northern Hemisphere assimilation run forecast for 100 mb heights (m) valid at 00Z, 26 August 1983.

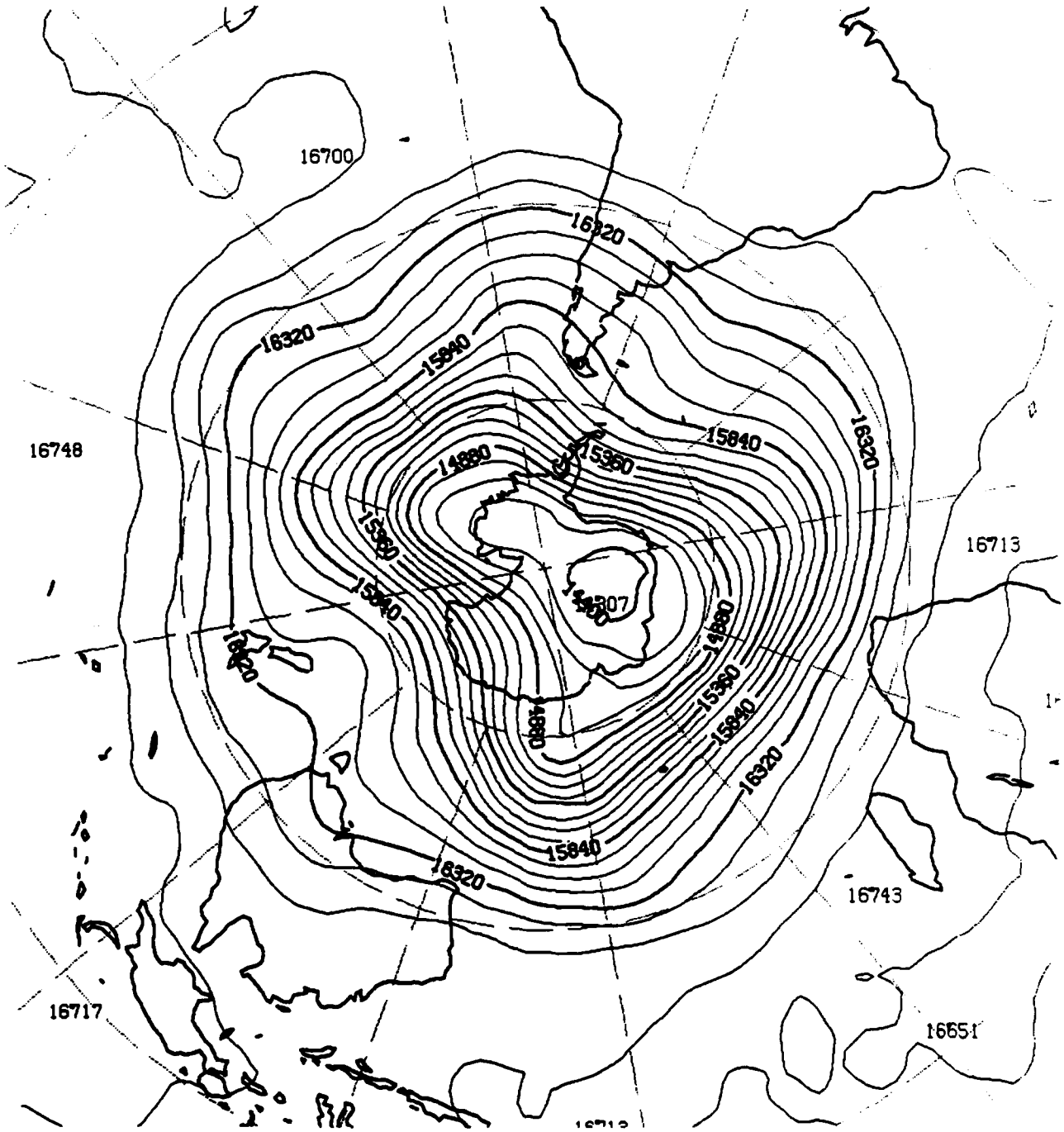

Fig. 32. 48-hour Southern Hemisphere assimilation run forecast for 100 mb heights (m) valid at 00Z, 26 August 1983.

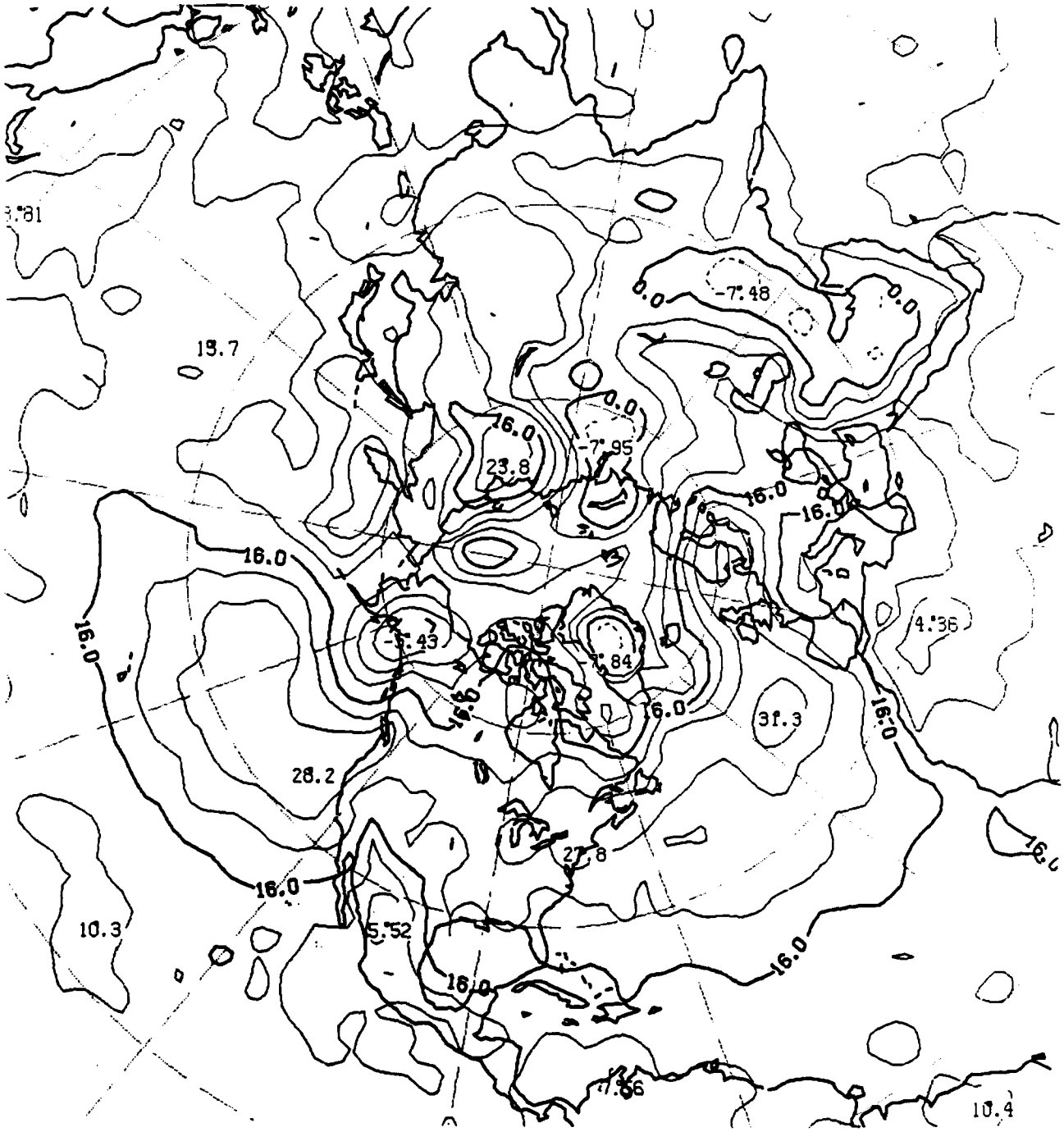

Fig. 33. 48-hour Northern Hemisphere control run forecast for sea-level pressure (mb) valid at 00Z, 26 August 1983.

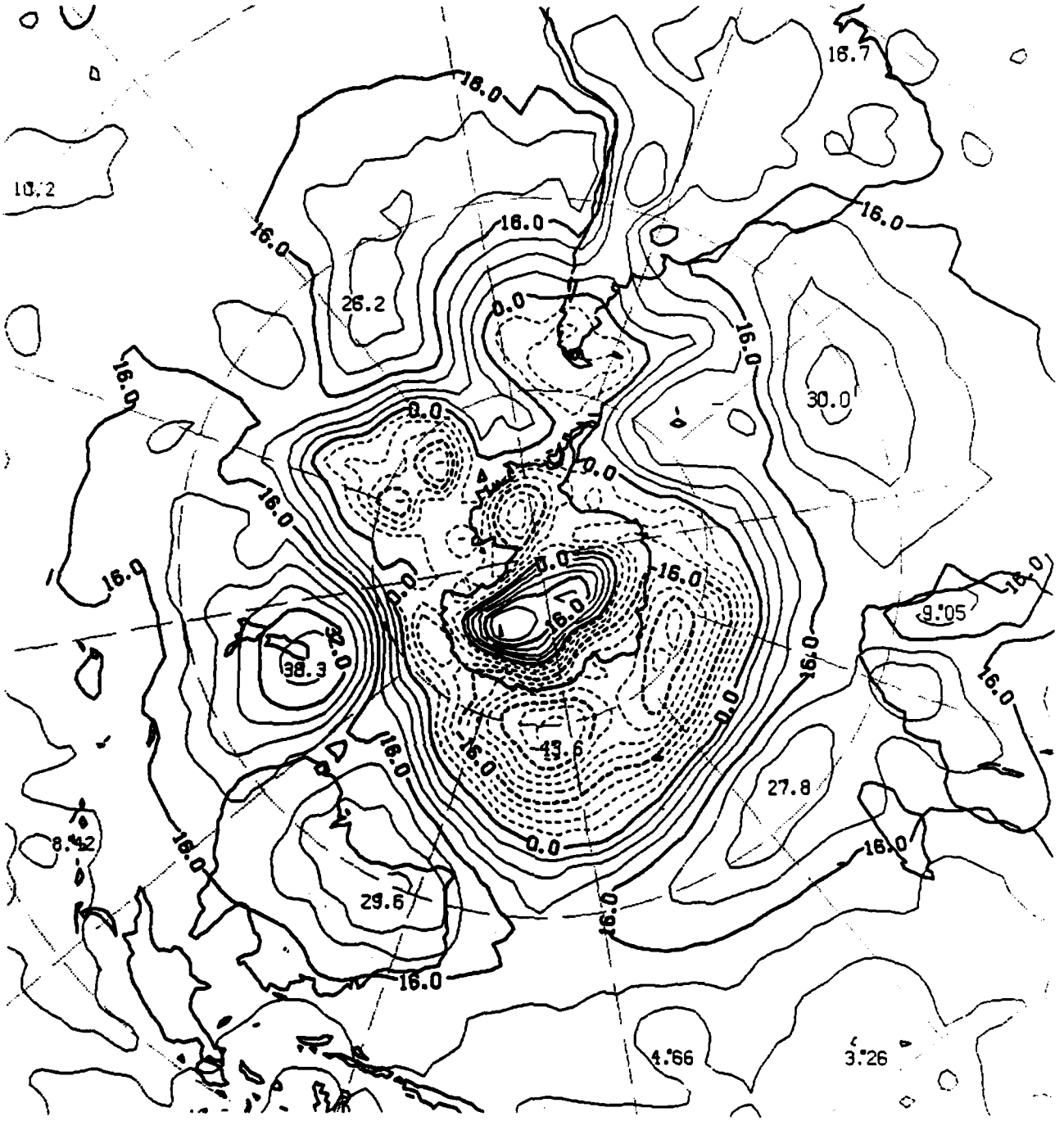

Fig. 34. 48-hour Southern Hemisphere control run forecast for sea-level pressure (mb) valid at 00Z, 26 August 1983.

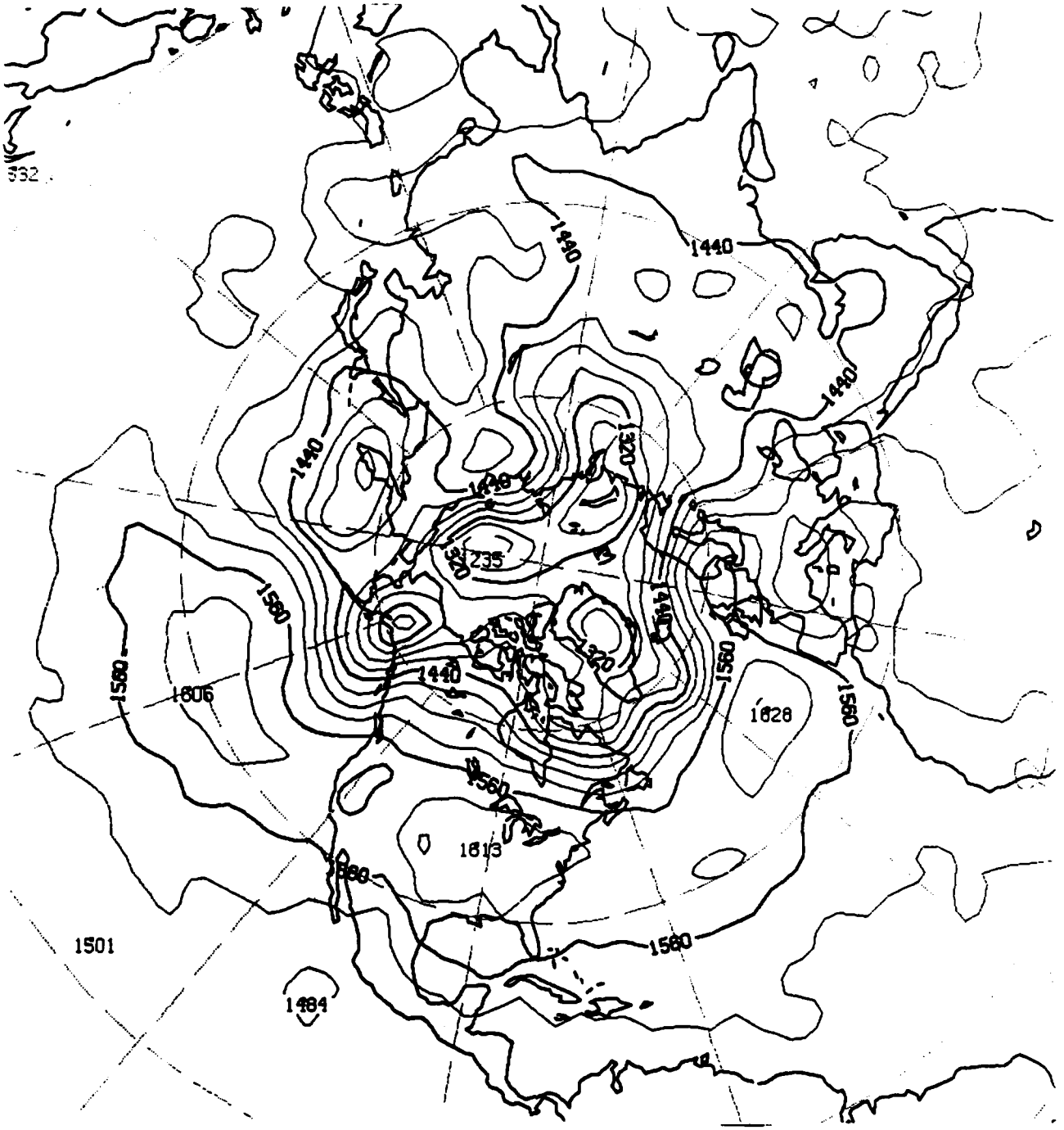

Fig. 35. 48-hour Northern Hemisphere control run forecast for 850 mb heights (m) valid at 00Z, 26 August 1983.

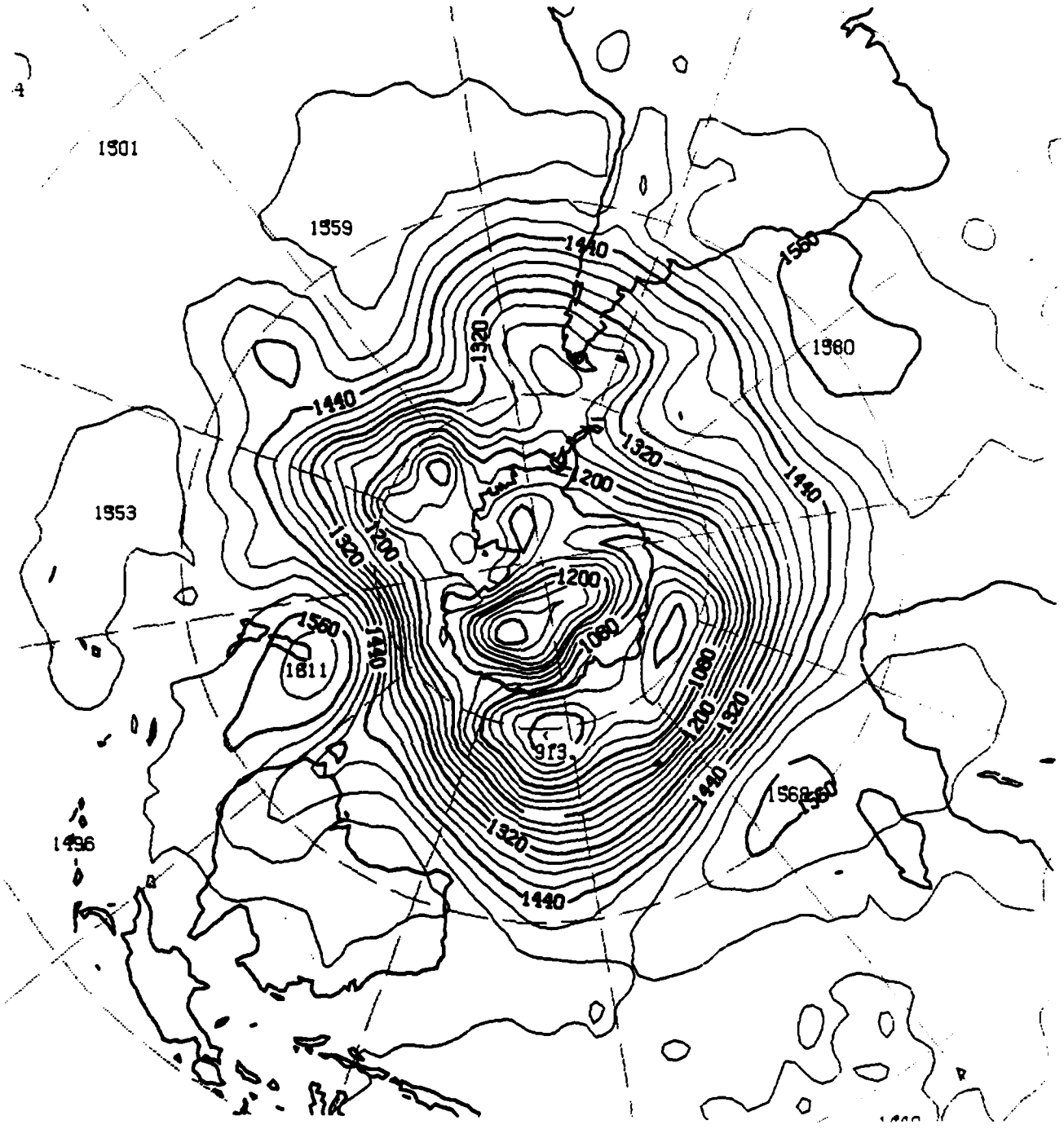

Fig. 36. 48-hour Southern Hemisphere control run forecast for 850 mb heights (m) valid at 00Z, 26 August 1983.

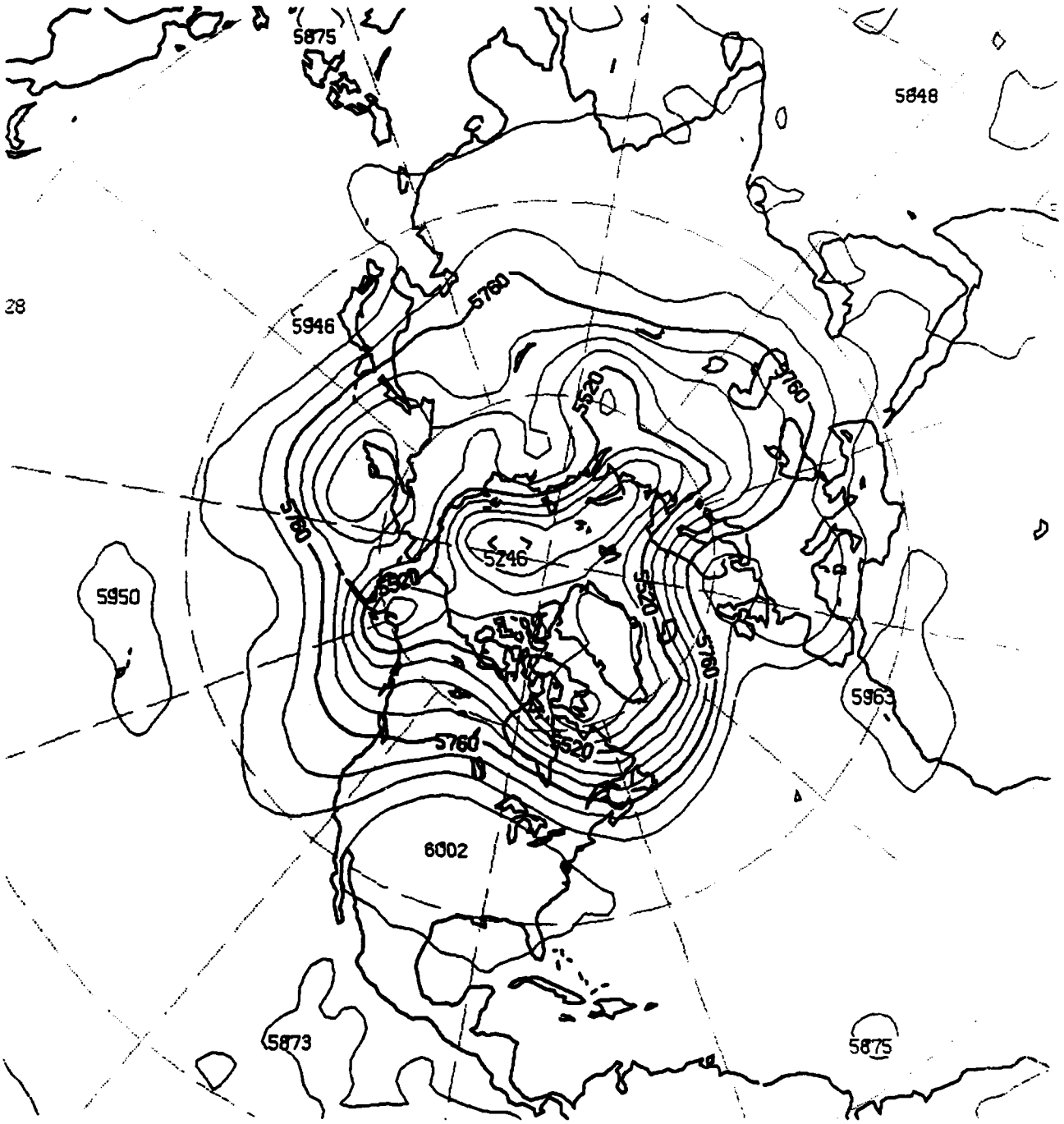

Fig. 37. 48-hour Northern Hemisphere control run forecast for 500 mb heights (m) valid at 00Z, 26 August 1983.

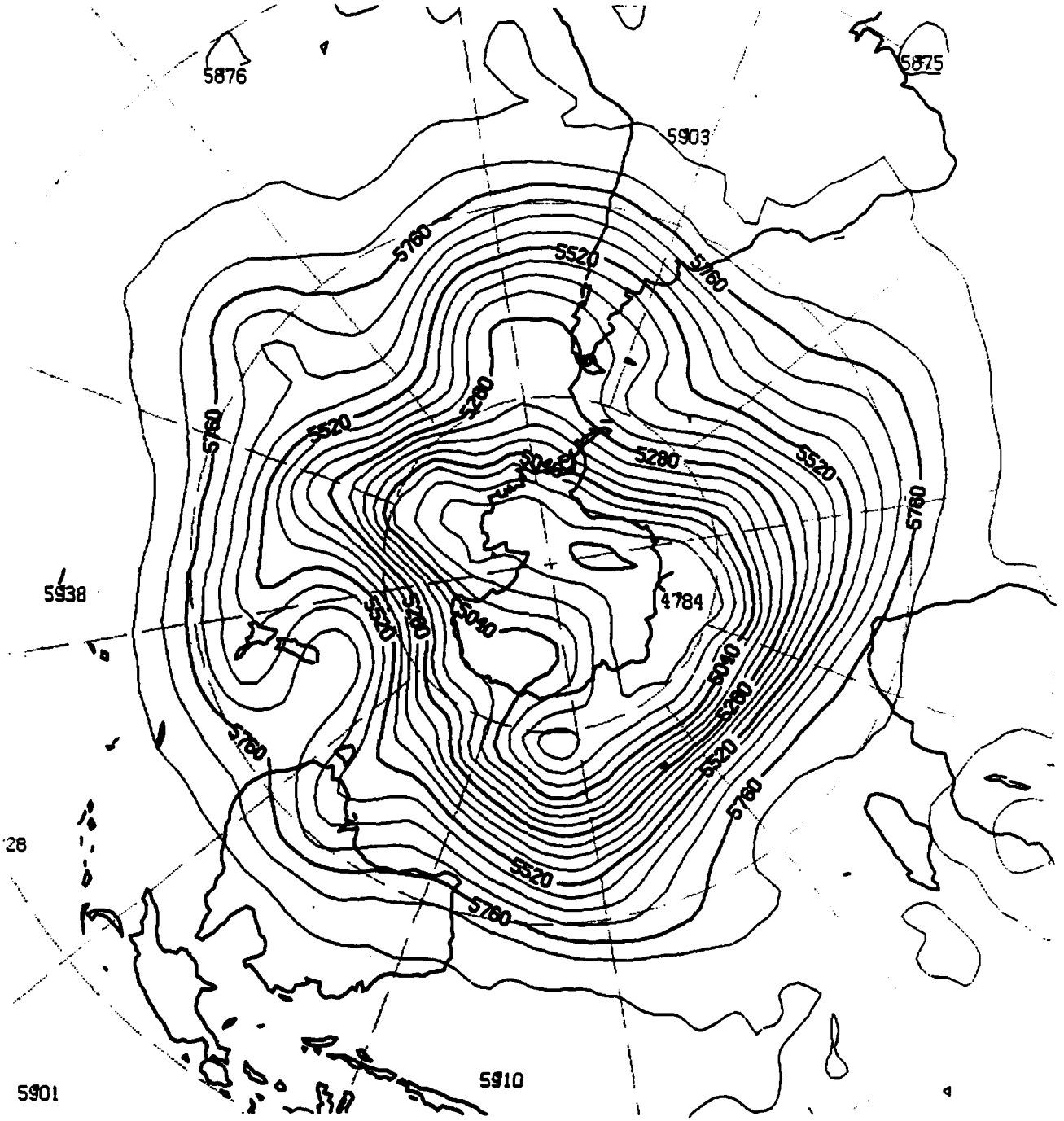

Fig. 38. 48-hour Southern Hemisphere control run forecast for 500 mb heights (m) valid at 00Z, 26 August 1983.

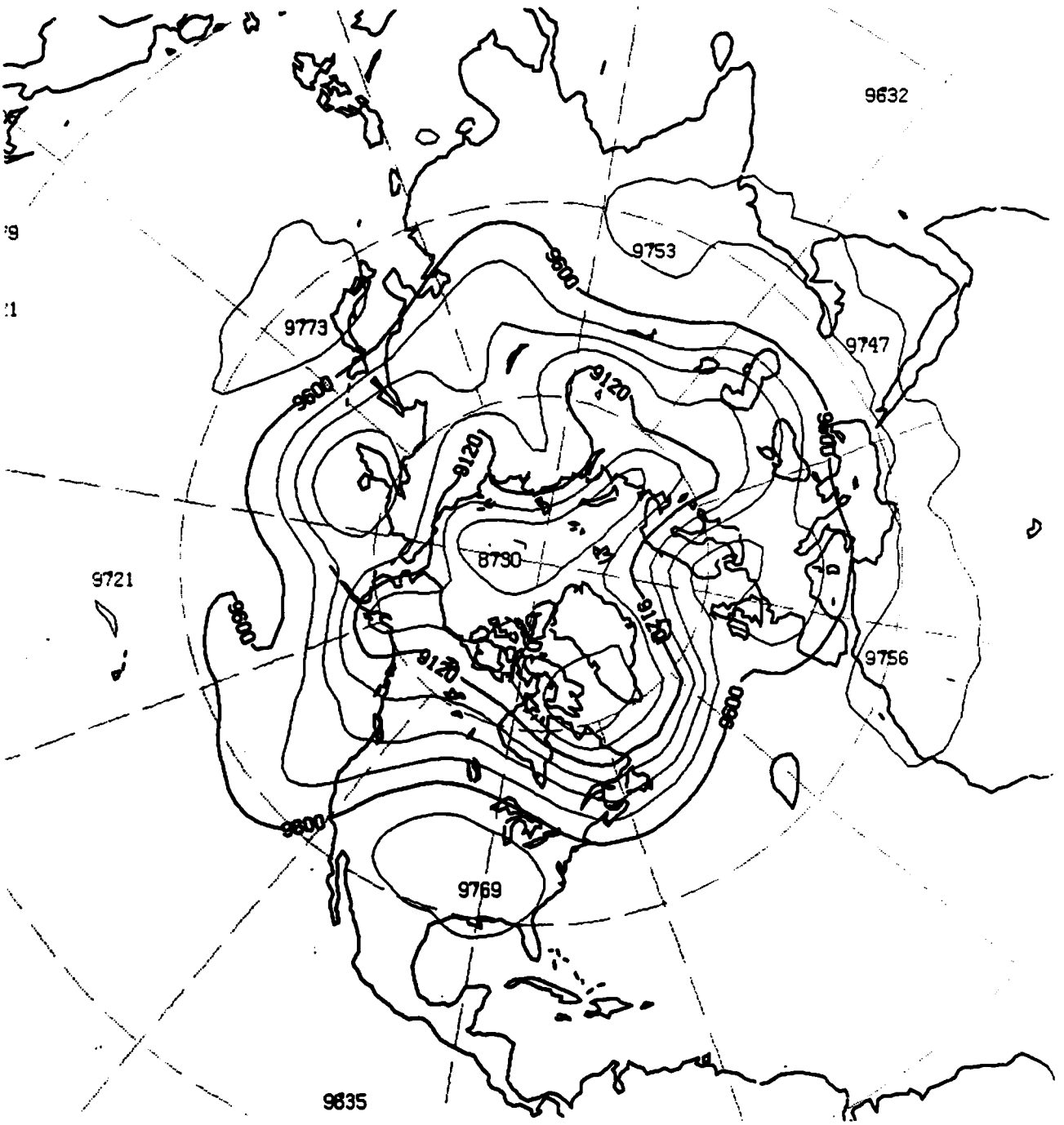

Fig. 39. 48-hour Northern Hemisphere control run forecast for 300 mb heights (m) valid at 00Z, 26 August 1983.

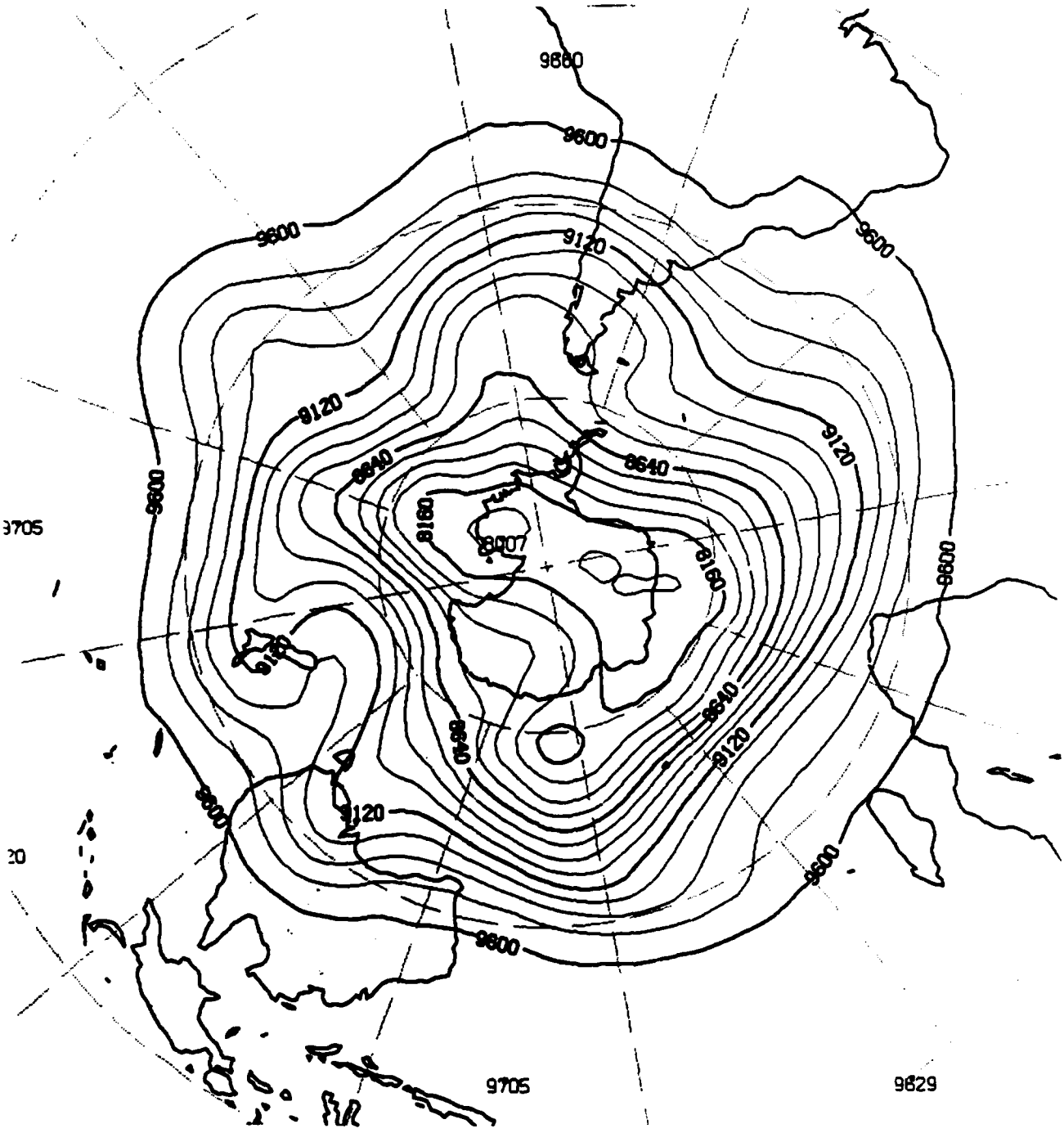

Fig. 40. 48-hour Southern Hemisphere control run forecast for 300 mb heights (m) valid at 00Z, 26 August 1983.

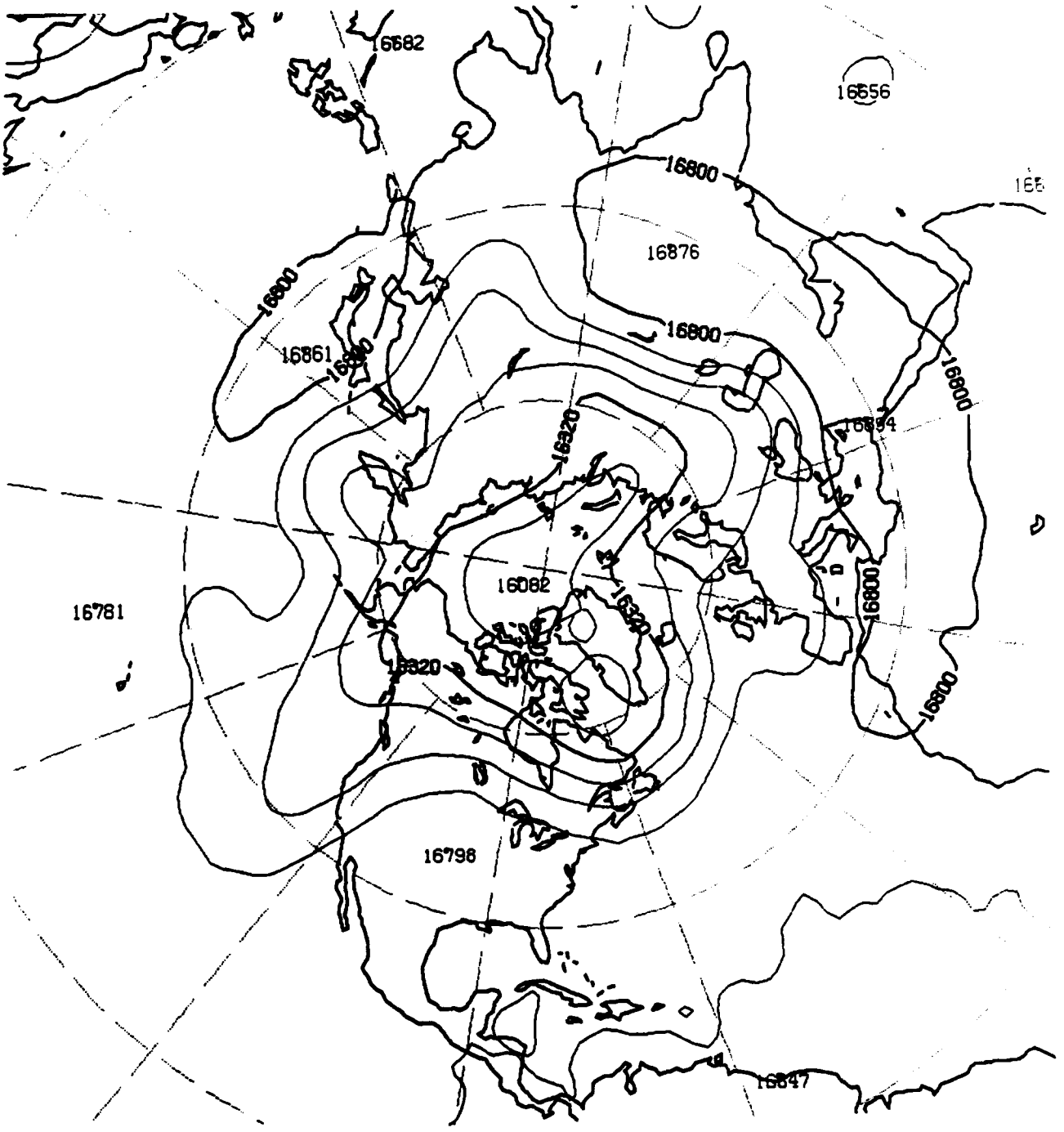

Fig. 41. 48-hour Northern Hemisphere control run forecast for 100 mb heights (m) valid at 00Z, 26 August 1983.

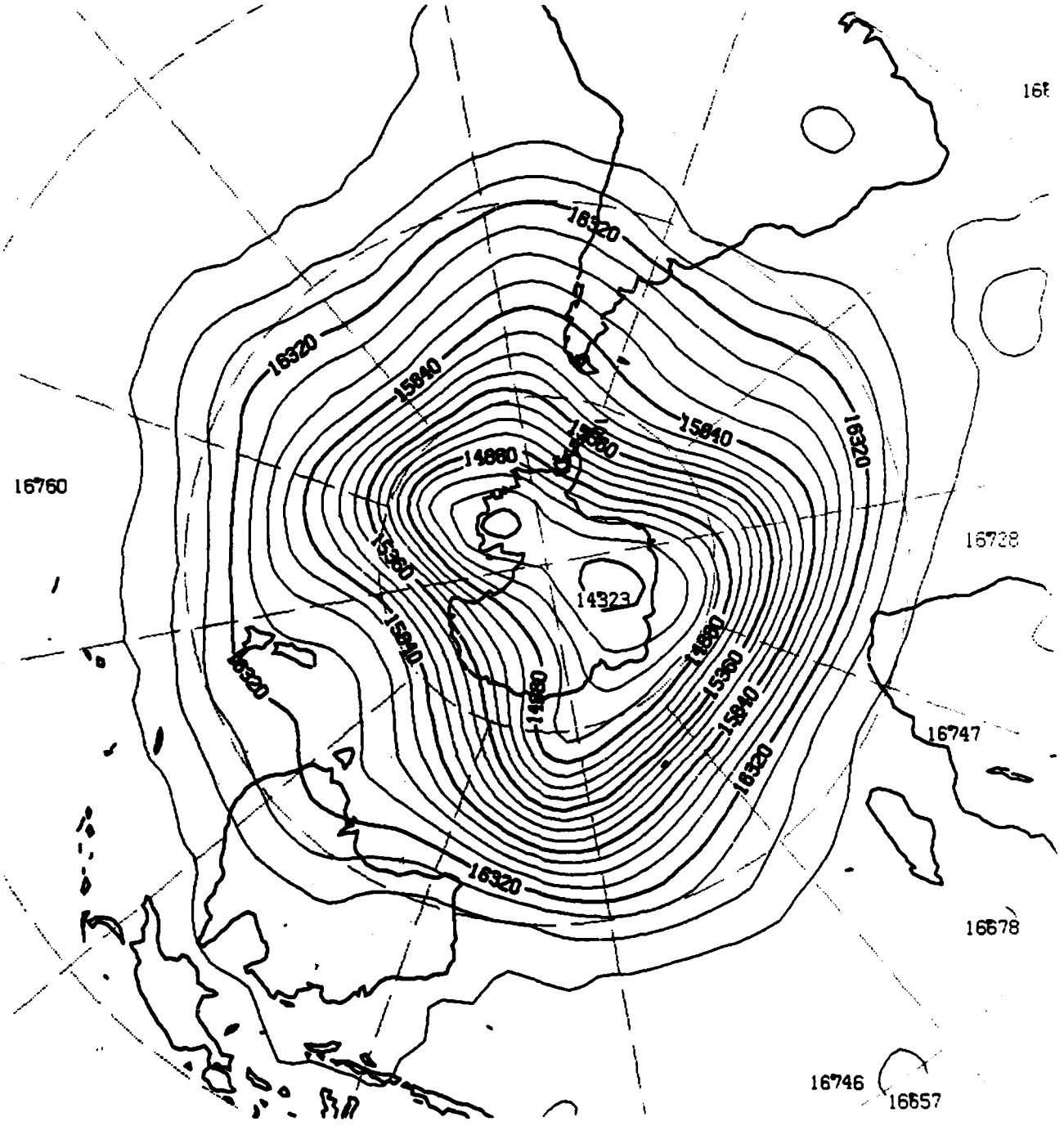

Fig. 42. 48-hour Southern Hemisphere control run forecast for 100 mb heights (m) valid at 00Z, 26 August 1983.

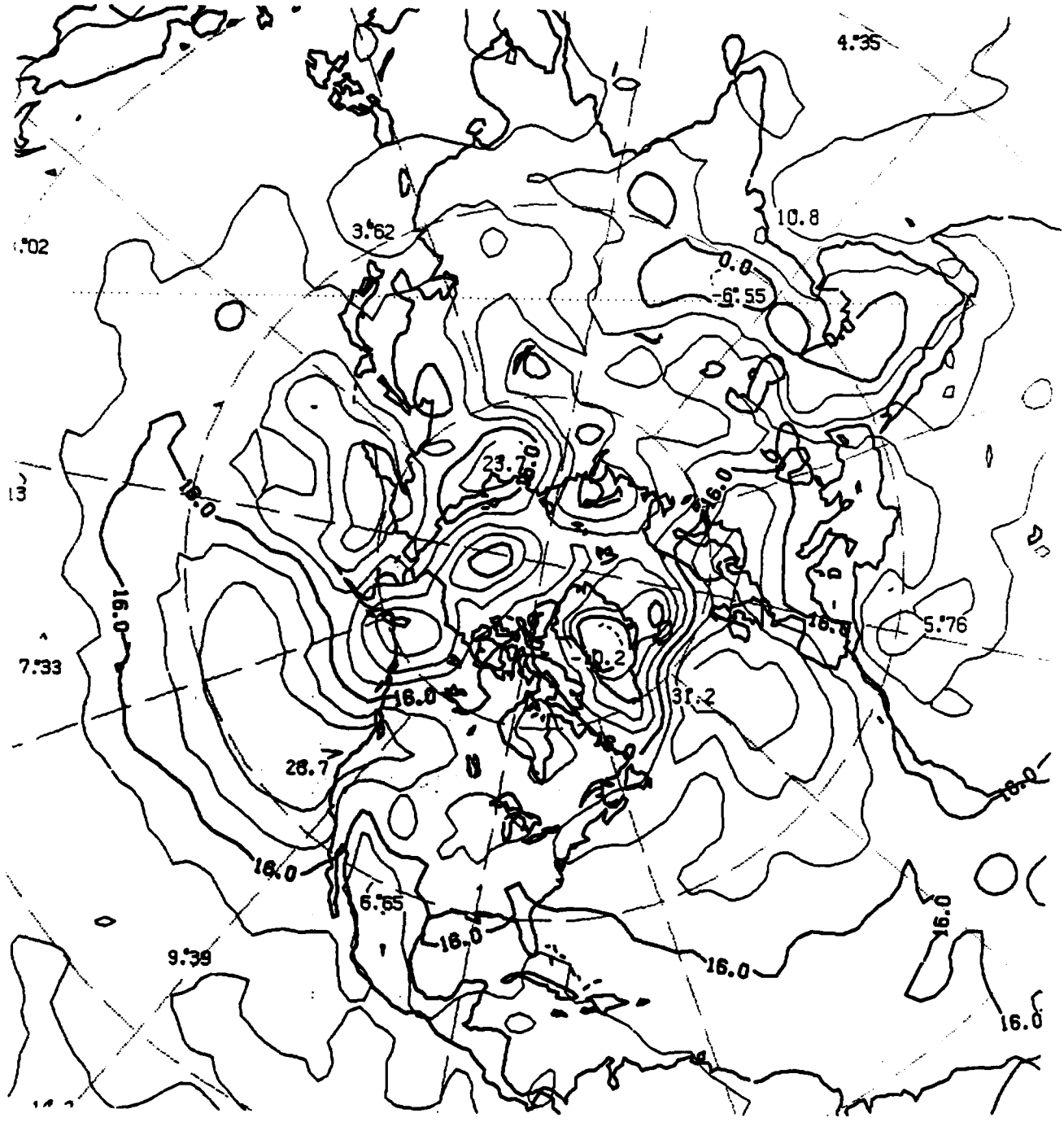

Fig. 43. 72-hour Northern Hemisphere assimilation run forecast for sea-level pressure (mb) valid at 00Z, 27 August 1983.

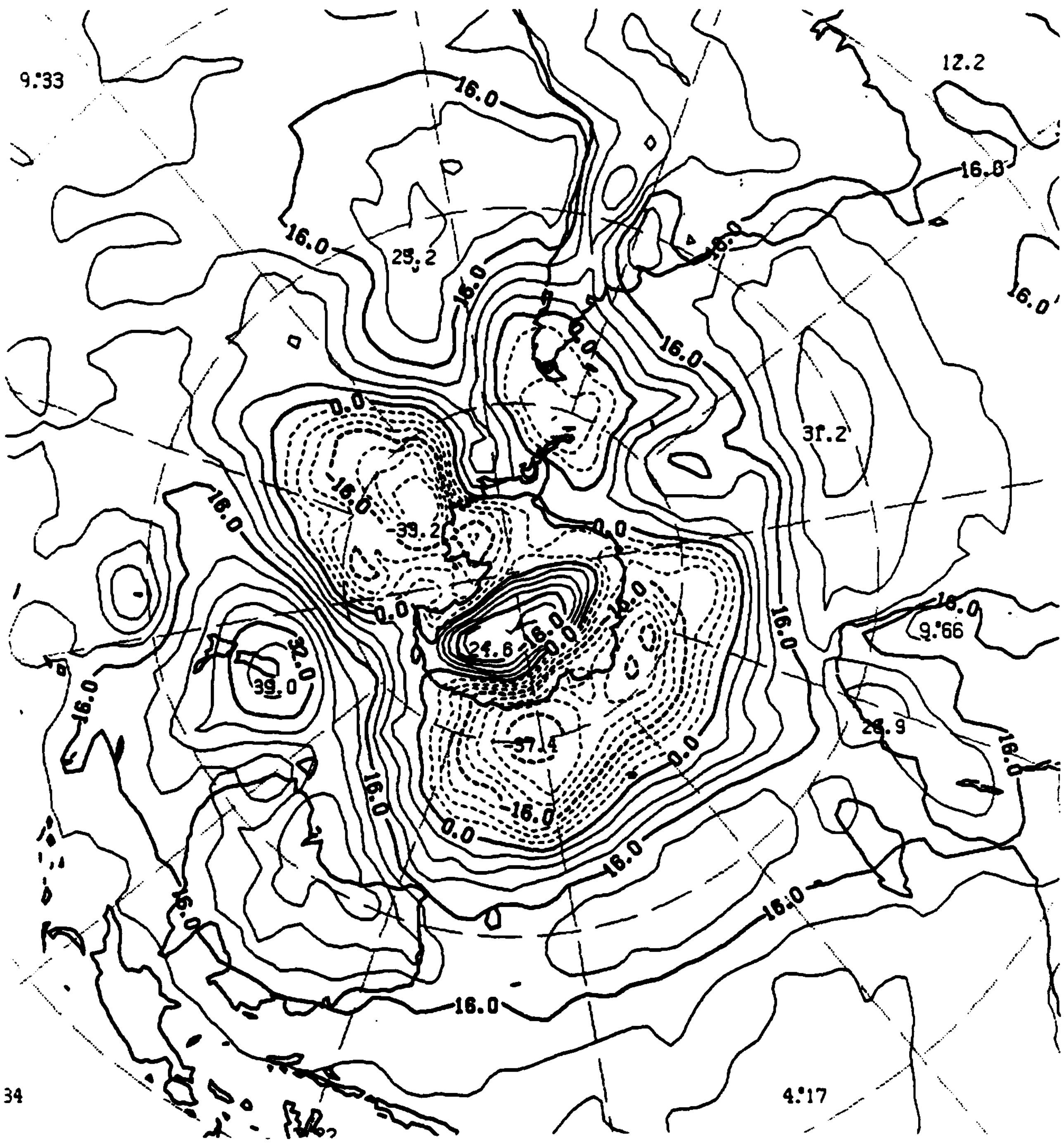

Fig. 44. 72-hour Southern Hemisphere assimilation run forecast for sea-level pressure (mb) valid at 00Z, 27 August 1983.

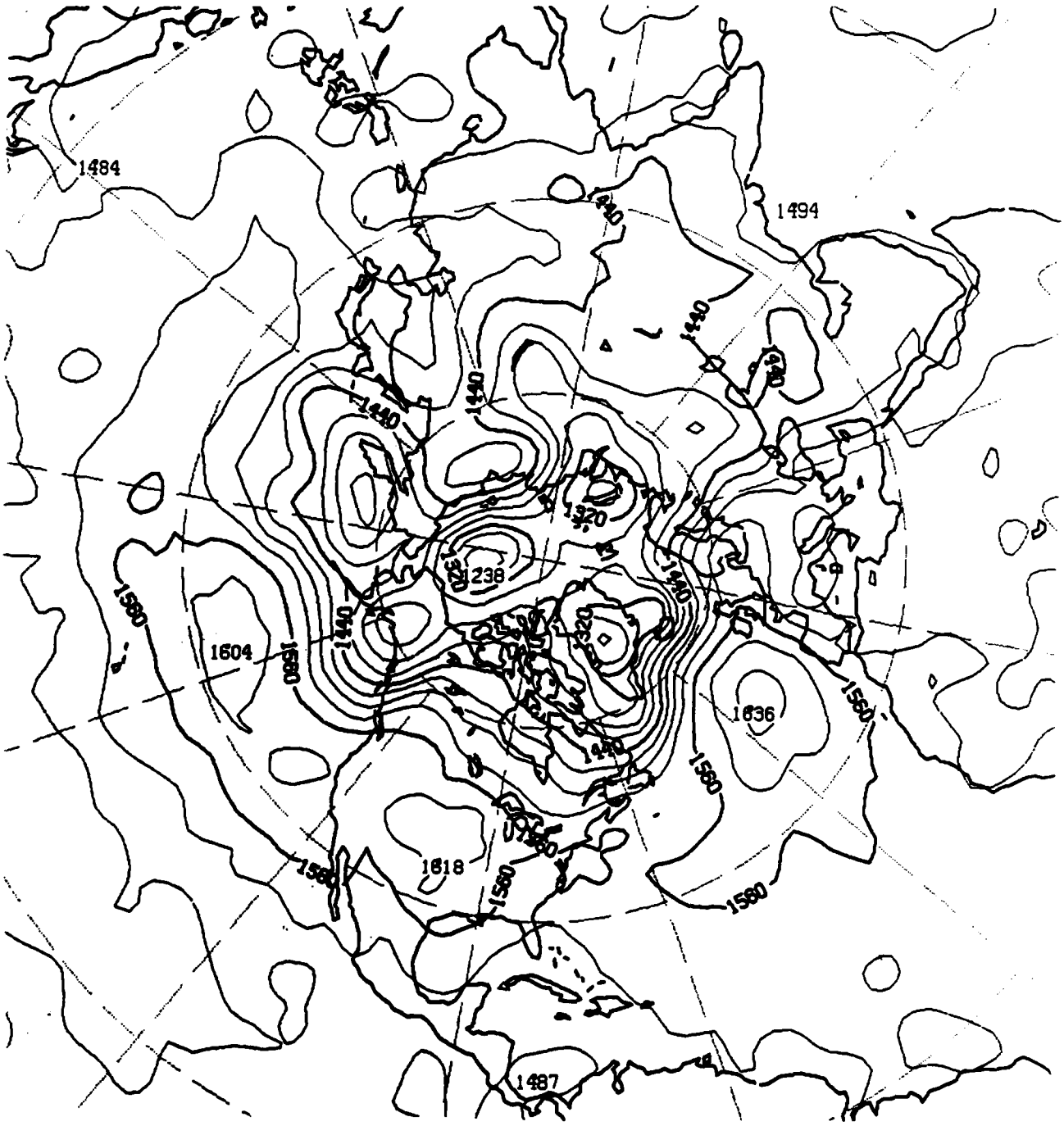

Fig. 45. 72-hour Northern Hemisphere assimilation run forecast for 850 mb heights (m) valid at 00Z, 27 August 1983.

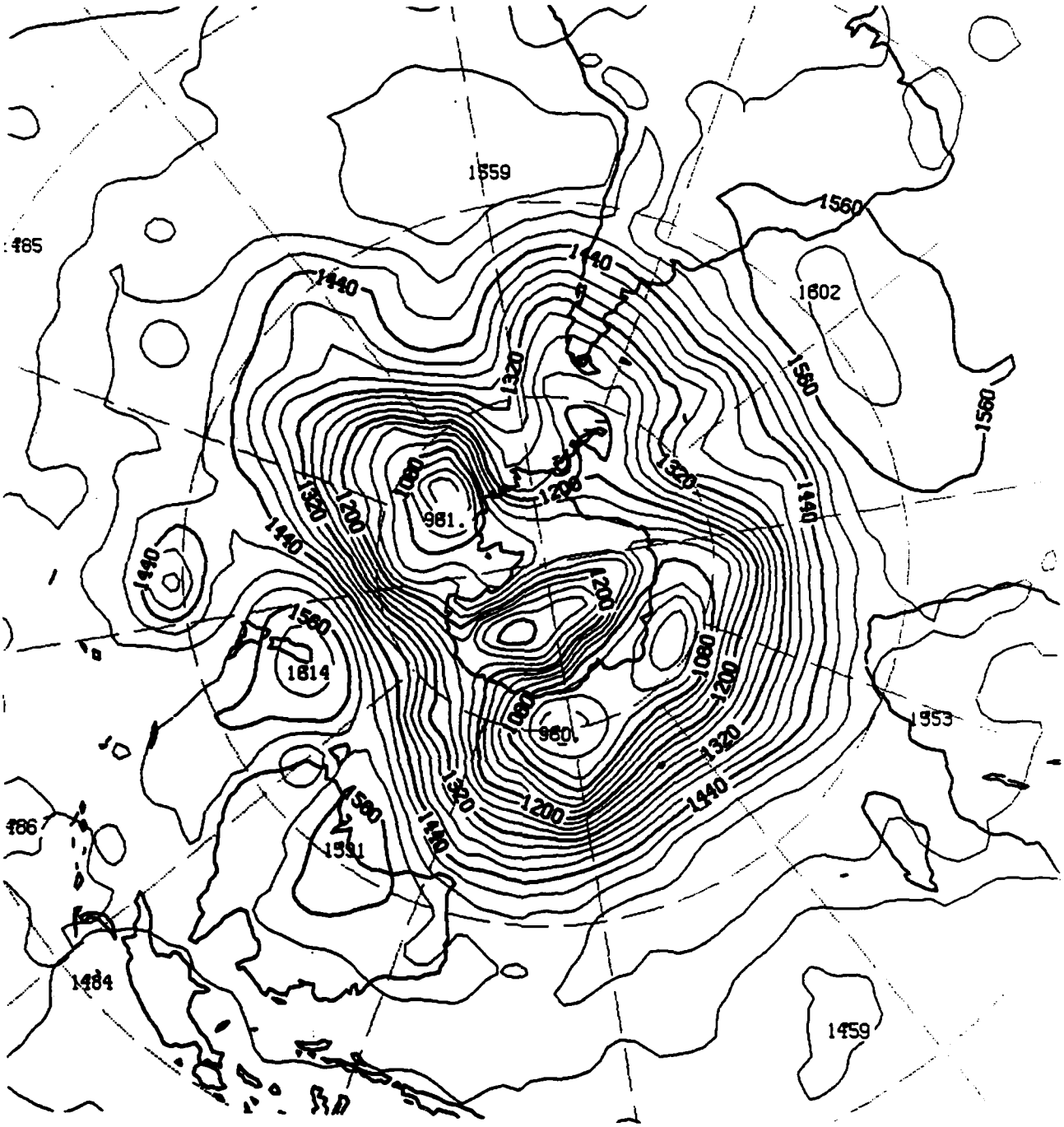

Fig. 46. 72-hour Southern Hemisphere assimilation run forecast for 850 mb heights (m) valid at 00Z, 27 August 1983.

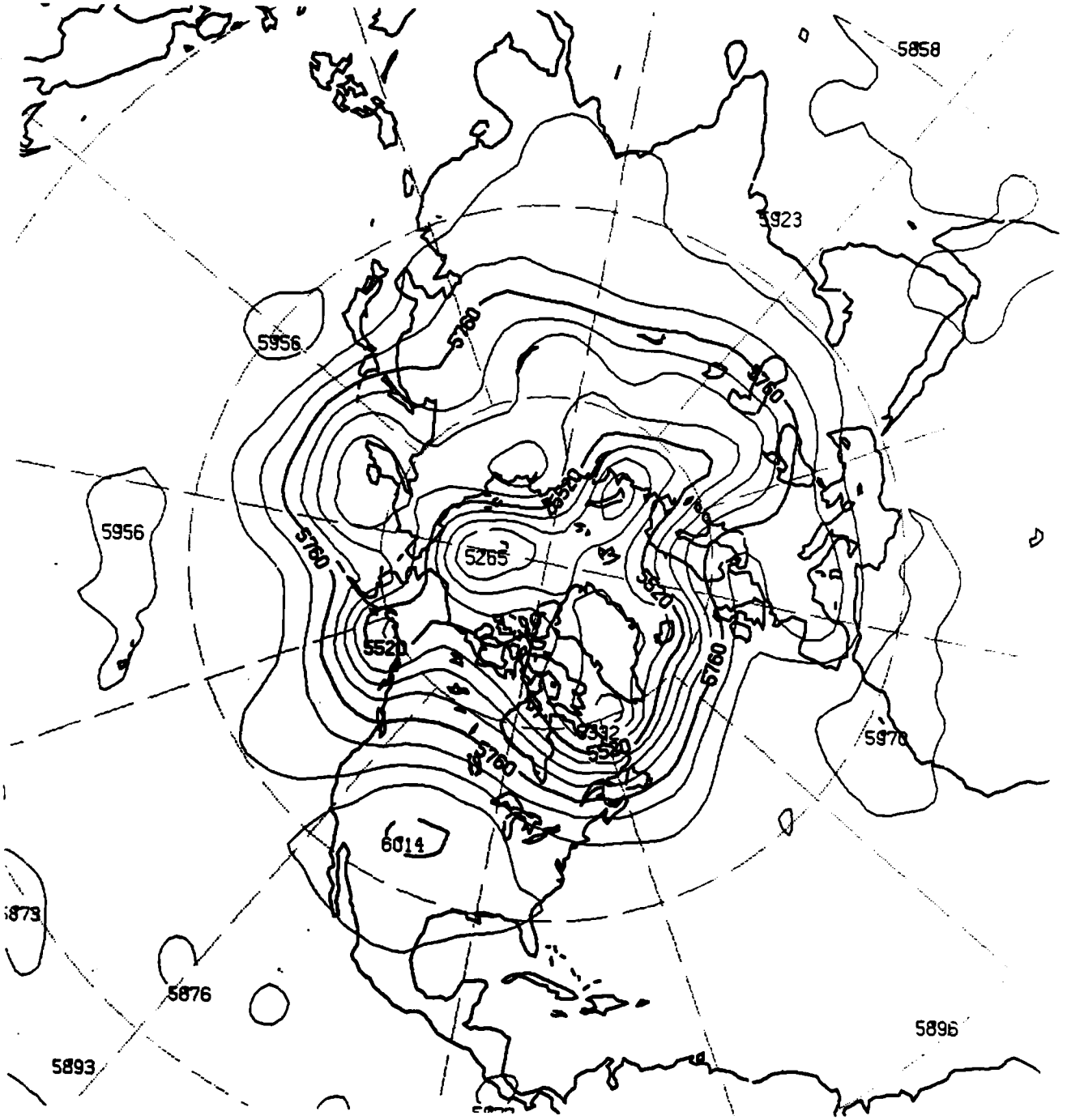

Fig. 47. 72-hour Northern Hemisphere assimilation run forecast for 500 mb heights (m) valid at 00Z, 27 August 1983.

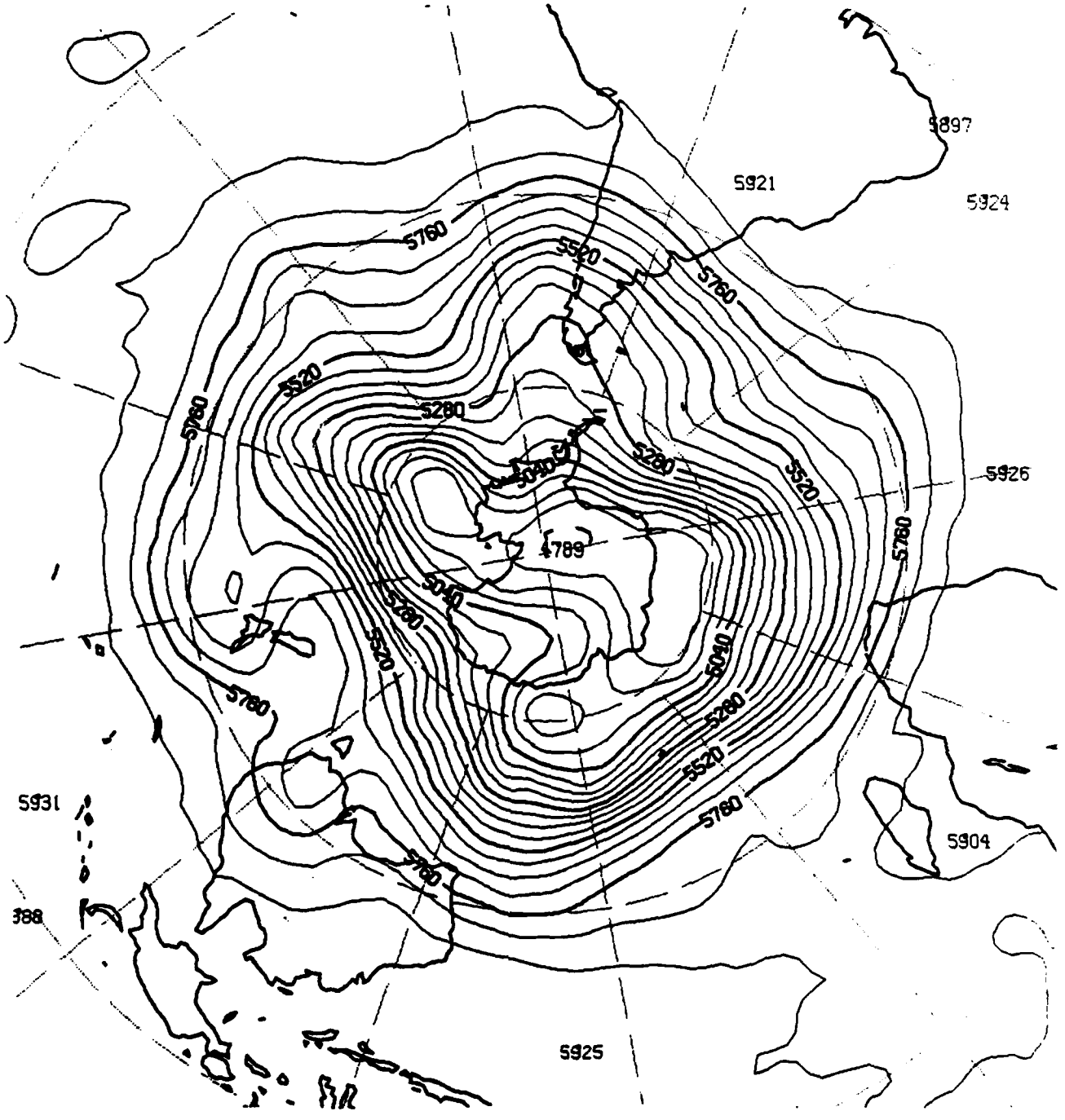

Fig. 48. 72-hour Southern Hemisphere assimilation run forecast for 500 mb heights (m) valid at 00Z, 27 August 1983.

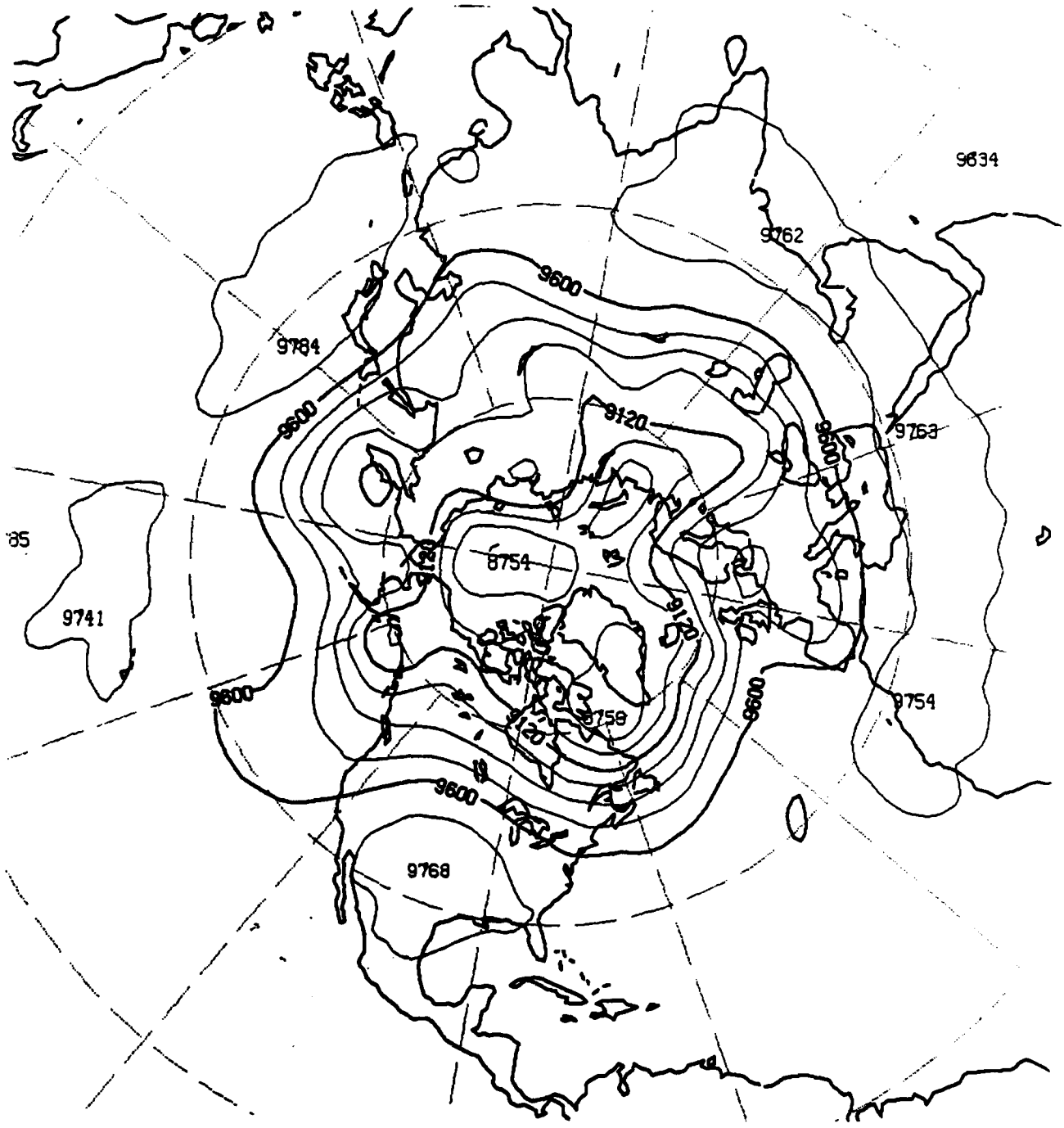

Fig. 49. 72-hour Northern Hemisphere assimilation run forecast for 300 mb heights (m) valid at 00Z, 27 August 1983.

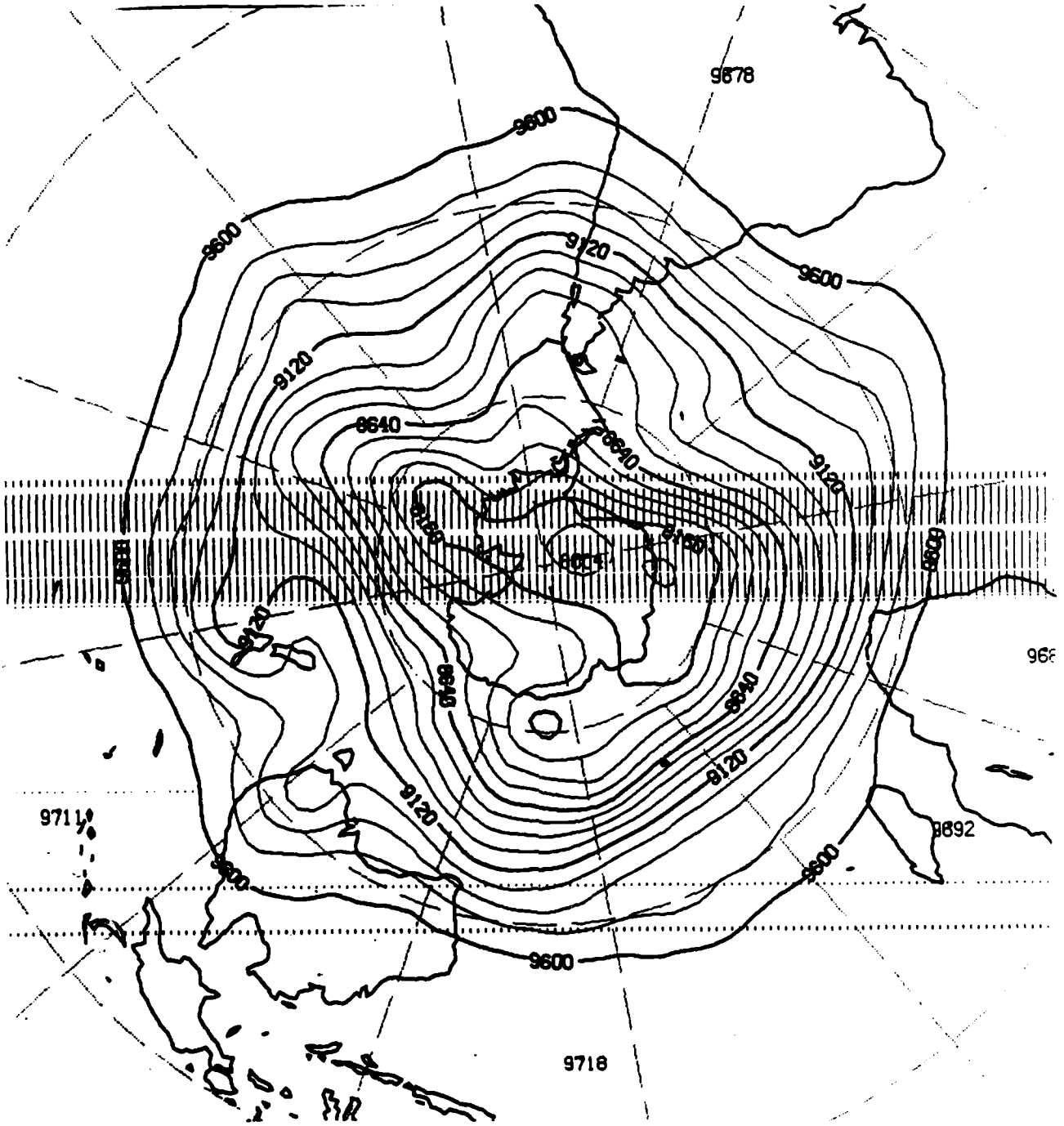

Fig. 50. 72-hour Southern Hemisphere assimilation run forecast for 300 mb heights (m) valid at 00Z, 27 August 1983.

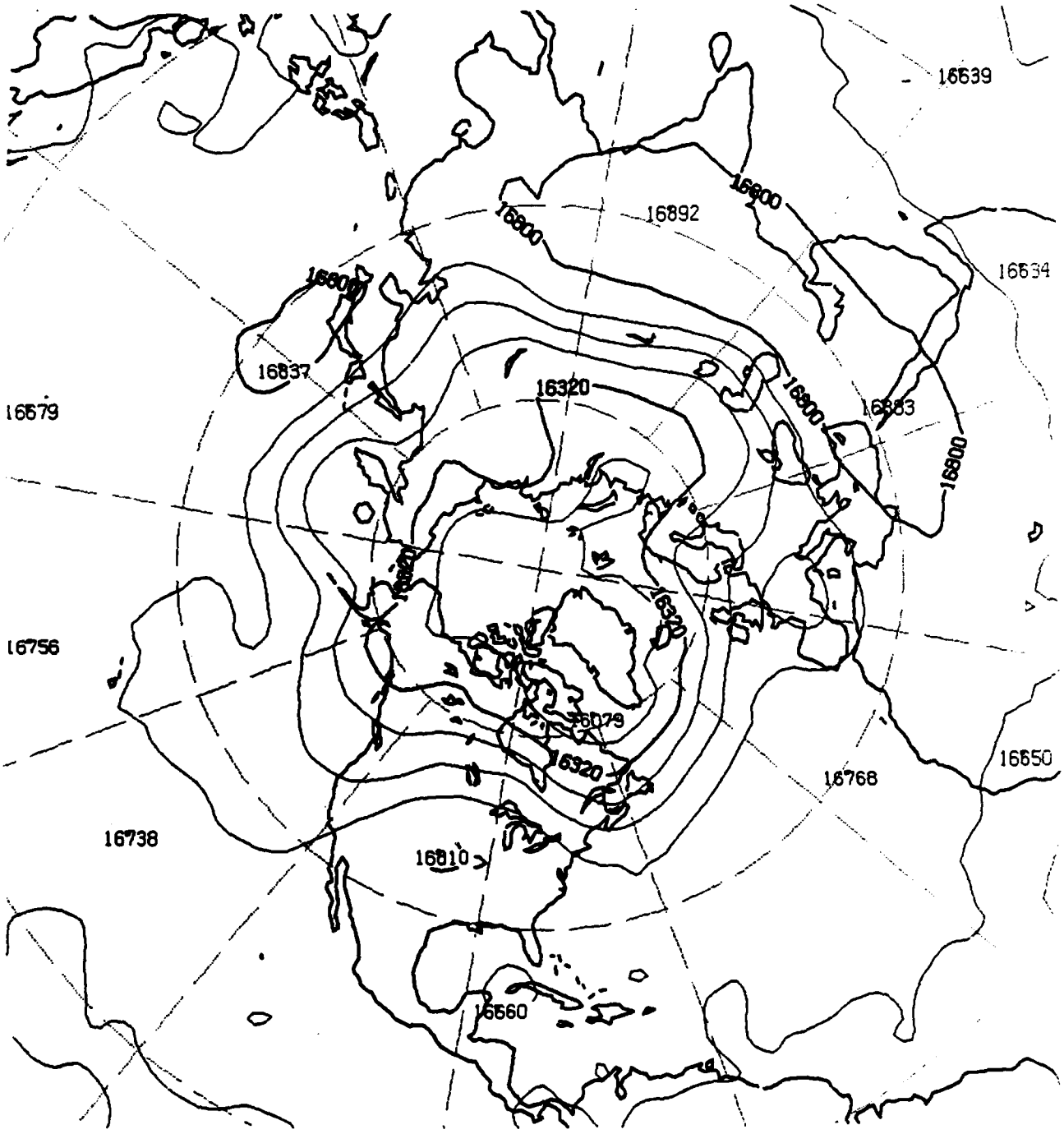

Fig. 51. 72-hour Northern Hemisphere assimilation run forecast for 100 mb heights (m) valid at 00Z, 27 August 1983.

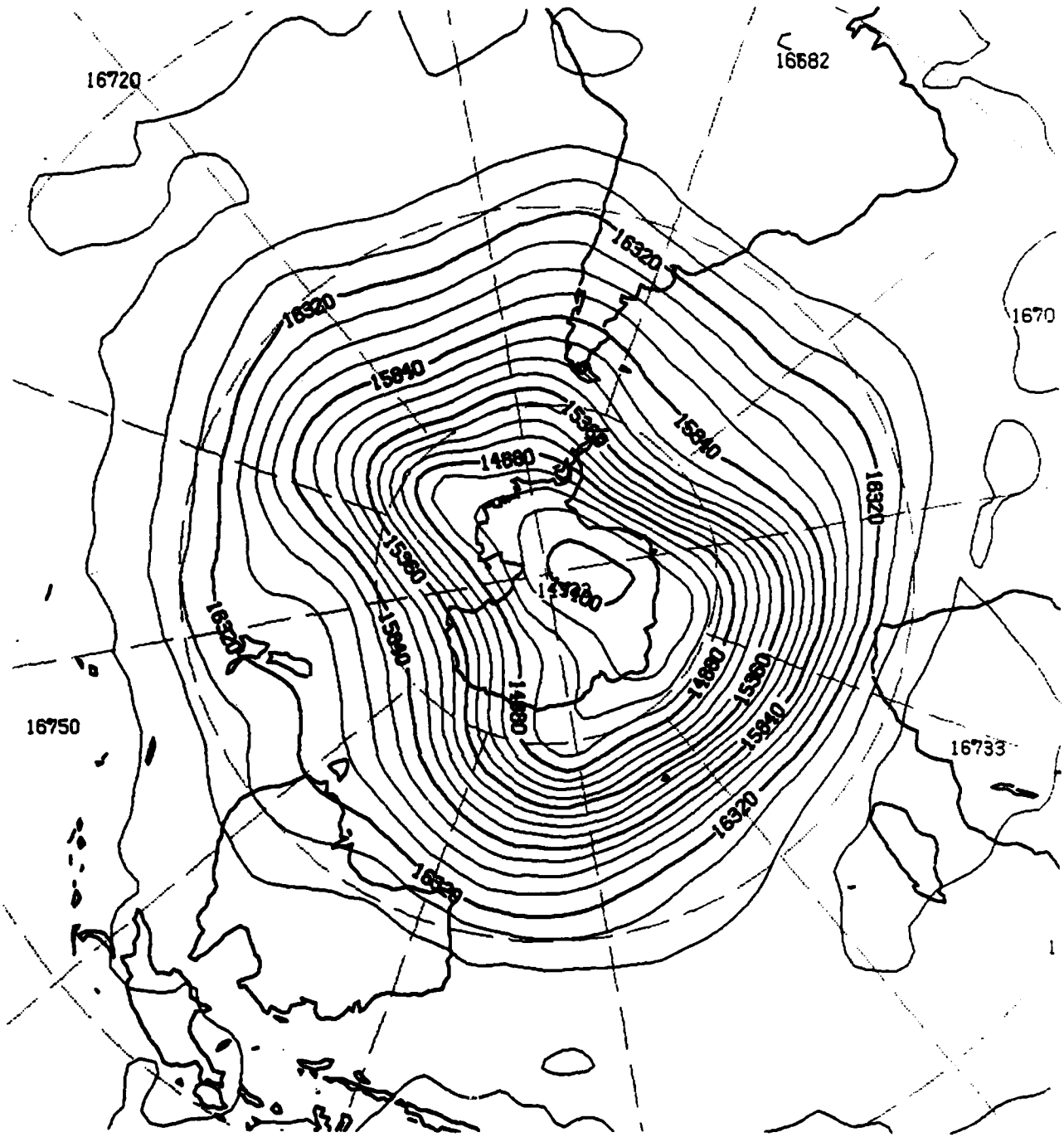

Fig. 52. 72-hour Southern Hemisphere assimilation run forecast for 100 mb heights (m) valid at 00Z, 27 August 1983.

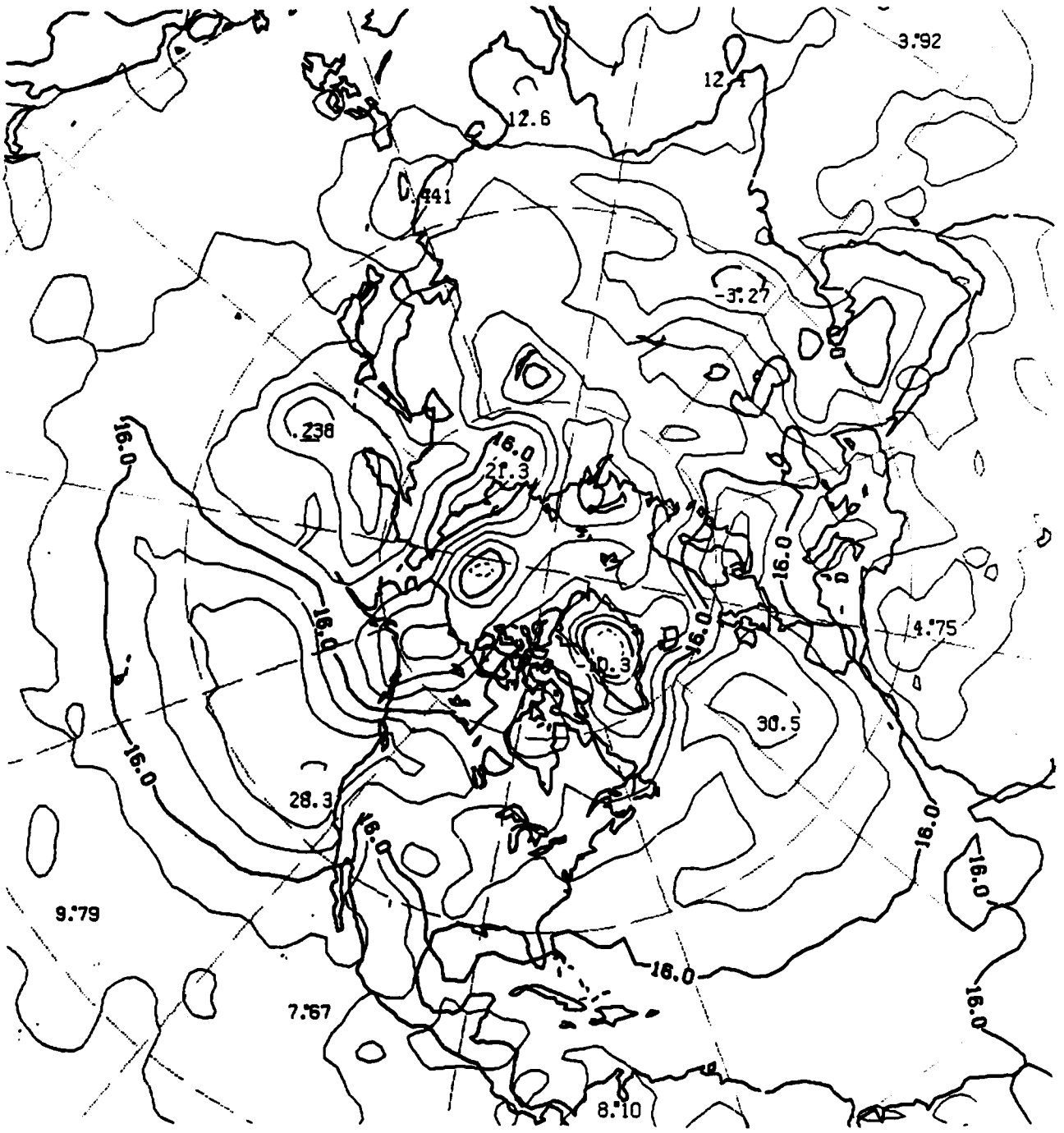

Fig. 53. 72-hour Northern Hemisphere control run forecast for sea-level pressure (mb) valid at 00Z, 27 August 1983.

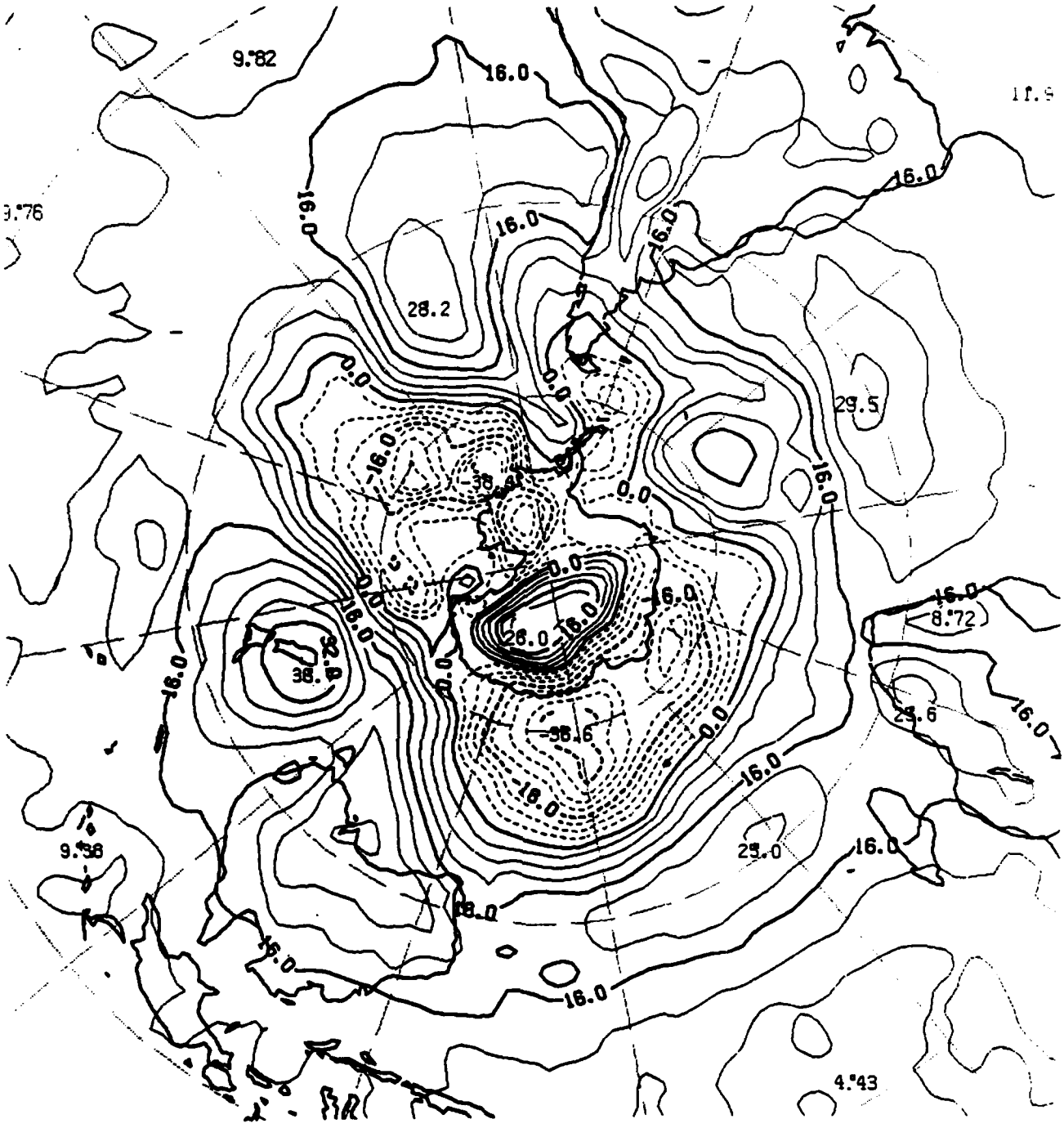

Fig. 54. 72-hour Southern Hemisphere control run forecast for sea-level pressure (mb) valid at 00Z, 27 August 1983.

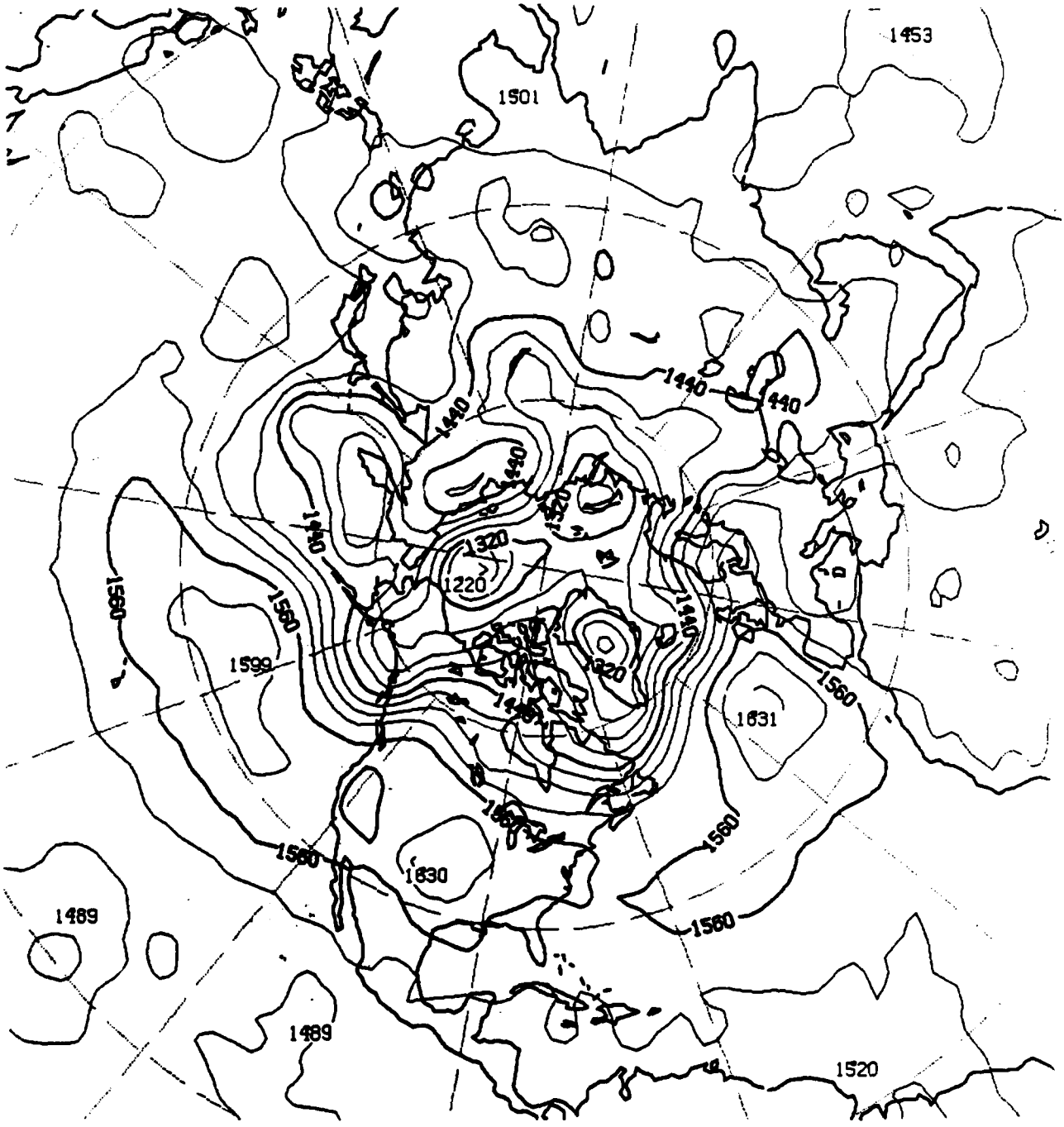

Fig. 55. 72-hour Northern Hemisphere control run forecast for 850 mb heights (m) valid at 00Z, 27 August 1983.

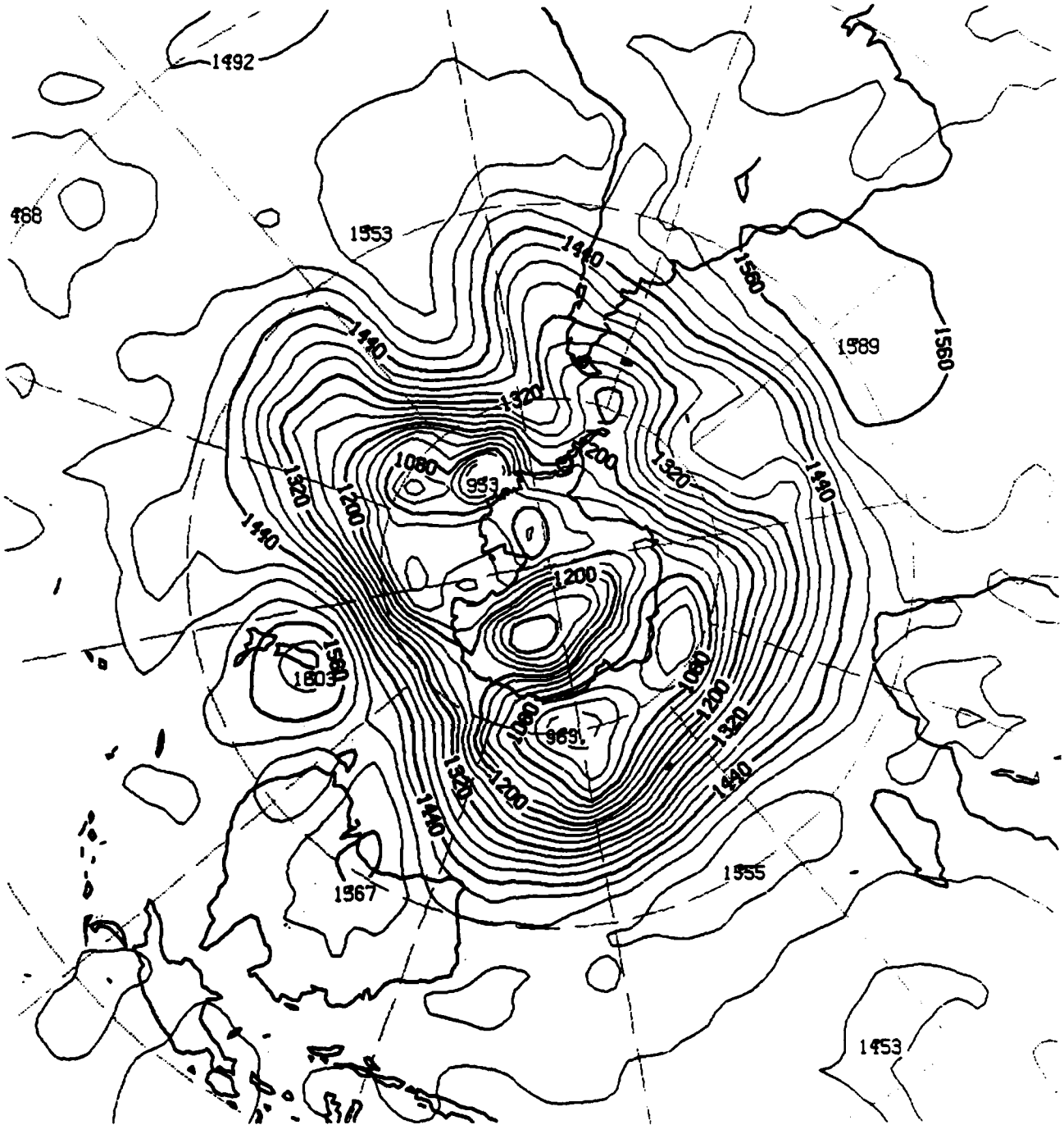

Fig. 56. 72-hour Southern Hemisphere control run forecast for 850 mb heights (m) valid at 00Z, 27 August 1983.

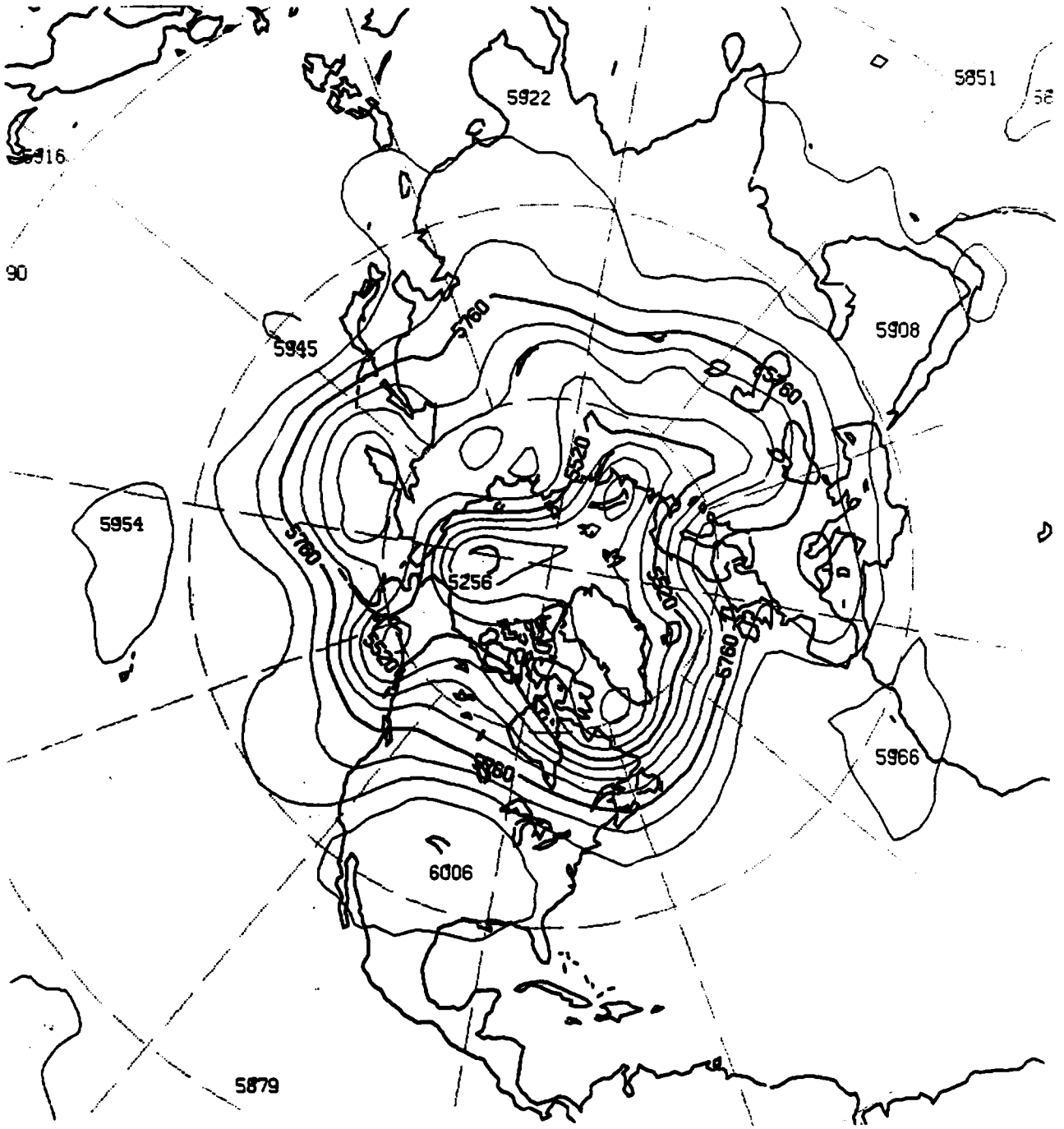

Fig. 57. 72-hour Northern Hemisphere control run forecast for 500 mb heights (m) valid at 00Z, 27 August 1983.

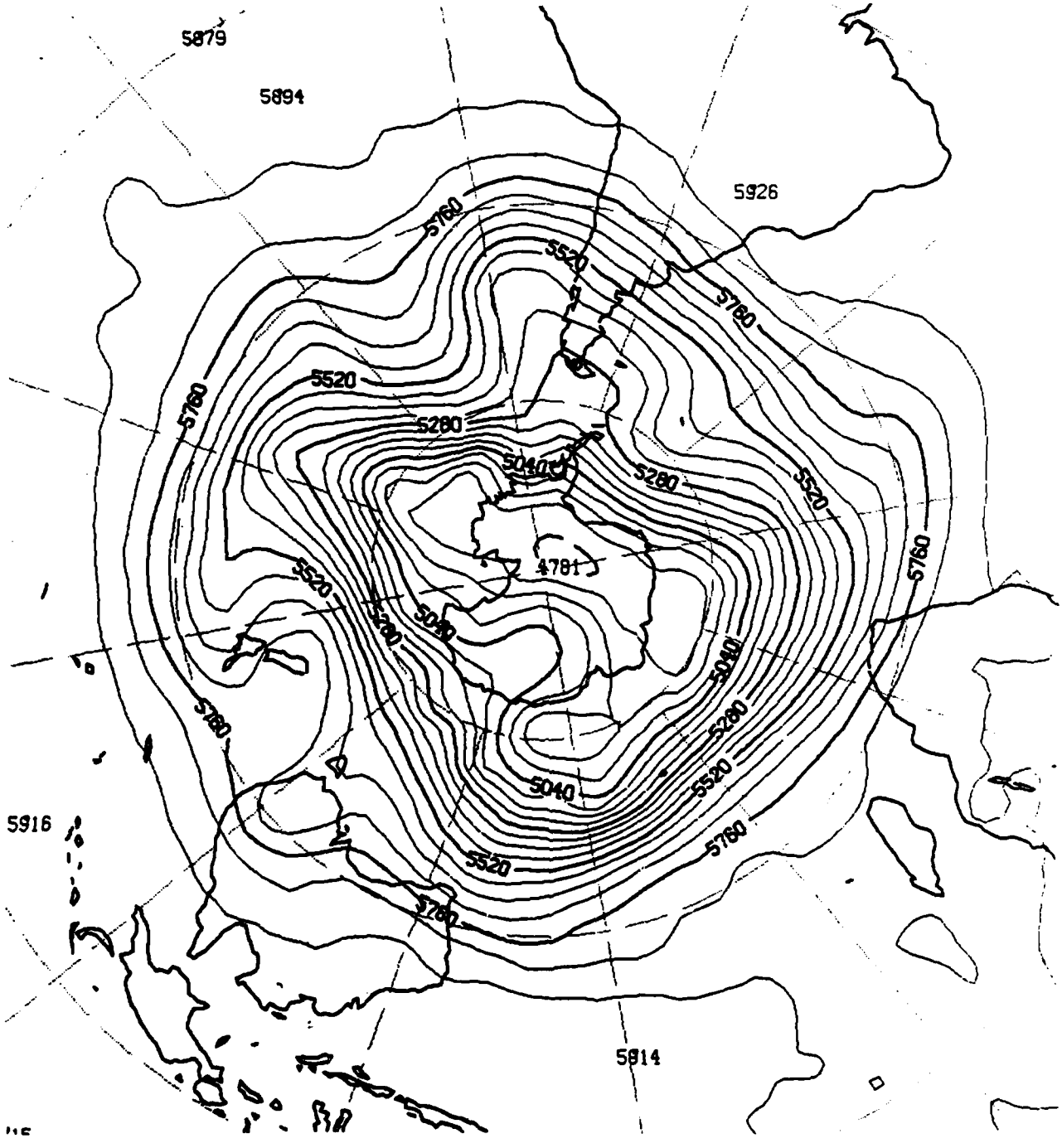

Fig. 58. 72-hour Southern Hemisphere control run forecast for 500 mb heights (m) valid at 00Z, 27 August 1983.

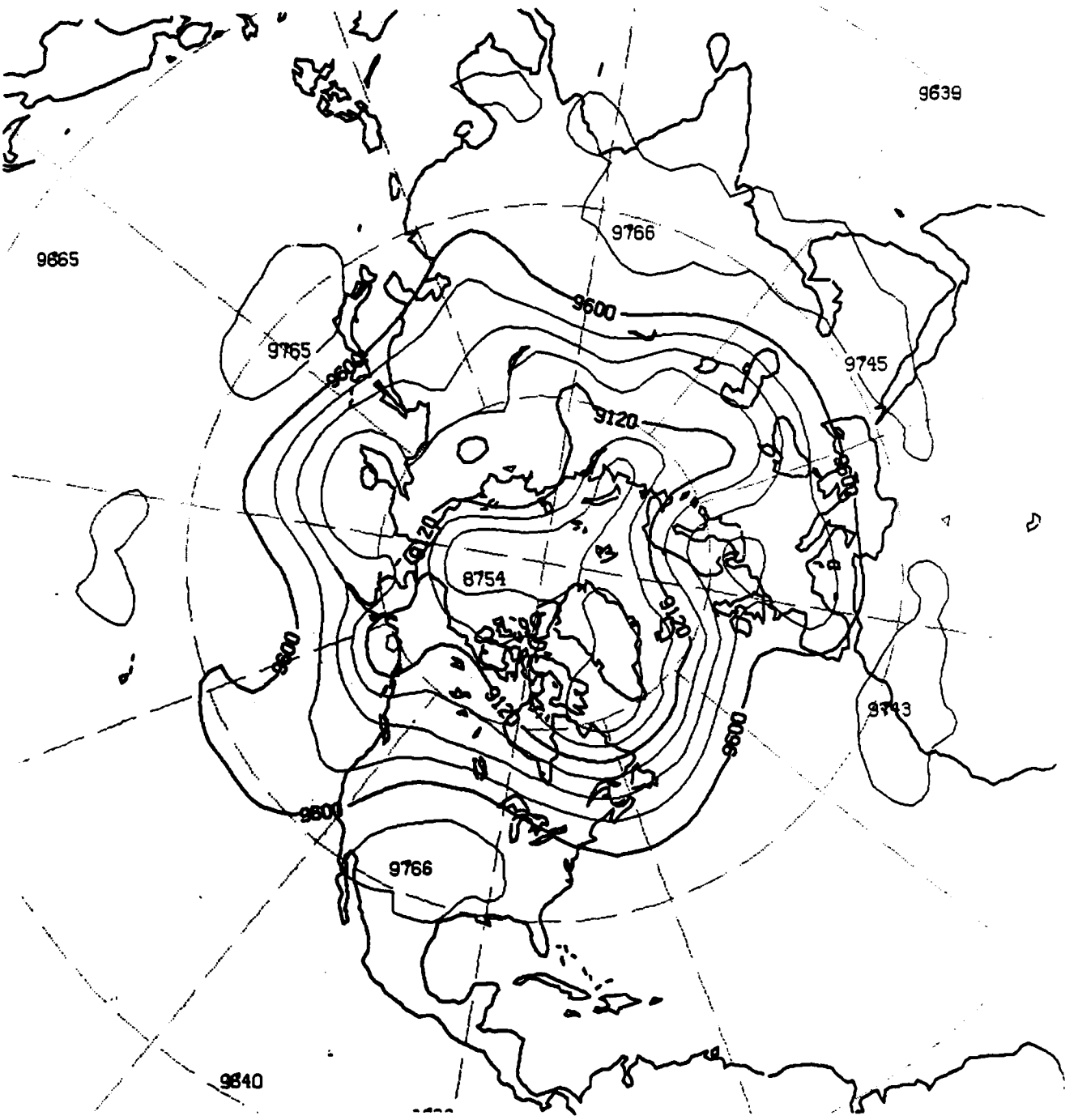

Fig. 59. 72-hour Northern Hemisphere control run forecast for 300 mb heights (m) valid at 00Z, 27 August 1983.

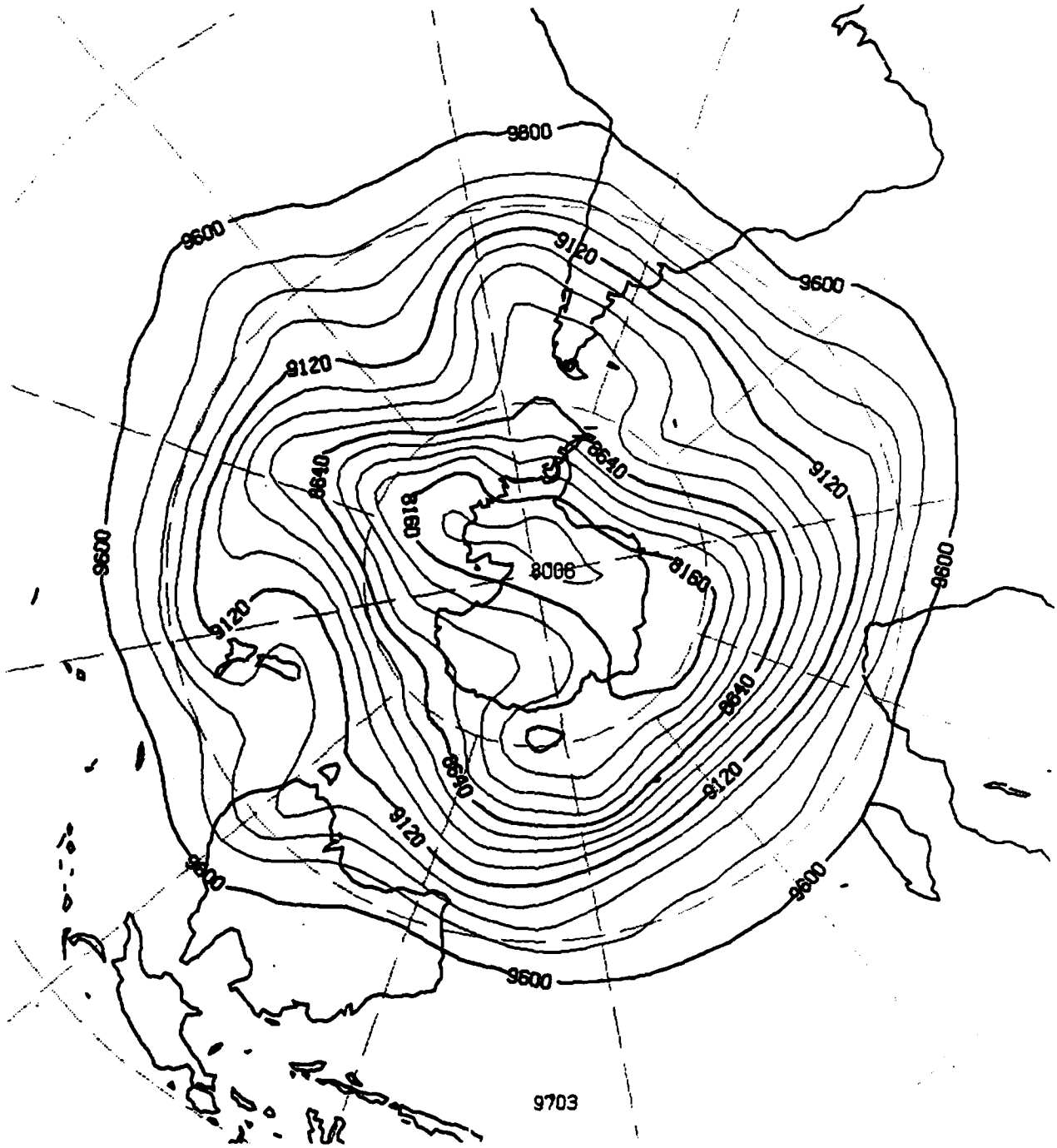

Fig. 60. 72-hour Southern Hemisphere control run forecast for 300 mb heights (m) valid 00Z, 27 August 1983.

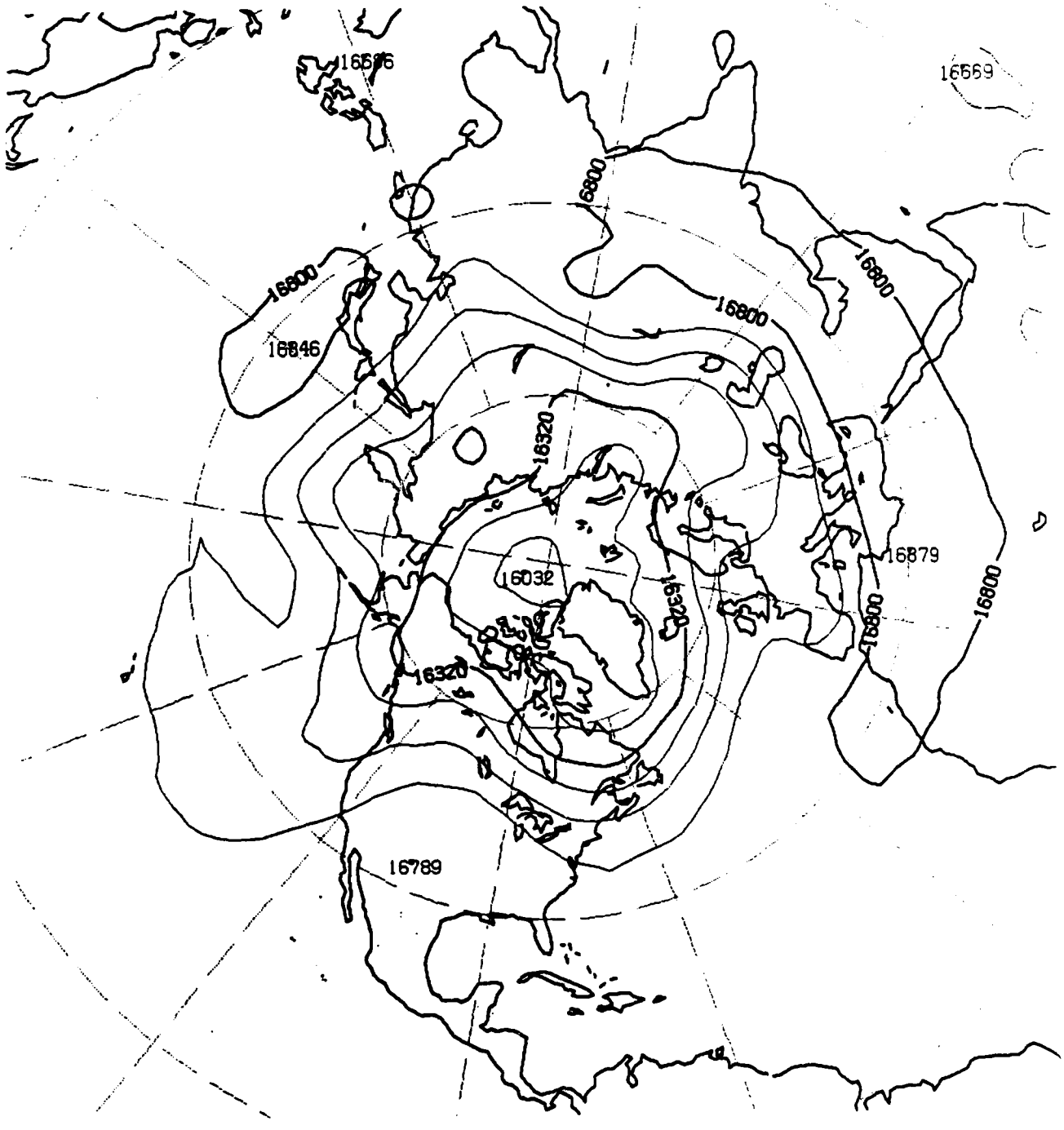

Fig. 61. 72-hour Northern Hemisphere control run forecast for 100 mb heights (m) valid at 00Z, 27 August 1983.

AD-A139 904 FOUR-DIMENSIONAL SATELLITE DATA ASSIMILATION(U) 2/2
COOPERATIVE INST FOR MESOSCALE METEOROLOGICAL STUDIES
NORMAN OK Y K SASAKI ET AL. JAN 84 N00014-79-C-0758
UNCLASSIFIED F/G 4/2 NL

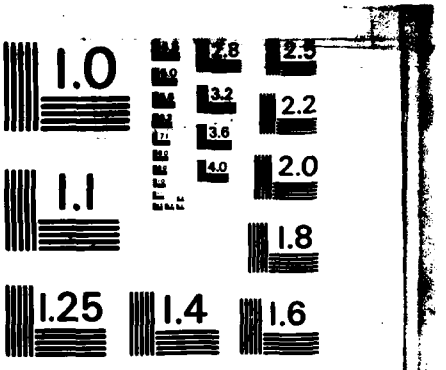

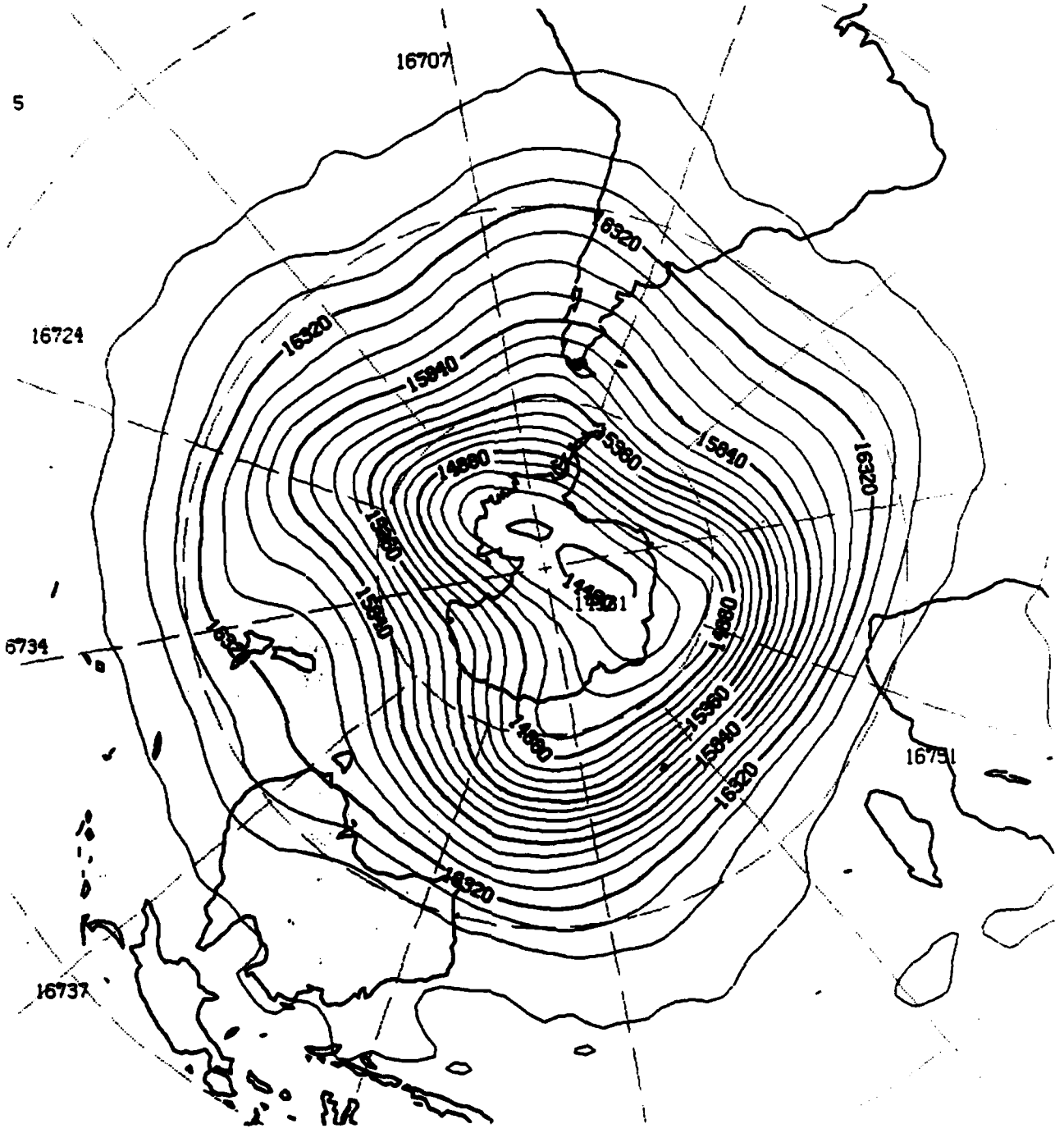

Fig. 62. 72-hour Southern Hemisphere control run forecast for 100 mb heights (m) valid at 00Z, 27 August 1983.